

**REPUBLIC OF TURKEY
AYDIN ADNAN MENDERES UNIVERSITY
GRADUATE SCHOOL OF NATURAL AND APPLIED SCIENCES
MECHANICAL ENGINEERING
2019-Ph.D.-006**

**A COMPUTATIONAL FLUID DYNAMICS (CFD)-
DISCRETE ELEMENT MODELING (DEM)
INVESTIGATION OF CENTRIFUGAL
SEPARATION PROCESSES OF
PARTICLE-LADEN FLOWS**

Orçun EKİN

**Supervisor:
Prof. Dr. Yunus ÇERÇİ**

AYDIN

REPUBLIC OF TURKEY
AYDIN ADNAN MENDERES UNIVERSITY
GRADUATE SCHOOL OF NATURAL AND APPLIED SCIENCES
AYDIN

The thesis with the title of “*A COMPUTATIONAL FLUID DYNAMICS (CFD)-DISCRETE ELEMENT MODELING (DEM) INVESTIGATION OF CENTRIFUGAL SEPARATION PROCESSES OF PARTICLE-LADEN FLOWS*” prepared by the PhD Candidate Orçun EKİN at the PhD Program at the Department of Mechanical Engineering was accepted by the jury members whose names and titles presented below as a result of thesis defense on 13/06/2019.

	Title, Name and Surname	Institution	Signature
President:	Prof. Dr. Yunus ÇERÇİ	Aydın Adnan Menderes University	
Member:	Dr. Öğr. Üyesi Mustafa ASKER	Aydın Adnan Menderes University	
Member:	Dr. Öğr. Üyesi Adem ÖZÇELİK	Aydın Adnan Menderes University	
Member:	Dr. Öğr. Üyesi Ali YURDDAŞ	Manisa Celal Bayar University	
Member:	Dr. Öğr. Üyesi Yiğit AKSOY	Manisa Celal Bayar University	

This Doctorate Thesis accepted by the jury members is endorsed by the decision of the Institute Board Members with file number and date.

Prof. Dr. Gönül AYDIN
Institute Director

REPUBLIC OF TURKEY
AYDIN ADNAN MENDERES UNIVERSITY
GRADUATE SCHOOL OF NATURAL AND APPLIED SCIENCES
AYDIN

I hereby declare that all information and results reported in this thesis have been obtained by my part as a result of truthful experiments and observations carried out by the scientific methods, and that I referenced appropriately and completely all data, thought, result information which do not belong my part within this study by virtue of scientific ethical codes.

25/06/2019

Orçun EKİN

ÖZET

PARTİKÜL İÇEREN AKIŞLARDA SANTRİFÜJ SEPARASYON İŞLEMLERİNİN HESAPLAMALI AKIŞKANLAR DİNAMİĞİ (HAD)-AYRIK ELEMAN MODELLEME (AEM) BİLEŞİMİ İLE İNCELEMESİ

Orçun EKİN

Doktora Tezi, Makine Mühendisliği Anabilim Dalı

Tez Danışmanı: Prof. Dr. Yunus ÇERÇİ

2019, XXVI+92 Sayfa

İnek sütündeki Somatik hücre sayısı (Somatic Cell Count-SCC) aşırı yüksek değerleri ürün kalitesine ve üretim kapasitesine önemli zararlar veren ‘Mastitis’ hastalığının açık belirtisi haline gelmesi sebebiyle, süt tesisinde sürü sağlığının önemli değişkenlerinden biridir. Dolayısıyla, SCC indeksinin, süt işleme tesisine kabulü sırasında yasalarla belirlenmiş sınırların altına indirilmesi gerekir. Bu çalışmada, süt temizleme işlemi, somatik hücrelerin ayrık partiküller, sütün ise partikül içeren, iki fazlı saf ve sürekli bir akışkan olarak modellenmesi yoluyla araştırılmıştır. Disk tipi bir santrifüj içerisinde partiküllerin çökme davranışları yanısıra sürekli akışkan karakteristiği, Euler-Lagrange bileşimi kullanan Ayrık Eleman Modelleme (AEM) ile bağlaşıklık Hesaplamalı Akışkanlar Dinamiği (HAD) yardımıyla incelenmiştir. Somatik hücreler için kabul edilen 6-20µm aralığında, 16.5µm ortalama partikül çapı için doğrulama noktasında %87.83'lük ölçüm verisine karşılık %91.05'lük ayırıştırma kabiliyeti hesaplanmıştır. Farklı besleme ve devir hızlarında, ayrıca farklı disk sayılarında gerçekleştirilen benzetimler, artan merkezkaç kuvvetler ve azalan besleme hızlarının partikül ayırışım oranlarını en üst düzeye çıkardığını göstermektedir. Ancak işlemin elverişliliği açısından bu üç değişkenin eniyilenmesi gerekliliğini ortaya koymaktadır.

Anahtar Kelimeler: santrifüj separasyon, Euler-Lagrange metodu, HAD-AEM, inek sütü, somatic hücre

ABSTRACT

A COMPUTATIONAL FLUID DYNAMICS (CFD)-DISCRETE ELEMENT MODELING (DEM) INVESTIGATION OF CENTRIFUGAL SEPARATION PROCESSES OF PARTICLE-LADEN FLOWS

Orçun EKİN

PhD Thesis, Mechanical Engineering Dept.

Supervisor: Prof. Dr. Yunus ÇERÇİ

2019, XXVI+92 Pages

Somatic cell count (SCC) in bovine milk is an important parameter of cattle health in a dairy farm, the exceeding numbers of which heavily indicate an infection in milk called ‘Mastitis’, reducing the overall quality of product and crippling the yield. Therefore, the SCC index of milk must be reduced below legal limits when admitted to a dairy compound. In this study, the clarification process of milk is investigated by modeling the somatic cells in milk as discrete particles, meanwhile the milk is assumed to be a continuous, pure substance; constituting a two-phase, particle-laden medium. The sedimentation behavior of particles along with flow characteristics of the continuous medium in a disk-stack centrifuge is investigated in terms of Computational Fluid Dynamics (CFD) coupled with Discrete Element Modeling (DEM) where a Euler-Lagrange scheme is employed. A 6-20 μm range for somatic cells is assumed, yielding an 87.89% separation efficiency against an 87.83% validation point; that is for 16.5 μm of average diameter of particles. Simulations performed on different throughput rates, rotational speeds of solid-bowl and number of disks employed imply that increasing centrifugal forces, applied with minimum throughput rates maximize the particle sedimentation, reducing the SCC index. However, an optimization between the three parameters are required to maintain operation feasibility.

Keywords: centrifugal separation, Euler-Lagrange Coupling, CFD-DEM, bovine milk, somatic cells

ACKNOWLEDGEMENTS

I would like to express my sincere gratitude to my advisor Prof. Yunus ÇERÇİ for the continuous support of my PhD study and related research, for his motivation, and immense knowledge. His guidance helped me in all the time of research and writing of this thesis. I could not have imagined having a better advisor and mentor for my PhD study. He has taught me more than I could ever give him credit for here. He has shown me, by his example, what a good scientist should be.

I am grateful to all of those with whom I have had the pleasure to work during this thesis study and other related projects. Each of the members of my Dissertation Committee has provided me extensive personal and professional guidance and taught me a great deal about both scientific research and life in general. I would also like to thank *HAUS Centrifuge Technologies* for all the engineering models and field test results they provided, helping this study find its foundation and conclusion.

Nobody has been more important to me in the pursuit of this thesis study than the members of my family. I would like to thank my parents; whose love and guidance are with me in whatever I pursue. They are the ultimate role models.

Orçun EKİN

TABLE OF CONTENTS

ÖZET	vii
ABSTRACT	ix
ACKNOWLEDGEMENTS	xi
1. INTRODUCTION	1
1.1. Basic Concepts of Sedimentation Theory	1
1.2. Filtration and Centrifugation	5
1.2.1. Filtering Centrifuge	6
1.2.2. Sedimenting (Solid Bowl) Centrifuge	7
2. LITERATURE REVIEW	9
3. MATERIAL AND METHOD	18
3.1. General Configuration and Operation Principles	18
3.1.1. Paring Disk	20
3.2. Performance Evaluation of Centrifuges by Classic Methods	21
3.3. Equivalent Surface Area for Disk-Stack Centrifuge	22
3.4. Milk and Milk Properties	24
3.4.1. The Bovine Milk	24
3.4.2. The Composition and Characteristics of Bovine Milk	26
3.4.3. Somatic Cell Count Effect on Quality of Raw Milk	27

3.5. Milk Processing Through Centrifugation	28
3.5.1. Requirements for Sedimentation	29
3.5.2. Raw Milk Clarification	31
3.6. Particle-laden Flow in Disk-Stack Centrifuges.....	33
3.6.1. Flow Characteristics in a Nutshell.....	34
3.6.2. Rule of Thumb: Methods to Process Evaluation.....	34
3.6.2.1. The Ambler Method.....	35
3.6.2.2. Kempken and Leung Calculations	36
3.7. Particle-laden Flow Modeling in CFD	38
3.7.1. Continuous Medium	38
3.7.1.1. Conservation of Mass	38
3.7.1.2. Conservation of Momentum.....	39
3.7.2. RANS Models for the Particle-laden Flow in Centrifugal Field	40
3.7.2.1. RNG $k - \epsilon$ Model.....	41
3.7.2.2. Standard $k - \omega$ Model.....	44
3.7.3. Particle-laden Flow in ANSYS Fluent Software: The CFD-DEM.....	47
3.8. The CFD-DEM Simulations in the Separation Field	51
3.8.1. Problem Definition	52
3.8.2. Pre-processing Setup and Particle Injections	54
3.8.2.1. Boundary Conditions	56
3.8.2.2. The DEM Setup	57

4. RESULTS AND DISCUSSION.....	58
4.1. Problem Validation.....	59
4.2. Sedimentation Performance for Various Cut-off Diameters.....	62
4.3. Scale-up Ability of the CFD-DEM Model.....	64
4.4. Particle Stagnation in Disk-stack	65
4.5. Turbulence Model Comparison for 3-D Flow Field.....	68
5. CONCLUSION.....	74
REFERENCES	77
APPENDICES.....	83
RESUME.....	91

LIST OF SYMBOLS

v_g : Particle velocity	P: Pressure
ρ_p : Density of discrete particles	k: Turbulence kinetic energy
ρ_m : Density of continuous medium	ε : Turbulence dissipation rate
μ : Dynamic viscosity	ω : Specific rate of dissipation
ω, Ω : Angular velocity	α : Inverse effective Prandtl number
N: Revolutions per minute	$\hat{\nu}$: Turbulent viscosity ($k - \varepsilon$)
n: Number of Disks	G_k : Turbulent kin. energy generation
F_g : Gravitational force	G_ω : Specific diss. rate generation
F_b : Buoyancy Force	Γ_k : Effective diffusivity of k
F_d : Drag Force	Γ_ω : Effective diffusivity of ω
ϑ : Stokes' Terminal Velocity	Y_k : Dissipation of k due to turbulence
Re: Reynolds Number	Y_ω : Dissipation of ω due to turbulence
Q: Throughput rate	σ_k : Turbulent Prandtl number for k
Σ : Centrifuge equivalent surface area	σ_ω : Turbulent Prandtl number for ω
d_{cutoff} : Particle diameter at cut-off	μ_t : Turbulent viscosity ($k - \omega$)
r_2 : Disk outer diameter	α^* : Low-Re buffer coeff. ($k - \omega$)
r_1 : Disk inner diameter	$F(M_t)$: Compressibility function
θ : Disk half-angle	\bar{u} : Mean fluid phase velocity
d_{min} : Minimum particle diameter	T: Integral time scale
d_o : Average particle diameter	T_L : Lagrangian integral time
\vec{V} : Velocity Field for cylindrical coord.	

LIST OF ABBREVIATIONS

<u>Abbreviation</u>	<u>Expansion of the Term</u>
BTSCC	: Bulk Tank Somatic Cell Count
CAE	: Computer Associated Engineering
CFD-DEM	: Computational Fluid Dynamics – Discrete Element Modeling
FSI	: Fluid-Solid Interface
LES	: Large Eddy Simulation
mAb	: Monoclonal Antibody
MRF	: Moving Reference Frame
N-S	: Navier-Stokes (Equations)
PDF	: (Gaussian) Probability Density Function
RANS	: Reynolds Averaged Navier-Stokes
RCF	: Relative Centrifugal Force
RMS	: Root Mean Square
RNG	: Renormalization Group
RSM	: Reynolds Stress Model
SCC	: Somatic Cell Count
SNF	: Solid Non-Fat
VoF	: Volume of Fluid

LIST OF FIGURES

Figure 1.1. The force balance for a particle confined in a gravitational field.....	2
Figure 1.2. A still representation of Coriolis effect during particle sedimentation on centrifuge, when the disk is rotated counter-clockwise.	4
Figure 1.3. Solid-bowl centrifuge (Leung, 2007).	5
Figure 1.4. Filter (screen) bowl centrifuge (Leung, 2007).	6
Figure 1.5. A filtering centrifuge with horizontal bowl for pharmaceutical applications. (Heinkel Drying and Separation Group, 2019).....	7
Figure 1.6. A see-through section of a nozzle centrifuge used in pharmaceutical applications (GEA Group Aktiengesellschaft 2019).....	8
Figure 2.1. A visualization of the two flow field definition approaches; Eulerian (left) and Lagrangian frame of references (Università Di Pavia, 2019).....	11
Figure 2.2. Outlet example of solid-bowl centrifuge (Kempken et al., 1995).....	14
Figure 2.3. Cylinder flow region of the tubular bowl centrifuge and mesh structure in a cross-section view in Lindner et al. (2013).....	15
Figure 2.4. One-eighth (45°) centrifuge modeling (Shekhawat et al., 2018).....	16
Figure 3.1. A generic solid-bowl centrifuge cross section view with main parts (van der Linden, 1987).....	19
Figure 3.2. Rib assembly on a typical disk stack (distributor is not shown) (Flottweg Separation Technologies, 2019).	20
Figure 3.3. A typical paring disk to separate either one of the liquid phases (Bylund and Svensson, 1995).	21
Figure 3.4. Schematic of disk-stack for cutoff diameter calculation (van der Linden, 1987).....	23
Figure 3.5. Main form and departments of cow's udder (Jelen, 2000).....	24

Figure 3.6. A parallel tandem milking parlor in a dairy farm.....	25
Figure 3.7. The 'state-of-the-art' Cream Separator by de Laval. Commercial brochure from Smithsonian archives (De Laval Separator Co. 1913. De Laval Cream Separators, Farm and Dairy Sizes, New York).	28
Figure 3.8. In-line Milk Standardization Process (Kilara, 2011).....	30
Figure 3.9. Milk distribution in clarifier bowl (left) and settling behavior of particles between disks (Bylund and Svensson, 1995).	32
Figure 3.10. Interphase location is decided according to volume fractions of liquid phases (Bylund and Svensson, 1995).....	32
Figure 3.11. Hydraulic discharge mechanism in a drop-bottom centrifuge (Bylund and Svensson, 1995).....	33
Figure 3.12. 2D representation of disk-stack; two disks (Ambler, 1959).	35
Figure 3.13. 24-disk bowl representation of two-phase clarifier.	52
Figure 3.14. Actual simulation domain is obtained by a three-step evaluation.	54
Figure 3.15. Detail of mesh view, 45° model with 0.25mm disk interval.	55
Figure 4.1. A schematic of a Flow Cytometry application (Abcam, 2019).	60
Figure 4.2. Residual graphics of RANS models applied to problem statement at steady state conditions: RNG k- ϵ and the Standard k- ω	61
Figure 4.3. The CFD-DEM method for problem definition converges at every time step, at the expense of simulation time.	62
Figure 4.4. Settling efficiencies at cutoff diameters.	63
Figure 4.5. Sedimentation efficiencies at increasing throughput rates.	64
Figure 4.6. Separation efficiencies at increasing bowl rates.	64

Figure 4.7. Particle stagnation in disk-stack during the process occurs regardless the turbulence model employed.	66
Figure 4.8. Particle tracks and occurrence of stagnation in disk-stack for Shekhawat avg. particle with RNG $k - \epsilon$ and the Standard $k - \omega$ RANS models.	67
Figure 4.9. Reynolds number survey near settler beach and through disk interval. Representation: Standard $k-\omega$; 7700 rpm, 1.436×10^{-2} kg/s.	69
Figure 4.10. Pressure distribution in the flow region for RNG $k - \epsilon$ and Standard $k - \omega$ RANS models.	70
Figure 4.11. Velocity distribution in the flow region for RNG $k-\epsilon$ and Standard $k-\omega$ RANS models.	71
Figure 4.12. Turbulence Kinetic Energy distribution in the flow region for RNG $k-\epsilon$ and Standard $k-\omega$ RANS models.	72
Figure 4.13. Mass flow rate quickly stabilizes for each calculation method.	73

LIST OF TABLES

Table 3.1. Composition of whole and skim milk solids (Spreer, 2017).....	26
Table 3.2. Operational distinctions of separator and clarifier.	31
Table 3.3. The number of disks in the CFD modeling against the number of disks on the original model.	55
Table 3.4. Some physical properties of Leukocytes with source publication.	56
Table 3.5. Boundary conditions set with applied modifications.....	56
Table 3.6. DEM Parameters	57
Table 4.1. Process parameters for example collection.	59
Table 4.2. Steady-state separation efficiency is validated through CFD-DEM modeling	60
Table 4.3. Minimum particle diameter calculation via theoretical approaches in different settler configurations.	62
Table 4.4. Stokes' terminal velocities and total mass of injection for cut-off particles from Table 4.2.	63



*To my mother;
who taught me how to read,
and how to cherish...*

1. INTRODUCTION

1.1. Basic Concepts of Sedimentation Theory

Based on density difference between the ‘phases’ in a multi-component medium, centrifugation is one of the most efficient ways of separating pure substances. Gravitational settling especially applies for particles in solutions, due to higher density differences they can provide. Field of applications for centrifugal separators expand regularly as manufacturers tend to increase the quantity and variety of experiments through these devices. Yet separating a group of particles from inside a continuous medium stands the core application of a centrifugal settler, although the properties of media and particles change from application to application. In this respect, however an indispensable branch of operation for centrifugal settlers, separating two or more ‘liquid’ components from a medium is considered a rare application, often limited to milk processing, olive oil processing etc.

Every field of application introduces distinct medium and particle characteristics; i.e. organic or inorganic with features like variable sizes, shapes, ability to accumulate, etc. In the context of this thesis study, organic particles (somatic cells or *leukocytes*) alongside with organelles and *cell-debris* within an organic substance (bovine milk) is considered. Another very popular application of sedimenting centrifuge is oil-field which introduces an environment where both continuous medium and particles are inorganic compounds. To maintain a concise language, however, all these components will be referred to as ‘particles’ throughout the document.

Practical centrifuge assessment based on principal parameters essentially originates from the Stokes's law (Stokes, 1851). If the sedimentation of a single particle – a sphere in a gravitational field is considered; as the velocity of this particle reaches a constant value (‘terminal velocity’), the net force on the particle is equal to the force resisting its motion through the liquid. This resisting force is called frictional or drag force.

The Euler-Lagrange approach utilized in the context of this study, along with many contemporary studies regarding fluid-solid interactions when the solids are non-soluble (discrete) elements in a continuous medium; originates from the Stokes’ law formulation. Stokes’ law (not to confused with Stokes’ theorem in vector calculus)

basically states that a sphere with a density of ρ_s will tend to sink or rise in a medium of density ρ_m , at a velocity of ϑ , which is called the ‘terminal velocity’ of this particle. For a particle with a higher density than that of its continuous medium ($\rho_s > \rho_m$), a force balance can be written (Eqn. 1.1) in which the gravitational force ' F_g ' of the particle is balanced out by buoyancy ' F_b ' and drag ' F_d ' forces, as in Fig. 1.1:

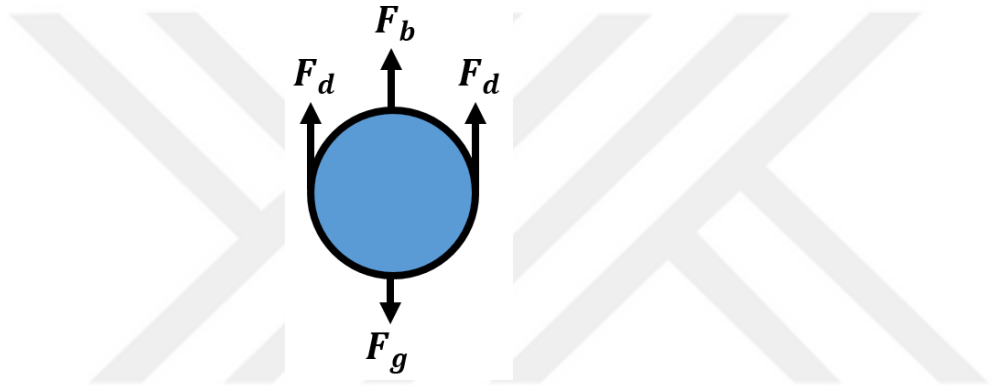


Figure 1.1. The force balance for a particle confined in a gravitational field.

$$F_g = F_b + F_d \quad [N] \quad (1.1)$$

where the gravitational and buoyancy forces are,

$$F_g = \rho_s \cdot V \cdot g \quad [N] \quad (1.2)$$

and

$$F_b = \rho_m \cdot V \cdot g \quad [N] \quad (1.3)$$

respectively. The drag force is expressed as;

$$F_d = 3\pi \cdot \mu \cdot d \cdot \vartheta \quad [N] \quad (1.4)$$

In Eqn.s 1.2-1.4, V represents the volume of the particle, μ is the dynamic viscosity of medium, d is the diameter of particle and ϑ is the terminal velocity. When Eqn. 1.1 is rearranged utilizing the involving forces balancing out the particle inside a gravitational region; the Stokes' law can be obtained as given in Eqn. 1.5. From the equation the sedimentation rate can be calculated as v_g (m/s).

$$v_g = \frac{gd^2(\rho_p - \rho_m)}{18\mu} \quad [m/s] \quad (1.5)$$

In Eqn. 1.5, 'g' is the gravitational acceleration of the earth, μ is the dynamic viscosity of the medium and $(\rho_p - \rho_m)$ is the density difference between the particle and the medium. Stokes' Law states that;

- The sedimentation rate of a given particle is proportional to the square of this particles diameter, d.
- The sedimentation rate is proportional to the difference between the density of the particle and the density of the liquid medium, $(\rho_p - \rho_m)$. As a natural result of this; the sedimentation rate is zero when the density of the particle is equal to the density of the liquid medium.
- The sedimentation rate decreases as the viscosity, μ , of the liquid medium increases.
- The sedimentation rate increases as the force field (g) increases.

The force field relative to the earth's gravitational field (Relative Centrifugal Force-RCF) exerted during centrifugation is defined by the Eqn. 1.6;

$$RCF = \frac{\omega^2 r}{9.81} \quad [m/s^2] \quad (1.6)$$

where r is the distance between the particle and the center of rotation in m; the rotor speed ω in rad/s can be calculated from the Eqn. 1.7 (where N represents the rotor rate, in rpm):

$$\omega = N \frac{2\pi}{60} = N \times 0.10472 \quad [rad/s] \quad (1.7)$$

Relative centrifugal force expression in Eqn. 1.6 is simply replaced with the gravitational force of the earth in the Stokes' Law to yield the theoretical minimum diameter calculation utilized to assess centrifuge performance of particle sedimentation. The mathematical justification of relative centrifugal forces has concerned many field engineers and researchers since the method was first introduced (as in Ambler, 1959). A considerable amount of valuable quantitative information can be obtained by applying some of these equations to data from experiments done in various centrifuges (Triebel, 2007). Also, the computational methods being developed and applied to many problems in the recent years opened a new possibility to model, assess and scale-up these machineries. Built-in models to determine particle behavior inside separation field made possible by considering Eulerian-Lagrangian algorithms and contact models such as Hertzian contact model (Hertz, 1882 and a relatively recent study; Tsuji, Tanaka, and Ishida, 1992).

Also, worth to note that inevitably involved due to motion on a body rotating along an axis at dramatic angular velocities, is the Coriolis effect. Due to centrifugal force, particles first shot near the inner circle of disk are dispersed along the radius. Although, as the tangential velocity increases along the radius of disk, the Coriolis effect forces the particles to fall 'behind' as they approach the outer circle of disk, where the highest relative tangential velocity occurs (Fig. 1.2).

The combined outcome of centrifugal force and the Coriolis effect contributes to the utilization and work of principle of disk-stack centrifugal separators: the particles are driven away outward through the disk radius and in the meantime toward the rib on the opposite side of the direction of rotation. The Coriolis effect also justifies the existence of ribs on the disk, along with the interval adjustment.

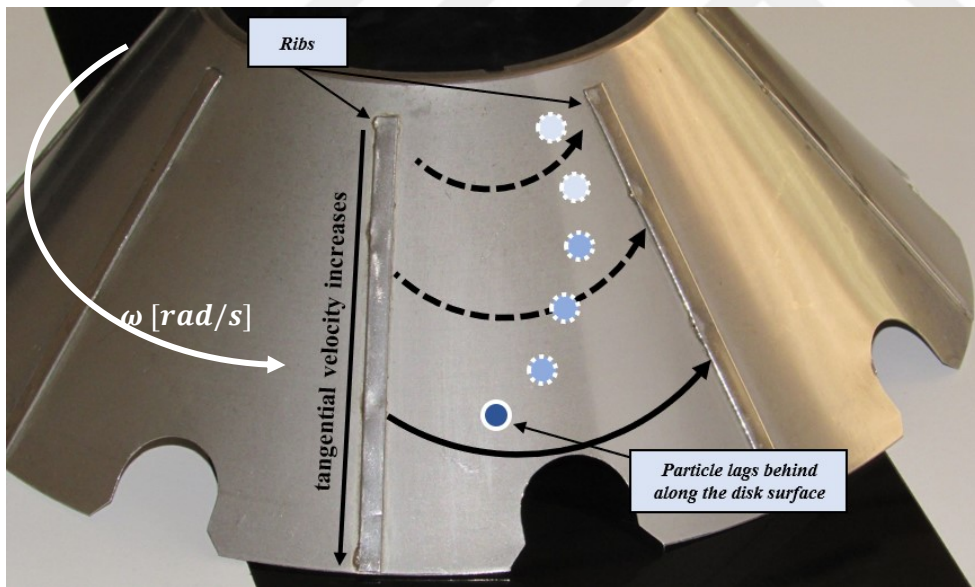


Figure 1.2. A still representation of Coriolis effect during particle sedimentation on centrifuge, when the disk is rotated counter-clockwise.

1.2. Filtration and Centrifugation

Before start discussing the solid-bowl centrifugal separators, it is important to underline a principal of application in mechanical separation processes: filtration vs. centrifugation. Traditional centrifugation, which is conducted with solid-bowl centrifugal separators, is explicitly utilized to separate ‘suspended’ solids from within the continuous medium. In other words, a solid-bowl centrifugal separator cannot separate dissolved solids. In addition to that, a solid-bowl centrifuge requires a density difference between the continuous fluid and suspended solids. In its principle operation, heavier particles, when exposed to drastic centripetal forces, drift along the radius of settler and sediment against the walls of solid bowl. This principle also applies in any static tank, subjected only to Earth’s gravitational pull; only in centrifugation, the gravity is replaced and extremely magnified by rotation around an axis Fig. 1.3.

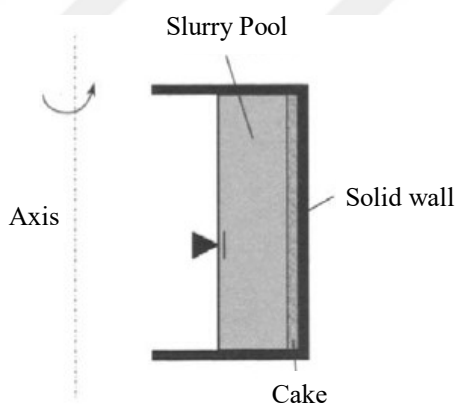


Figure 1.3. Solid-bowl centrifuge (Leung, 2007).

In a filtering centrifuge, on the other hand, not even the density difference between the phases is necessary. The operation involves a meshed structure (filter) the porous characteristics of which can be intricately adjusted to the properties of multi-component fluid. The components are driven through the filter, again, by means of centrifugal forces.

Filtering a multi-component fluid is the only practical way of mechanically separating dissolved particles from a continuous liquid: particles coarser than the filter openings are confined inside the mesh while liquid phase(s) pass through the structure (Fig. 1.4), later to be discharged from the system, in a batch or continuous

process. To summarize, solid-bowl centrifuges rely on density difference between components in a suspension which is not a constraint in filtering centrifuges. Although this appears to be a drawback in day-to-day applications involving centrifugation, the solid-bowl centrifuges have the ability of sedimenting particles of any size without changing any moving part or assembly *during* operation, as long as there is a significant density difference between the continuous liquid and particles.

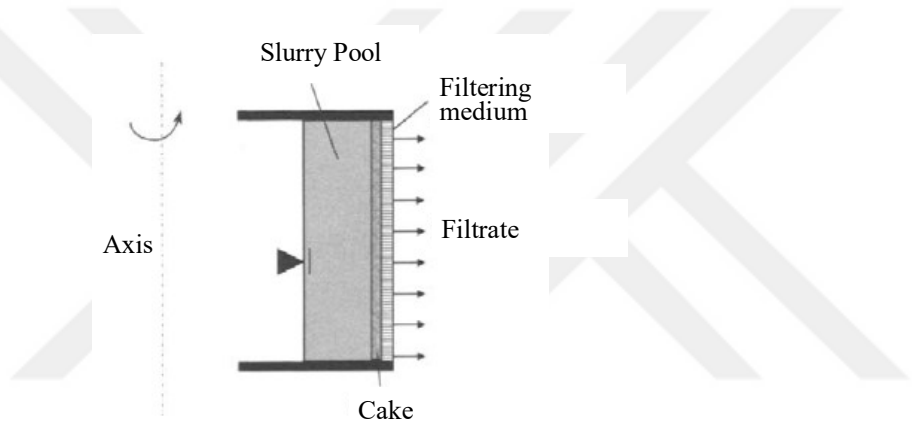


Figure 1.4. Filter (screen) bowl centrifuge (Leung, 2007).

1.2.1. Filtering Centrifuge

A typical filtering centrifuge, similar to solid-bowl centrifuges, is capable to perform operations other than filtering solid particles such as wash-cleaning and deliquoring. These operations can be performed both in a batch or a continuous process. Regardless of the volume of batch, the filtering centrifuge is charged with product and operates the medium through different processes expressed above. Small-batch centrifuges involve spin-tube, basket types while peeling and siphoning filter centrifuges handle larger batch sizes. Centrifuges commonly known as screenbowl and pusher (Fig.1.5) are the examples of continuous process filter centrifuges.



Figure 1.5. A filtering centrifuge with horizontal bowl for pharmaceutical applications. (Heinkel Drying and Separation Group, 2019)

Suspension (or ‘sludge’) is fed continuously into a screenbowl centrifuge, where supernatant is also continuously extracted from the system. Suspension, comprised of organic or inorganic components, cannot be discharged in a continuous manner and after a time depending on the particulate nature of suspension, starts to occupy in the porous environment. As the filter is clogged up, both time and the efficiency of filtration process are affected negatively, after a point which the filter is required to be extracted and cleaned or replaced. As mentioned above, particle size variance is another issue with filter-centrifuges. Suspended components must be greater than filter openings by a safe proportion, which in most cases limits the minimum particle diameter can be extracted from the medium to be larger than $1\mu\text{m}$ (Concha A., 2014).

1.2.2. Sedimenting (Solid Bowl) Centrifuge

Similar to filtering centrifuges, solid bowl centrifuges can be designed and operated both for batch and continuous process. Yet the majority of applications emphasize solid-bowl centrifuges ability to separate particles without any clogging problems in continuous operating and particle sizes of a very large scale that can be easily sedimented out. Batch processing solid bowl separators involve zonal centrifuges, spintubes and in a wide variety of applications, the ultracentrifuge family. Suspended solids forced to the solid walls of centrifuge and accumulate at this area (mostly a conical volume at a greater radius, for cleaning purposes). Solids removal is performed once the device is completely stopped.

Disk-stack centrifuges are the most common types of continuously operated solid-bowl centrifuges. Particle-laden medium is fed to the bowl volume, accelerated immediately to the angular velocity maintained, where particles, due to their higher density, forced outwards to the solid walls. Particles sedimented against a solid containing volume, where the sludge is discharged either at intervals (drop-bottom) or continuously as in a nozzle-centrifuge (Fig. 1.6). Unlike the decanter centrifuge, a disk-stack centrifuge operates on a dilute fluid.

In the context of this study, solid-bowl centrifuges, specifically disk-stack centrifugal separators are investigated in terms of mathematical models of performance evaluation and computational methods to assess and scale-up the devices with various physical and operational parameters. Since the process in the scope is milk clarifying (hence the medium is assumed to be ‘two-phase’) hermetic designs are not considered, as there is no foaming risk in particle sedimentation.

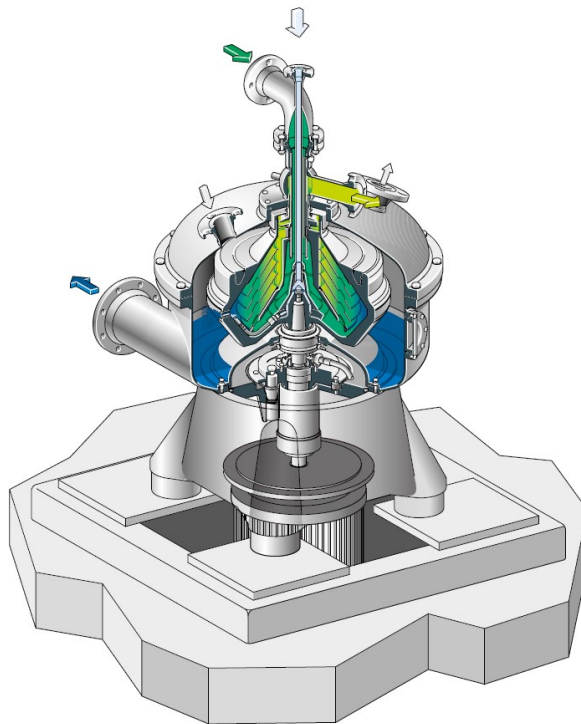


Figure 1.6. A see-through section of a nozzle centrifuge used in pharmaceutical applications (GEA Group Aktiengesellschaft 2019).

2. LITERATURE REVIEW

Particle-laden flows has always been a popular topic amongst mechanical, chemical, and food engineers, along with the overlapping studies including oilfield applications, mineral and edible oil industries, internal combustion etc. Prior studies usually tend to emphasize and understand the behavior of particles confined or suspended in a continuous fluid, say, beverage or water, in a pure mathematical way by employing principal physics. As mentioned before, Stokes' law was the first physical cornerstone ever to have been utilized toward explaining the sedimentation of particles suspended in a medium. That idea coined the terminal velocity concept into sedimentation of solid particles in a medium. For design, estimation and scale-up purposes, the preliminary research on the sedimentation phenomenon has been satisfactory. After all, the empirical equations are sturdy, especially when backed up with proper theory. Therefore, many product assessments by prominent manufacturers around the globe were earlier performed based on this de facto.

Although these well-established methods still linger and referred to frequently, the fact that a conventional centrifugal disk-stack separator is applied to a novel application regularly proves a more substantial design and performance estimation approach is rather critical. In this study, a mathematical method (backed by the experimental data, of course) has been developed to correspond this need. A CFD-DEM mainframe handles the configuration of product properties, separator geometry and operating conditions, and gives the best result as to estimate product performance of this particular multi-phase (particle-laden) fluid. Literature survey therefore commenced in the vicinity of this core to prevent losing our focus as the particle-laden flows are a vast chapter in fluid dynamics and general physics.

However fundamental, engineering applications of Stokes' law and terminal velocity concept are often nested with computational methods handled for specific problems. Many studies incline to solve sedimentation or transportation character of numerous particles in a continuous medium. Analytically solving force balances for many suspended particles, without computational methods, involve great verbosity, especially when total mass of discrete phase becomes dominant over continuous phase. Kartushinsky et al. (2016), inspected the terminal velocities of suspended particles in pipe flows with different characteristics. Implementing the model by using Eulerian schemes for both continuous medium and particles, flow

direction and mass concentration effects on particle distributions and axial velocities of both phases are investigated. The difference between the settling velocities of phases is observed to approach to zero, therefore an alternative drag force definition is suggested to regulate the axial component of momentum equation. In their study, Náraigh and Barros (2016) discussed the flow of a suspension through an inclined channel. By applying a pressure drop throughout the channel and sustaining a laminar-steady state flow, gravitational/inertial effects on the suspension is investigated. A novel diffuse-flux model is suggested to admit the particle properties better into the modeling equations and allow for a more detailed parameter study on Stokes' force balance in inclined channels. The study shows a resemblance to the current study, since two-dimensional handling of any disk-stack settler will amount to a laminar-fully developed flow of a suspension, exposed to gravitational forces and pressure gradient (Poiseuille flow). Also Akbarzadeh and Hrymak (2016) investigated both the solid-solid and solid-liquid interaction in a rectangular duct with Poiseuille and Couette formulated flows. Handling particle collision equations, hydrodynamic, thermophoretic forces within a two-way coupling scheme. Particle residence times are investigated when both phases have close length scales, i.e. with unit Reynolds and Stokes numbers. A specific bend in duct geometry is used to observe settling times of particles around the radius which turned out to be longer than that of flat surfaces.

Calculating the force equilibrium in particle-fluid interactions through Euler-Lagrange coupling is a popular method in particle-laden flow investigations, as long as mesh-bonded methods are preferred for solution mainframe. A Euler-Lagrange coupling suggests two distinct solution algorithms for each parties of a particle-laden flow analysis. In Eulerian specification, the flow field is handled as a fixed region and every point in that region is solved simultaneously as the time advances. In Lagrangian specification on the other hand, only a portion or a fraction of this flow field, which contains the particle, is considered, and the physical properties of this unitary element are solved as it moves through flow field and in time (Fig. 2.1).

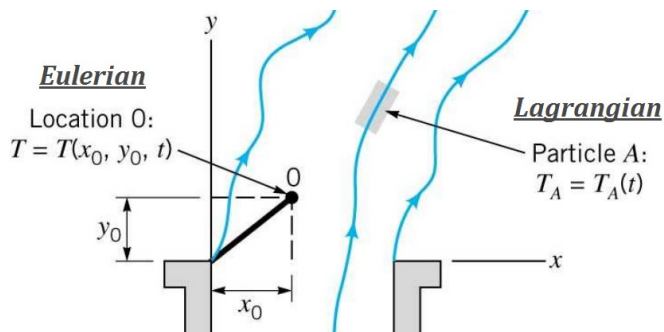


Figure 2.1. A visualization of the two flow field definition approaches; Eulerian (left) and Lagrangian frame of references (Università Di Pavia, Physics Department, 2019).

In Euler-Lagrange methods, a finite element in a flow regime represents both the continuous fluid and the discrete element, unlike mesh-free methods (as in Liu and Liu, 2010; Monaghan, 2005; Ndimande, Cleary, Mainza, and Sinnott, 2019). In other words, despite they are ‘followed’ with their own coordinate frames, particles do not occupy a number of finite elements. Their physical properties are calculated as they passed through the mesh, which is spread over the flow regime (Eulerian Frame of Reference). This generalized character of the approach encouraged many researchers in the field of fluid dynamics in time to simulate a variety of physical phenomena through computational methods. During the survey, studies treating Euler and Lagrange approaches separately, instead of a coupling were also encountered: Zhang and Chen (2007) investigated the two modeling methods to predict particle behavior in ventilated environments in their study. To handle the workload of continuous medium, the Standard $k-\epsilon$ turbulence model is utilized. First Eulerian, then Lagrangian particle tracking results obtained, then compared with experimental data. Although compelling in terms of computational demand, the Lagrangian method proved to be better in transient conditions due to superior accuracy, the Eulerian particle tracking displayed competitive success in steady-state scheme. In a similar study, Saidi et al. (2014) investigated the scatter, settling and accumulation behavior of particles in gaseous phase during inhalation process and through lung alveoli. Eulerian and Lagrangian schemes are approached separately, then their results are compared to find the most effective option to represent a hypothetical situation, instead of an experimental one. In the first scenario, segregation of particles, initially stationed homogeneously on a horizontal plane is modeled with a pressure difference applied to encourage the particle dispersion. In the second scenario, the Eulerian and Lagrangian approaches utilized separately to model airflow between the two parallel plates where a parabolic

velocity profile is applied. Particle concentrations generated by the two methods are compared. This scenario resulted in a significant variety in particle fates, calculated by the two methods: Euler and Lagrange schemes deviated in results, considerably. It is emphasized that substituting Lagrangian approach for its Eulerian counterpart cannot guarantee the reliable results in low concentration cases (also in Thunman et al., 2002). In the last scenario, particle-laden flow in lung alveoli is investigated. The two methods again tested for a 3-D realistic model of lung bifurcation with increasing (so that, the disperse phase becomes 'dense' phase) number of particles. As expected, with the number, hence the mass of discrete elements rises, the results of Eulerian approach 'converge' with those of Lagrangian methods, therefore one method can compensate for the other. Still, the Lagrangian method generates a more convincing result for particle dispersion and segregation.

The results gathered from Eulerian and Lagrangian schemes, when they are used separately for different problem definitions show more or less deviation, depending on the initial, and boundary conditions, as well as the density of discrete phase simulated. As mentioned above, this deviation is minimized when the discrete phase density increases. In many cases though, the particulate phase is scarce when compared to continuous medium; a state where the Lagrangian approach becomes prominent. In applications such as Arsalanloo and Abbasalizadeh (2017) suggested, the Eulerian algorithm is utilized to simulate the continuous fluid where the Lagrangian method handles the particulate phase simultaneously to harness the competence of Euler-Lagrange coupling. In their study, particle segregation and deposition in a bent pipe geometry, exposed to swirling flow. The Eulerian continuous phase solver utilizes a Reynolds Stress Equation model, a choice which makes the study significant as a classic modification of k- ϵ model was not preferred. Instead of a moving reference frame (MRF), the swirl feature is generated using spiral vanes. Particle deposition is discussed by reporting the particle Stokes number. Results show the Lagrangian approach deliver a reliable base for particle behavior in both aspects investigated in the study: the effects of vanes' heights on the swirl generated and particle dispersion and larger particles, having greater Stokes numbers, have better predictability when compared to smaller particles.

Euler-Lagrange coupling can be extended to inspect also heat transfer phenomena within particle laden flows. Towards this scenario, Maskaniyan, Rashidi, and Esfahani (2017) in their paper investigated the discrete characteristics of Al_2O_3 particles in a channel, equipped with a feature with elevated temperatures. Particle

sizes are limited to 30-500nm interval whereas volume fractions are adjusted to deliver a disperse phase simulation. The effects of forces in a two-way coupling of particles and continuous medium involving Brownian and thermophoresis forces where a laminar flow enforced (with $Re \leq 100$). It is found –yet arguably that the nanometer scale particles do not follow the continuous fluid’s streamlines, but instead diffuse across the streamlines. An increase in the deposition inclination of particles with increasing particle size is also emphasized. Also in a recent study of Chang et al. (2019), a 3-D simulation of particle settlement in inclined vessels by implementing an Euler-Lagrange coupling is presented. It is shown that the occurrence of turbulence through the vessels actively reduce the settling behavior of discrete particles where particle size, hence particle inertia becomes significant on a particles fate. Larger diameter-better settling behavior encourages many different applications where Euler-Lagrange coupling will thrive. The study also states that, the best angle of inclination for particle suspension can be calculated through simulations where dissipation of potential energy becomes a decisive parameter.

Solid bowl centrifuge applications of particle-laden flow modeling are difficult to come across. Available studies involving a disk-stack centrifuge are either lack of detailed modeling and validation research, or limited to experimental results, rather than CFD-DEM simulation of the sedimentation process. Studies subsequent to Ambler (1959) offer more or less the same theoretical concept to estimate the minimum particle sizes; a concept that comes arguably with heavy assumptions and oversimplification of process. Kempken, Preissmann, and Berthold (1995) in their study, considered a Westfalia prototype disk-stack centrifuge and tested it to inspect the mammalian cell sedimentation ability. Experiments were conducted via cell counting and comparison of examples from inlet and outlet streamlines of machinery. Analyses give insight at a certain extent, due to filtration capacity of device utilized to determine the particle sizes on both streams which, as implied in the study, is reliable between 1-5 μm . Above the measurement limit, however, the centrifuge establishes a basis regarding the particle sedimentation ability: larger particles having exposed to greater inertial forces and therefore more easily sedimented against the centrifugal forces applied by the machine, as seen on Fig. 2.2.

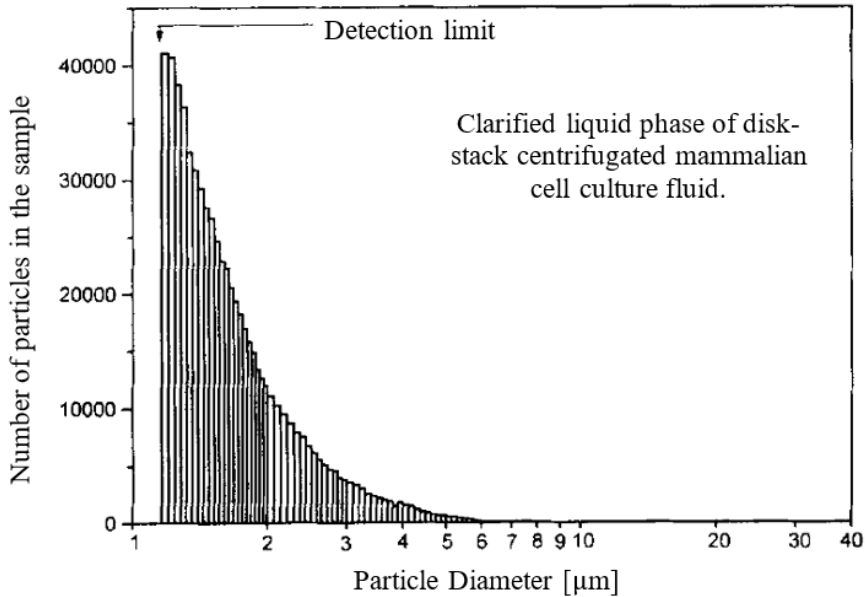


Figure 2.2. Outlet example histogram of solid-bowl centrifuge (Kempken et al., 1995).

Despite Kempken paper did not suggest any mathematical mainframe, it represents one of the stepping stones of this thesis study in terms of centrifuges reliability in particle size-sedimentation rate behavior. One of the first direct approaches to centrifugal settlers via CFD-DEM modeling was given in the study of Lindner, Menzel, and Nirschl (2013). Without revealing the specifics about the CFD-DEM algorithm or the particle-laden flow characteristics, several numerical studies using water and air as continuous media are investigated for a solid bowl centrifuge. A two-way turbulence coupling is implemented to discuss about the particles' effect on the continuous media. Instead of running the Lagrangian equations on a pseudo-transient scheme, the researchers prefer to perform simulations on a completely transient model.

While a two-phase of continuous medium suggests Volume of Fluid (VoF) model in ANSYS Fluent, the researchers also considered contact modeling of discrete particles (Hertz, 1882). Although the centrifuge model utilized is adopted only for simulation purposes (Fig. 2.3) and a Euler-Lagrange scheme is not openly suggested, the paper still has its unique place among other studies considered. This kind of modeling of a centrifugal system however, misses the elusive nature of sedimentation in terms of computational methods.

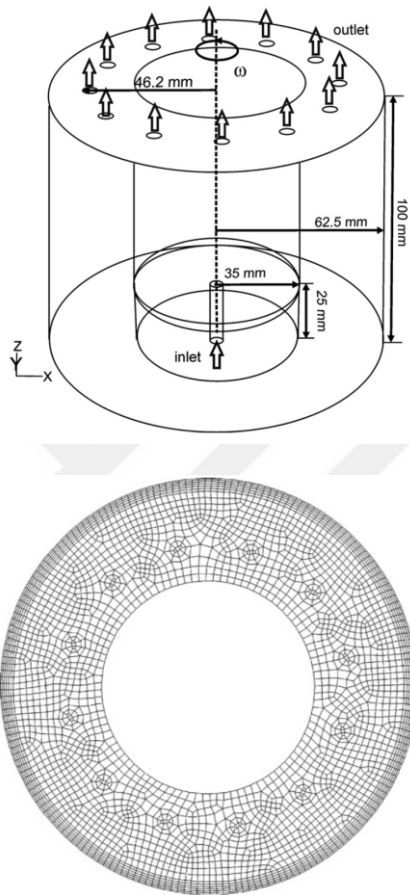


Figure 2.3. Cylinder flow region of the tubular bowl centrifuge (above) and mesh structure in a cross-section view in Lindner et al. (2013).

In some applications of disk-stack centrifuges, the discrete particles represent the valuable substance, instead of continuous medium. In their study, Shekhawat et al. (2018) investigated the separation performance and production of Therapeutic Monoclonal Antibodies (mAb's). In regular clarifying applications, the fate of the sedimented particles are not considered. Although when it comes to 'harvest' cells from inside the fluid region, cells viability against abrupt centrifugal field becomes the most important constraint. An Eulerian-Eulerian model is implemented where the researchers used Gidaspow drag model (Gidaspow, 2012) to better realize the stresses generated on the particles. A standard $k-\varepsilon$ model is selected to simulate the continuous medium. The study offers an empirical approach and to relate the theoretical cell break-up rate to turbulence effects due to centrifugal forces.

Employing a 3-D simplified model of an actual disk-stack centrifugal separator for the simulations, the paper in terms of this thesis study, offers a couple of important outputs:

- The average particle size for somatic cells which is $16.5\ \mu\text{m}$, was adopted from this study; along with Zlotnik's publication (Zlotnik, 2012).
- Model simplification by reducing the number of disks and taking only the separation volume between two subsequent ribs on a disk (that is, the '45° model').

Although reducing the number of disks without reducing the total volume of the centrifuge (Fig. 2.4) seems inconvenient, the study puts forward a good compromise between simplification and realistic simulation.

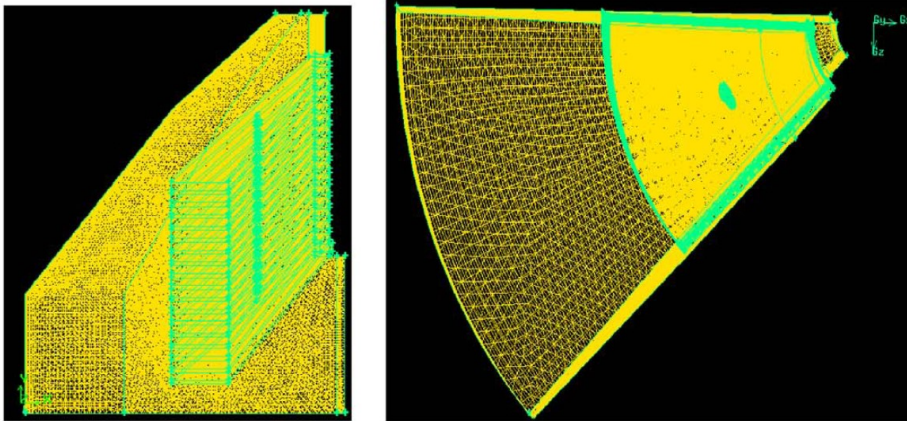


Figure 2.4. One-eighth (45°) centrifuge modeling (Shekhawat et al., 2018).

Bovine milk and milk properties became an inevitable part of this study as the centrifuge to be investigated in terms of CFD-DEM modeling and Euler-Lagrange multiphase approach is originally a milk clarifying machine. In milk clarifying, one specific type of discrete element is discussed in detail: the somatic cells. Somatic cell count of a specimen gives clues about milk quality as well as herd health as dairy compounds admit milk from different farms in large batches (Aytekin and Boztepe, 2017). Perhaps the most important information acquired through the somatic cell count (or 'index') is the mastitis, an infectious disease which is the one of the most common causes of profit losses in dairy industry (Melo, Gomes, Baccili, Almeida, and Lima, 2015).

Containing lipolytic and proteolytic enzymes, somatic cells (dominantly white blood cells, otherwise known as 'leukocytes' or 'leucocytes') help the animal fight back mastitis. Therefore, the production of somatic cells in cow's udder increases as the disease advances. However, the very same enzymes also destroy milk fat and proteins. This simple mechanism of nature becomes the most effective way of detecting the Mastitis and taking the measures to increase herd health and milk yield of a farm. One of the first in-depth investigations of the bovine milk in terms of solid-organic contents was published by Zlotnik in 1947. Detailing the somatic cell (pseudo-polymorphs) content and delivering a range for the group, that is 6-20 μm , this study established a basis for several publications to follow (such as in recent studies of Dosogne et al. (2010), Li et al. (2014), Rola et al., (2014) and van Reis et al. (1991).

Status quo on particle-laden flows, as seen on above examples, involves studies on a wide variety. Along with any scenario where solid particles are confined in a continuous medium; liquid 'acting' like a discrete phase (water vapor or spray corpuscles, flue gasses, wet granular flows etc.) within continuous medium can also be modeled with ease. The number of published studies, however, reduces to only a few when particle-laden flow in a solid bowl separator is in question. In this study, we focus on this very topic, hopefully surpassing the level of detail of previous literature via improved methodology and proper utilization of computational abilities of contemporary hardware. It is important to note that, introducing novel applications every now and then, the centrifugal separation can provide promising research on the plane where computational methods and experiment can cooperate.

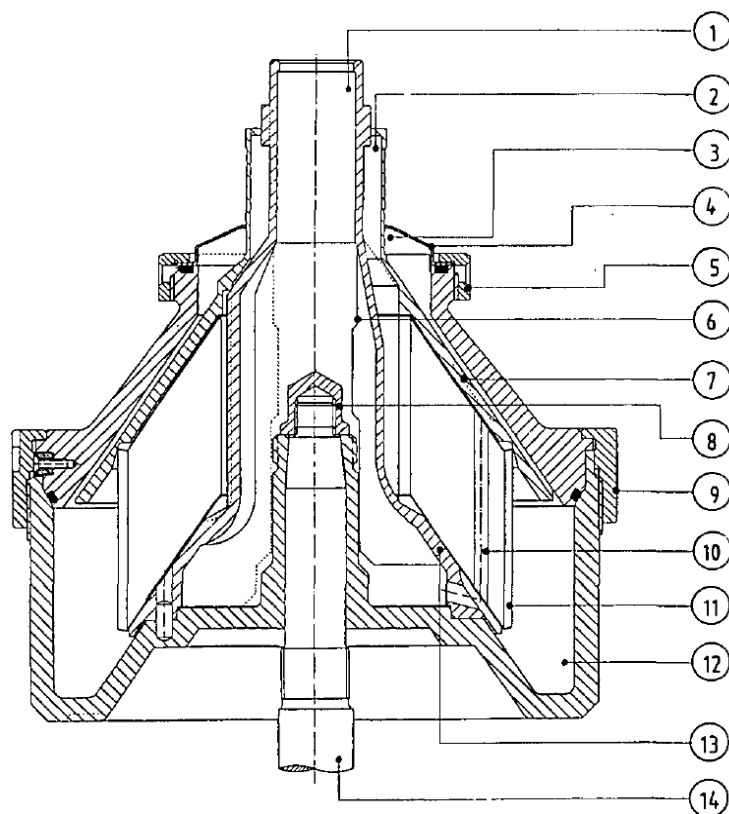
3. MATERIAL AND METHOD

3.1. General Configuration and Operation Principles

Disk-stack centrifugal separators continuously sediment particles against the solid containing portion of bowl volume, as a common procedure. Distinction between the particular types of disk-stack centrifuges appear in the way how the solids later ejected from the bowl volume. Two major applications are available as to solids discharge: nozzle and drop-bottom centrifuges.

In nozzle separators, particles are discharged from inside the separation volume, as soon as they reach the outermost radius of bowl where nozzles are located at intervals, removing particles continuously, along with a small ratio of liquid phase. The alternative design involves an intricate hydraulic system with a translational bottom part and a fixed upper part Fig. 3.1. The bowl is comprised of two parts, where bottom part is 'dropped' by means of hydraulic triggering, allowing sedimented solids to discharge with a portion of fluid. The applicability of a drop-bottom centrifuge to any particle-laden flow however, heavily depends on the particle fluidity and plasticity, since they must be able to move through the opening without smearing to surfaces.

In drop-bottom disk-stack centrifuges, the intervals at which the sedimented solids are discharged from the separation volume is determined by the mass concentration of the discrete phase. As mentioned before, the nature of discrete (disperse) phase depends on the medium. When liquid clarification involves the bovine milk sediments (in this study, somatic cells and cell debris), experimental results show a 10-min interval proved to be sufficient in most of the applications. Analyses performed in the scope of this study assumes the same durations while calculating cell stagnation and settling percentages, hence the centrifuge performance. The main parts of a generic centrifugal separator are given in Fig.3.1.



- | | |
|-----------------------|-------------------------|
| 1. Feed entrance | 8. Top nut |
| 2. Light phase outlet | 9. Lock ring |
| 3. Heavy phase outlet | 10. Interphase channel |
| 4. Gravity disk | 11. Disk-stack |
| 5. Lock ring | 12. Solid holding space |
| 6. Axial rib | 13. Distributor |
| 7. Top disk | 14. Spindle |

Figure 3.1. A generic solid-bowl centrifuge cross section view with main parts (van der Linden, 1987).

Once introduced through feed entrance, the medium reaches to the distributor, a precision-cast disk with several openings located around its periphery. The number of openings on distributor must be equal to the number of ribs on disks (Fig.3.2) Distributor also carries the disk-stack through indentations, canceling possible relative movement of disks. When reached to the distributor, medium immediately accelerates to the bowl speed.

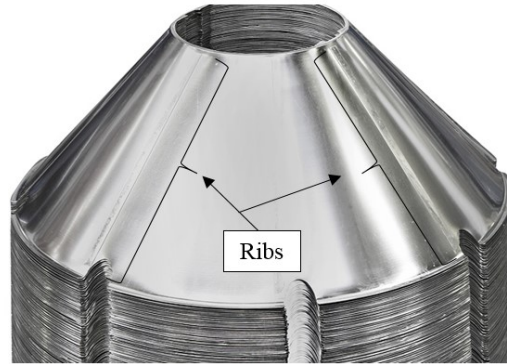


Figure 3.2. Rib assembly on a typical disk stack (distributor is not shown) (Flottweg Separation Technologies, 2019).

Disks act as a filtering element, reducing the relative velocity throughout the channels to provide a laminar flow region. Dense particles are thrown outwards and the majority settled quickly against the solid wall. Some particles arbitrarily escape through the disk-stack, later to be forced outwards against lower density fluid-flow. Several particles still can beat the drastic centrifugal forces and escaped through clarified phase outlet. Bowl assembly is set and locked on to the spindle which is driven by electric motor. Direct (via gearbox) and belt transmission systems are available in different applications (van der Linden, 1987).

3.1.1. Paring Disk

In the centrifugal separator, the clarified liquid (milk, in this study) is extracted from the bowl volume by a special accessory called the paring disk. When also a liquid-liquid separation is necessary (as in cream and skim-milk separation), two, instead of one paring disks are assembled. Paring disk utilization is a very common application so that some of the manufacturers called their disk-stack centrifuges 'paring disk' centrifuges. Paring disk, in form and analogy, is a centrifugal pump impeller. Only in a rotating bowl, paring disk becomes a stationary part, plunged into the separation volume, splitting columns of continuous medium at certain proportions. Through the paring disk, the kinetic energy of continuous medium is translated into pressure, which creates a pressure balance between the pressure inside the bowl and pressure lost in the peripheral piping. When downstream of machinery is throttled down, the pressure inside the bowl is balanced out instantly, thanks to paring disk Fig.3.3. In this study, pressure outlet of the milk clarifying centrifugal separator is maintained at 2.2 Bar for testing and validation purposes.

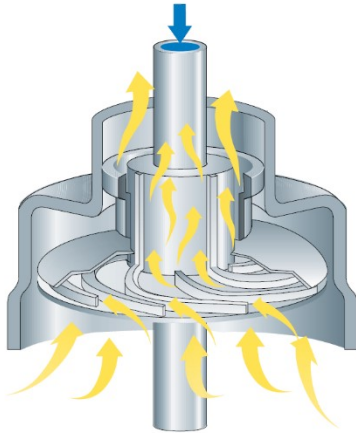


Figure 3.3. A typical paring disk to separate either one of the liquid phases (Bylund and Svensson, 1995).

3.2. Performance Evaluation of Centrifuges by Classic Methods

Centrifugal separators are designed and developed considering a specific product, a suspension or emulsion, containing a certain set of insoluble particles and operation requirements such as throughput rate and downstream pressure values (Baccioni and Peri, 2014). In design phases, manufacturers often refer to rule-of-thumb constraints, experience and some empirical factors far from being convenient. Inverse engineering is also an aspect when designing a new product to operate on a specific medium. Mathematical formulae based on some principal concepts of fluid dynamics, also one of the features of this thesis study, is a prominent source material as to estimate a centrifuges ability to sediment particles. These formulae (Ambler, 1959; Leung, 2007), although rely on heavy assumptions and oversimplification in flow and particle characteristics, provide an insight before an actual investment on a specific centrifuge is realized.

Violent centrifugal forces (3,000~10,000g) combined with drag forces and Coriolis Effect form a very complex flow region for both continuous medium and discrete particles. The formulae, on the other hand, implies there is a laminar flow regime between every subsequent pair of disks, where the magnitude of flow divided into equal portions and sedimentation is conducted in a mild environment. This approach was first coined by a Sharples Corp. engineer, Charles M. Ambler in his publication of 1959. Emphasizing the similarities between a centrifugal settler device and a common settling tank exposed only to the Earth's gravity, the study lied the foundations of what centrifuge manufacturers called 'the Sigma Concept' today.

The Sigma number is specific to a centrifuge and it reveals the equivalent ‘area’ of a settling tank (or pond) if the settling tank was exposed to gravitational field that the centrifuge is exposed. As the definition states, the Sigma concept can apply to every solid-bowl centrifuge settler; decanter centrifuge (a horizontal settler with a helix-shaped conveyor instead of disk-stack; more suitable for sludge or slurry medium) or centrifugal separator.

Along with the Sigma concept, formulae depending on the Stokes’ Velocity also generate the minimum particle size (or diameter; since particles are explicitly assumed to be spherical in nature) which is another important input of centrifuge scale-up. Although several studies following Ambler’s publication came up with alternative forms of these two calculations, the results these formulae generate fall within a rather narrow range. Yet the two prominent examples of centrifuge assessment next to Ambler’s calculation are investigated in this thesis study.

Although the calculation methods can give an insight on the minimum particle size can be sedimented under certain geometrical (disk half-angle, inner and outer radii etc.) and process features, no calculation method estimates the ratios at which the minimum diameter particle can be sedimented out. That fact becomes another constraint for performance evaluation and scale-up studies. This thesis study benefits from the computational capacity of modern computers, combined with a Computer Associated Engineering (CAE) program, ANSYS Fluent to better implement the sedimentation process of raw milk particles. Reducing the assumptions originally made by prior methods and studies and harvesting the data calculated by modern numerical methods are planned to be the novelties of this study.

3.3. Equivalent Surface Area for Disk-Stack Centrifuge

The sigma value Σ (Eqn. 3.1) is equivalent surface area (m^2) of any centrifugal settler to the area of a conventional settling tank, exposed to unit gravitational field, the magnitude of which is ‘1 x g’ (Records and Sutherland, 2007):

$$Q = 2\theta_g \Sigma \quad [m^3/s] \quad (3.1)$$

where Q is the total throughput rate of centrifugal settler device, with the Stokes’ terminal velocity for a particle of diameter, d (Eqn 3.2):

$$\vartheta_g = \frac{\Delta\rho g d^2}{18\mu} \quad [m/s] \quad (3.2)$$

where $\Delta\rho$ is the density difference between particles and the continuous medium and μ is the dynamic viscosity of continuous medium. The sigma (Σ) value for a disk-stack centrifuge then becomes (Eqn. 3.3):

$$\Sigma = \frac{2\pi n \omega^2 (r_2^3 - r_1^3)}{3g \tan\theta} \quad [m^2] \quad (3.3)$$

where n represents the total number of disks utilized (Fig.3.4). Notice as the Sigma calculation in Eqn. 3.3, when substituted into Eqn. 3.2 and rearranged; becomes minimum (or cut-off) particle diameter formula:

$$d_{min} = \frac{3.67}{\sqrt{\pi}} \sqrt{\frac{\mu \cdot \tan\theta}{\Delta\rho \cdot n \cdot \omega^2 \cdot (r_2^3 - r_1^3)}} \quad [m] \quad (3.4)$$

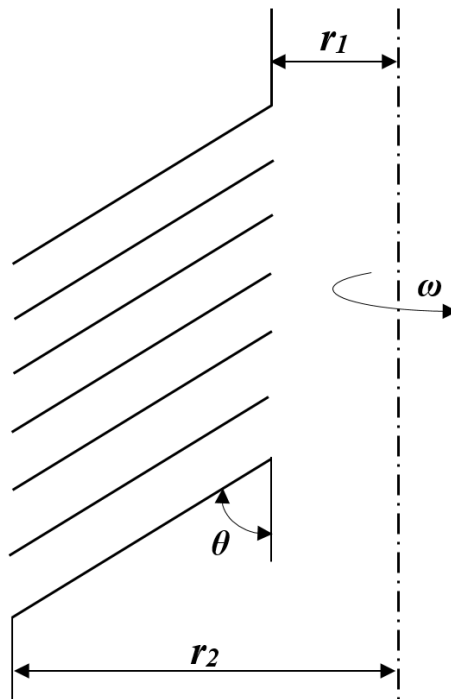


Figure 3.4. Schematic of disk-stack for cutoff diameter calculation (van der Linden, 1987).

3.4. Milk and Milk Properties

3.4.1. The Bovine Milk

Milk is indispensable for young mammals first years of its life. Not only the nutrients required for growth and energy, milk also contains material to protect calf from infections and support its immune system. A calf requires at least 1,000 liters milk for proper growth and the cow needs to produce this amount for each calf. As an inevitable side effect of domestication of dairy mammals, this figure increased remarkably in the course of millennia: while specific breeds of dairy cows can produce 6,000 liters per calf, extreme examples show they can yield up to 14,000 liters per calf. A heifer cannot reach sexual maturity until around 15 months of old. Also accounting the gestation period for these animals which is about 300 days; a cow starts producing milk at least 2 years. The average life of a dairy cow varies between 4-6 years. Since cows can give birth every year, total milk yield of a cow throughout her life span falls between 10,000-20,000 liters (Spreer, 2017).

Cow's udder is a hemisphere with two separate divisions. Each half is also divided in two smaller creases, each one having one teat. This allows cow to theoretically produce four qualities of milk. Crease structure and alveoli detail can be seen on Fig. 3.5. It is important to note that blood flow through the udder reaches up to 90,000 liters per day; it takes about 800 liters of blood to make one liter of milk.

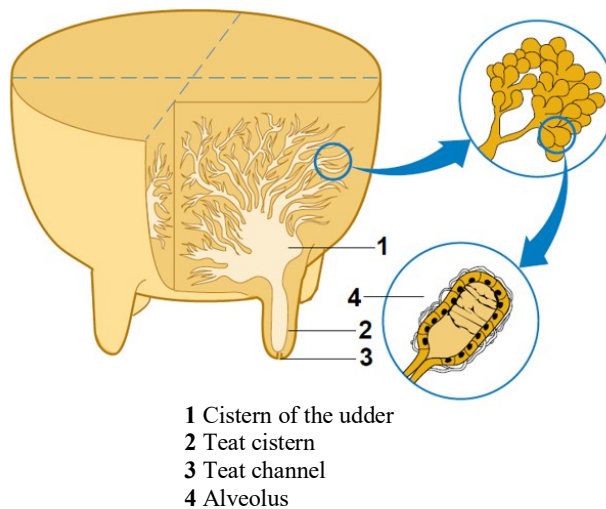


Figure 3.5. Main form and departments of cow's udder (Jelen, 2000).

Milking can be a highly automated process at the expense of proper investment (Fig. 3.6). Parlor design, implementation and automation has been investigated by many companies and researchers in detail (Reinemann, 2013). Although many dairy farms today still prefer hand milking, as it has done for thousands of years. Allowing mother to feed her calf first is essential, as separating the calf may cause frustration during milking. Contemporary breeds of dairy mammals produce large amounts of milk enough to feed calf and in the same time, for commercial use.

A dairy is mostly a local compound, collecting daily milk from farms in its precinct. Depending on a farms output, milk can be delivered to dairy compound in churns holding 30-50 liters of milk, or it can be transported via trucks with refrigerating trailers. Strainers are utilized to separate very coarse sediments, animal hair or skin, whether manually when milk is delivered in churns, or through in-line fittings during mass loading (Park and Haenlein, 2013). As an organic substance, milk is prone to spoil by micro-organisms rapidly unless properly chilled following milking. The micro-organisms in milk structure are very active above room temperature and their rate of multiplication becomes violent at around 35°C. The product therefore chilled to 4°C right after it leaves cow's udder and kept at this temperature which minimizes the micro-activity inside medium (Bylund and Svensson, 1995).



Figure 3.6. A parallel tandem milking parlor in a dairy farm (Microdairy, 2019).

3.4.2. The Composition and Characteristics of Bovine Milk

Bovine milk is a pure substance, denser and more viscous (around three times more viscous when compared to water with 3.003×10^{-3} Pa.s) with a slightly yellowish white color. Under proper conditions, it has a characteristic, sweet taste, a mellow odor and a soft texture without any flocculation. Processed milk is a principal ingredient in dairy products family including some of the traditional desserts (Kilara, 2011). Dairy-derived materials for use in food processing originate from milk.

When qualified in a chemical-physical perspective, milk is comprised of several components, each having typical concentrations within the matrix, such as fats, carbohydrates, proteins etc. and liquid phases, namely cream, whey and skim-milk. Phases can be separated in centrifugal separators if device allows for a secondary liquid phase extraction. Single-phase centrifugal separators are called ‘clarifiers’ and their use are confined to sedimentation of particles. Approximate fractions of components of raw milk structure are given in Table 3.1.

Table 3.1. Approximate composition of whole and skim milk solids (Spreer, 2017).

Component	Whole Milk Solids [%]	Skim Milk Solids [%]
Fat	29.36	1.08
Protein, casein	22.22	31.18
Whey protein	4.76	7.53
Lactose	38.10	52.15
Ash (minerals)	5.56	8.06

Organoleptic characteristics of milk changes during the lactation period of cow, which is around 300 days after the cow gives birth. The milk the cow produces in the first week following the birth is called ‘colostrum’, the traces of which can be found in 3~5 weeks milk. Colostral milk within the first week of lactation has not commercial value (Spreer, 2017). In addition to lactation period factors like breed of the cow, feeding habits and exercise of animal, milking season and intervals, age and current health strongly affect the milk character (Kilara, 2011).

3.4.3. Somatic Cell Count Effect on Quality of Raw Milk

Somatic Cell Count (**SCC**) is a measure of the white blood cells (leukocytes) in the milk structure and a quality assurance criterion accepted world-wide. Although allowed SCC in pasteurized milk varies depending on the regulations apply in different countries, 750,000 cells per milliliter (mL) is considered to be critical in terms of infectious diseases, most popularly mastitis. Increasing SCC values indicates poor herd health, and the process yield of every cultured product is reduced (Hagnestam-Nielsen et al., 2009). High quality milk, on the other hand, has SCC values typically less than 100,000 per mL. Heat-tolerant bacteria causing mastitis, such as staphylococci and streptococci, can be detected via dramatic increase in SCC values, reaching up millions, in some cases. Inflammatory response or an infected mammary quarter also cause SCC to rise and exceed allowable limits. Thus, an abnormal SCC is a good indicator inflammatory diseases or mastitis.

Elevated SCC's also suggests that milk flavor is affected negatively due to bacteria population, as stated previously. Healthy milk with proper chemical-physical structure should provide a cream-like appearance with smooth swallow texture. Bacteria can produce rancid flavors (acidic-salty or bitter) that immediately cause sickness when the milk is consumed.

For milk admission in dairy compounds, the Bulk Tank SCC (*BTSCC*) index can be utilized for a quality assurance mechanism. Examples are collected before admission of milk batch and analyzed. Milk then processed through a sedimenting centrifuge; in the majority of applications, a disk-stack centrifuge. Milk examples prior to admission and first clarification process is compared. Milk is admitted after satisfying BTSCC results obtained. Compounds perform tests from different farms continuously as a routine and avoid suppliers with constantly abnormal SCC counts in their products (Jayarao et al., 2010). A properly commissioned disk-stack centrifuge, however, is able to sediment 80%-95% of somatic cell content of milk, reducing the index below 100,000 cells/mL (Walstra et al., 1999).

3.5. Milk Processing Through Centrifugation

Sedimentation via centrifugation is a relatively new method. The application of process started with the invention of centrifugal separator designed for milk-cream separation by Swedish engineer Gustaf de Laval, the first of which he successfully patented in 1894 (Fig. 3.7).

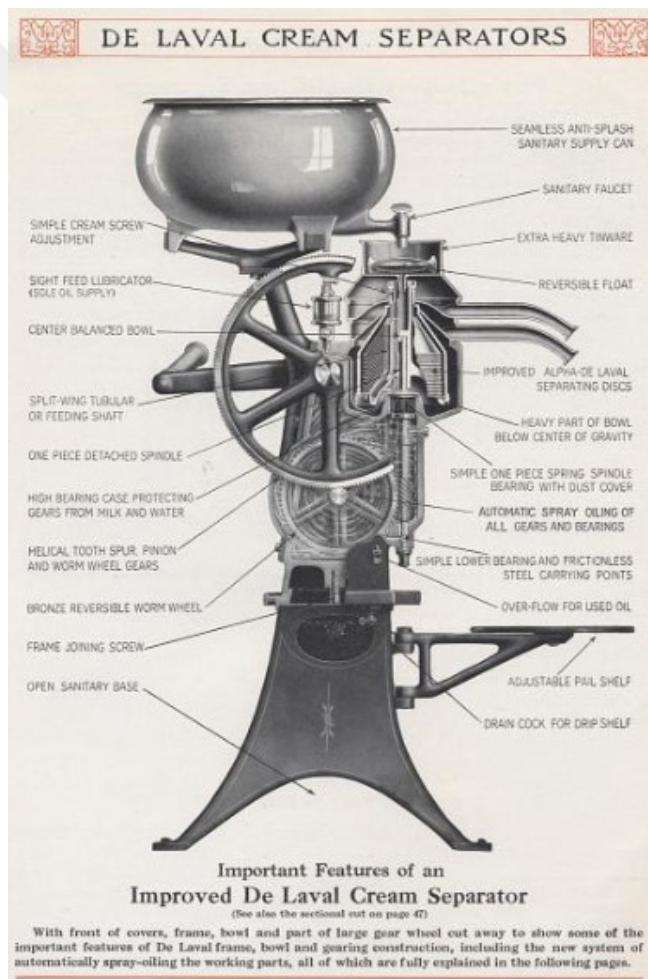


Figure 3.7. The 'state-of-the-art' Cream Separator by de Laval. Commercial brochure from Smithsonian archives (De Laval Separator Co. 1913. De Laval Cream Separators, Farm and Dairy Sizes, New York).

Prior to that invention, the sedimentation was conducted in stationary containers, against gravity, which was the only way as sedimentation by gravity took place anywhere and anytime. Clay particles moving in puddles will soon settle, leaving the water clear. Clouds of sand stirred up by waves or by the feet of bathers do the same. Oil that escapes into the sea is lighter than water, rises and forms oil slicks on the surface. Milk clarifying is no exception: milk transferred into a container right after lactation. When allowed to wait for a while, the fat globules accumulate on the surface open to air where they form a cream layer. This layer can be removed by a putty knife or even by hand. In the following titles however, sedimentation via centrifugation will be discussed.

3.5.1. Requirements for Sedimentation

When the problem is handled in mechanical engineering point of view, chemical-physical features of milk summarized previously become verbosity. In the scope of this study, milk is a pure substance with three 'phases', one of which is assumed to be continuous: skim milk. To specify further, the remaining liquid phase, fat globules, is assumed to be perfectly dissolved inside milk matrix. The remaining component of this system is particles, mainly comprised of udder cells, animal hair, small fractions of indigested straw, and finally, somatic cells (leukocytes).

A solid-bowl centrifuge cannot separate solids dissolved in continuous medium. Therefore, phases to be separated must not be soluble in each other. Centrifugation also cannot separate solution substances, as they can only be crystallized then be separated from the continuous medium. Although addition of crystallizers or flocculating additives are not in the context of this study. Also, the phases to be separated must come in different densities, specifically particles must have greater density, therefore higher gravity. In that, targeted particles in milk satisfy these conditions as they cannot be dissolved in milk and have a greater density (Bylund and Svensson, 1995).

When three-phase centrifugal separator utilized, fat globules inside milk can be separated at great ratios. Once skim-milk is obtained however, the cream can be introduced into milk, this time allowing for combination to be controlled, such as whole milk and 1%, 2% fat etc. This operation is called 'standardization'. Standardization process can be performed once the milk is admitted to the compound. In the admission stage, however, only two-phase centrifuges operated

to decimate BTSCC index. A typical milk example contains 1 kg of sediment for 10,000 liters. For somatic cells, this figure is far less: around 500,000~750,000 cells/ml.

Finally, temperature at which the separation will take place is also an important parameter. Separation of fat globules realized in relatively low temperatures (especially at storage temperature; 4°C) reduces the fat recovery performance. On the other hand, low temperatures assure higher viscosity, therefore increasing particle sedimentation performance of a clarifying centrifuge. This is another important reason why the milk goes through clarifying process at milk admission: milk transferred from the farm is maintained at storage temperature, best suited for reducing BTSCC, then admitted and heated up to further processed in standardization Fig. 3.8.

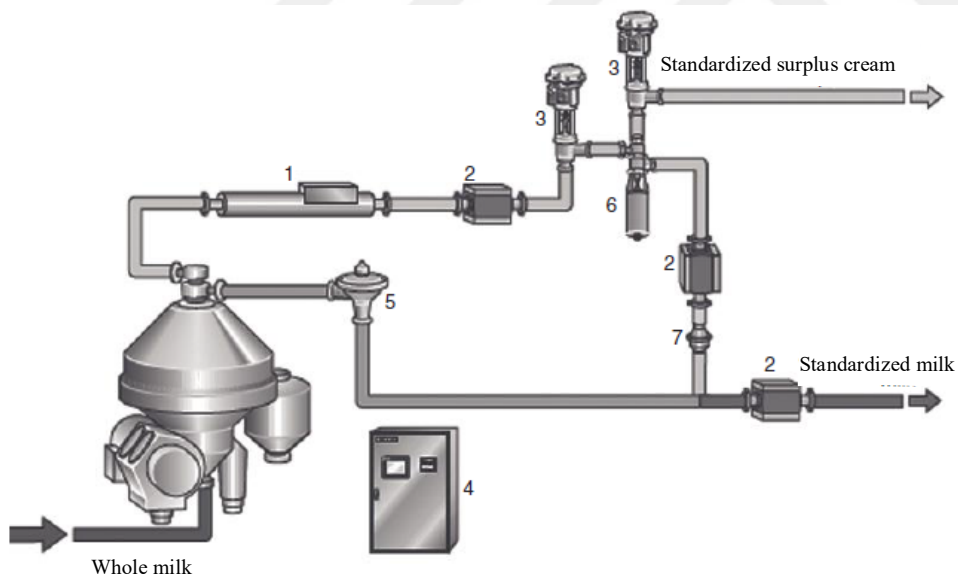


Figure 3.8. In-line Milk Standardization Process. 1, density transmitter; 2, flow transmitter; 3, control valve; 4, control panel; 5, constant pressure valve; 6, shut-off valve; 7, check valve (Kilara, 2011).

3.5.2. Raw Milk Clarification

Once introduced into centrifuge bowl, the milk is confined to pass through the disk-stack to leave the separation volume as the clarified milk outlet is located along the rotational axis, that is the center of disk stack (Fig. 3.9 and 3.10). Through the disk-stack, particles within milk structure are forced outwards continuously, based on two reasons:

- Low relative velocity of continuous medium allows for a laminar-fully developed flow throughout the channel,
- Particles, having a higher density than that of milk, based on the Stokes' velocity, tend to move against the stream.

Sedimentation based on gravity is reliable and applies theoretically for any particle when density condition is satisfied. Particles are accumulated in the solids containing portion of centrifuge that is basically the outermost solid wall of bowl assembly. Particle discharge then can be performed via nozzles or a drop-bottom mechanism, depending on the design of centrifuge and particle content of medium.

A clarifier and a milk separator differ from each other with a couple of aspects, as seen below Table 3.2:

Table 3.2. Operational distinctions of separator and clarifier.

Machinery	Treatment	Perforation on disk and distributor	Paring Disk
Separator	Three-phase	Towards the inner radius (full circle)	Double
Clarifier	Dual-phase	At the outer radius (half-circle)	Single

A centrifugal separator handles fat globules in cream formation. Therefore the machinery must allow for an 'interface' between the two liquid phases along with the discrete particles, therefore the double paring disks and disk perforation. Theoretical location of interface can be calculated via volume fractions of skim-milk and fat globules, then both the distributor and disks are manufactured on that proportions. In a clarifier on the other hand, the milk is treated as one pure substance without any nonhomogeneous components but the discrete particles. This assumption simplifies the machine, reduces the number of paring disks required to one and targets only to sediment particles, in our study the somatic cells.

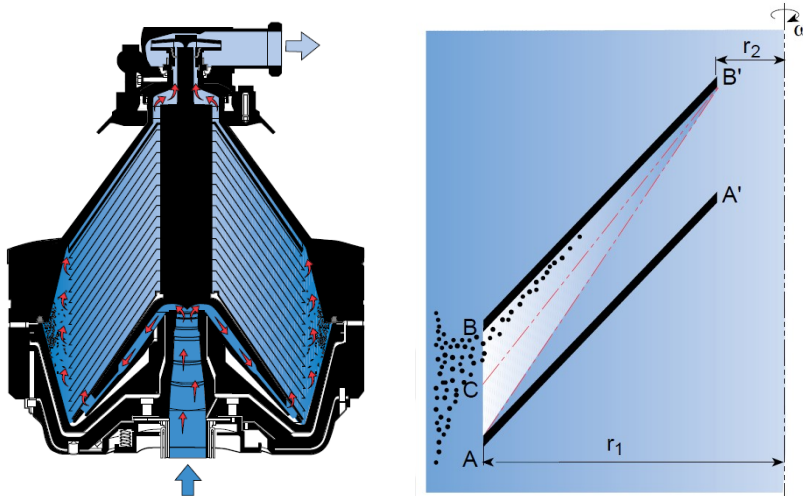


Figure 3.9. Milk distribution in clarifier bowl (left) and settling behavior of particles between disks (Bylund and Svensson, 1995).

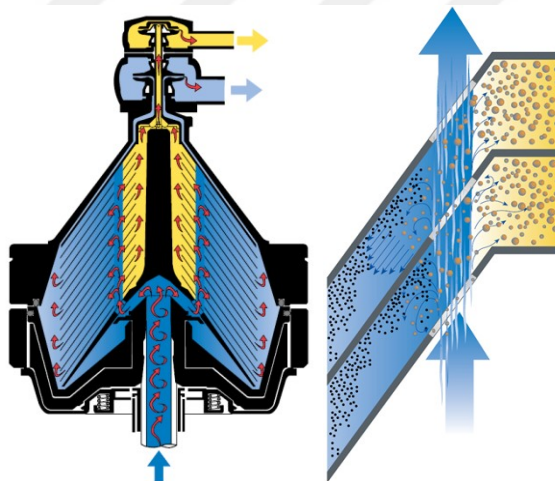


Figure 3.10. Interphase location is decided according to volume fractions of liquid phases (Bylund and Svensson, 1995).

Somatic cell separation is not the only outcome of clarifying process: epithelial cells from cow's udder, pulverized straw even dust particles from farm environment can be found in trace quantities. However, a greater fraction of particles are comprised of white (leukocytes) and red blood cells and bacteria. 1 kg total sediment out of 10,000 liters raw milk is considered to be a good estimation. Separator or clarifier, active volume (including disk intervals through the stack) in a solid-bowl centrifuge amounts to 10-20 liters. In our study, a clarifying centrifuge of 10 tons/hour throughput capacity with a 15-liter ($\approx 0,0151 \text{ m}^3$) bowl is investigated.

Discharge timer in drop-bottom centrifuges is set according to particle accumulation (Fig. 3.11). A trial-error basis can give the best discharge interval, on the condition that between discharges, examples are collected and analyzed: in a properly compacted discharge load, liquid lost should be minimum. Alternatively, examples can be analyzed for BTSCC index prior to clarifying. In this case, discharge interval is calculated manually for the optimum accumulation of particles. Normal intervals of discharge is around 30-60 minutes (Bylund and Svensson, 1995).

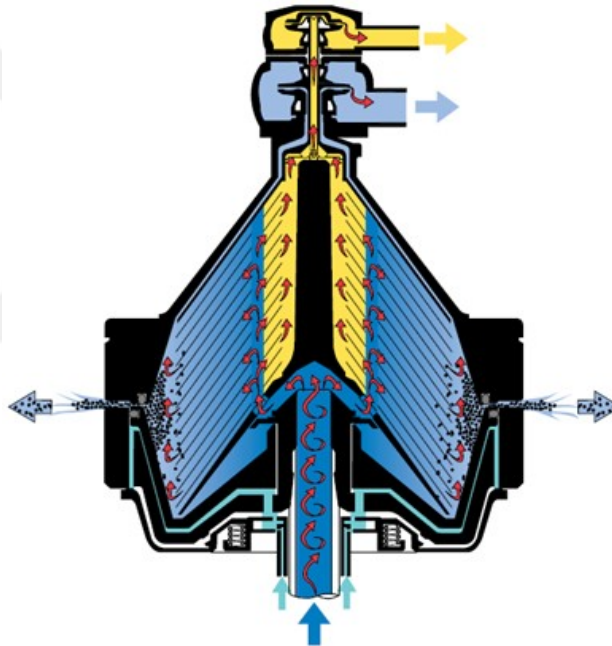


Figure 3.11. Hydraulic discharge mechanism in a drop-bottom centrifuge (Bylund and Svensson, 1995).

3.6. Particle-laden Flow in Disk-Stack Centrifuges

Simulating the particle-laden flow through a centrifugal separator and examining CFD-DEM representation against physical measurement of field samples has been the core of this study. Although a distinct machine operated on a specific medium (bovine milk) is investigated; the study aims to reveal a basis that will be applied any scenario, regardless of medium, particle it involves or the machinery to be operated on. Once completed under certain conditions, the results of this study might be able prove a steady basis to process optimization and product development cycles of related machinery.

3.6.1. Flow Characteristics in a Nutshell

The method adopted in this thesis study involves Eulerian definition continuous phase and Lagrangian definition of particle tracking, i.e. by employing a standard two-way turbulence coupling model (Subramaniam, 2013). The approach to solve the particle-laden flow question inside a centrifugal field also required the following criteria;

Dense phase representation is avoided since there are two distinct materials involved; hence no fluidization is considered. Due to obvious density differences between the particles (here, somatic cells-SC) and continuous medium, the Brownian motion modeling is also avoided,

Since dense phase modeling is not necessary, no particle collision models, i.e. DEM Collision, are assumed; which is, every single particle is affected only by the centripetal forces, wall collisions (no-slip boundaries) and the Coriolis Effect.

The particle content of whole milk is investigated in detail during the three years of thesis research. Although solids in the milk composition other than fat (solid-non-fat, SNF) have been the subjects of many previous assertions and publications, as stated before, this thesis study only involves the mechanical separation of a single group of sediments from the continuous medium by means of centrifugation. This group of SNF is selected to be the somatic cells, as the increasing number of which indicates infectious diseases like mastitis and therefore being explicitly investigated. This gave the researcher the upper hand of assessing the particle characteristics from the literature and quantities in both inlet and outlet from laboratory analyses, as the counting techniques are numerous, relatively accessible and commonplace.

3.6.2. Rule of Thumb: Methods to Process Evaluation

As the main inclination of the study remains as to set a mainframe on efficient particle separation based on multi-phase fluid characteristics and operating conditions for a disk-stack centrifugal separator; there is also a secondary aim that will be investigated along the way. There have been methods specifically utilized for designing, scaling-up and even inverse-engineering the disk-stack separators. As stated previously, empirical formulae derived from Stoke's Law have been heavily referred to in product engineering phases of centrifugal separators. In the greater scope, these methods (Ambler, 1959; Kempken et al., 1995; Leung, 2007) are quite

adept to estimate but the lower limit of particle equivalent diameter that can be deposited based on the medium and particle properties; geometrical features of an individual disk and operating conditions such as throughput rate and bowl rotational velocity.

The methods explicitly utilized to estimate the minimum size that can be separated under certain conditions for a particular machine will be emphasized in this section. Calculated data will be later compared/verified against CFD and experimental results from actual machinery.

3.6.2.1. The Ambler Method

In 1959, Charles M. Ambler put forward the first complete and definitive performance assessment formula by employing the aforementioned Stokes' law. When applied to a single particle trapped inside a continuous fluid on an inclined channel exposed to centrifugal forces, the configuration of Stokes' law gives the minimum diameter which can be sedimented out from the volume, that is the unit disk interval (Fig. 3.12).

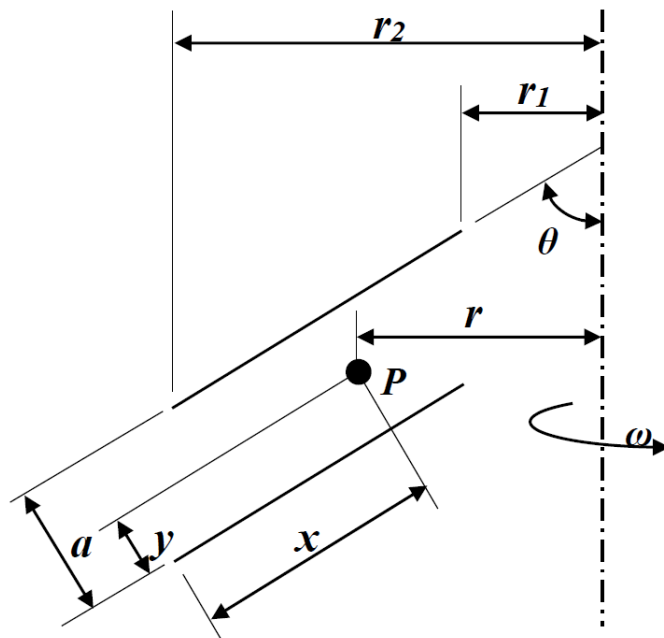


Figure 3.12. 2D representation of disk-stack; two consecutive disks (Ambler, 1959).

When disk settler configuration in Fig. 3.12 considered, the confined particle P is assumed to have settled once it contacts against the wall, that is, the upper disk surface. In this case, the Stoke's velocity and volumetric flow rate depending on the operating conditions and settler geometry can be expressed as in Eqn. 3.5 and 3.6;

$$v_g = \frac{\Delta\rho d^2 g}{18\mu} \quad [m/s] \quad (3.5)$$

$$Q = \frac{4\pi n v_g \omega^2}{3gC} (r_2^3 - r_1^3) \cot\theta \quad [m^3/s] \quad (3.6)$$

Where $\Delta\rho$ stands for the difference between continuous medium and particle densities, d is particle diameter, n is number of consequent disks in the stack and ω represents rotational speed of disk stack, in rad/s.

When parameters are introduced, the Ambler formula calculates the minimum particle of equivalent diameter that can be sedimented in disk stack. An inverted version of this emphasis also explains the reason these formulae are widely utilized: given the geometric aspects and fluid-particle properties, the Ambler formula gives the engineer the approximate volumetric (or mass) flow rate to separate a group of particles of specific size.

Ambler also coined the term “cut-off”, a state of operation when half the particles of diameter ‘ d ’ are sedimented and half escaped to mainstream. The parameter C on Eqn. 3.5 stands for the fraction of distance a (disk-interval) that is filled with the stream of fluid, and is unity either when the machine operates at cut-off or the particles of diameter d are separated altogether. As will be seen below, the consecutive formulae also utilized the principles of Ambler approach.

3.6.2.2. Kempken and Leung Calculations

Disk-stack centrifuges are utilized on a broad scale from oilfield applications to dairy products processing, as investigated in this study. Methods to estimate particle separation capabilities of machines have increased as the machinery became more and more common in the field of multi-phase flows. In the scope of this study, two of these studies are investigated and their results are compared to CFD-DEM simulations, along with Ambler approach.

Summarizing the target particle group as ‘mammalian cells’ in their study, Kempken et al. investigated the separation performance of three-phase disk-stack settlers, by utilizing a formula derived from Stoke’s Velocity formulation (Eqn 3.7).

$$d_{min} = \frac{3}{\omega} \sqrt{\frac{Q}{(r_2^3 - r_1^3) n \tan \theta}} \sqrt{\frac{3\mu}{\pi \Delta\rho}} \quad [m] \quad (3.7)$$

where η is dynamic viscosity of the continuous medium, z is the number of disks, and θ is the half-angle of disks. Similar to Ambler approach, Eqn. 3.7 gives an insight about the minimum particle size a centrifuge can sediment based on the parameters involved. An approximation to sedimentation percentage of this minimum size, however, was not suggested. As seen on Eqn. 3.7, increasing rotational speeds (hence, centrifugal forces) of bowl and decreasing volumetric flow rates guarantee the minimum particle size is achieved. In this respect, the minimum particle size is estimated for the device investigated during the process.

Wallace Leung (Leung, 2007) also settled his approach on the fact that the disperse phase is dilute, therefore the presence of solids do not affect the continuous fluid flow. Flow through an individual channel (i.e. disk interval) is suppressed and laminar, allowing Stokes’ law to hold. Leung has employed the ‘‘cut-off’’ utilizing the original idea of Ambler back in 1959, according to which at cut-off point, half the particles of diameter x_c will be sedimented and half not. Leung standardized his equation to give a constant, (Le number) through which the minimum particle size can be calculated, using average particle size Eqn. 3.8.

$$\frac{d_c}{d_o} = \frac{3}{\sqrt{\pi}} Le \quad (3.8)$$

Where d_c is cutoff diameter and d_o is the average particle diameter. Additional contributing discussion of researchers such as Triebel (2007) and van der Linden, (1987) must be also credited. Stemmed from the Stokes’ law, all the study to define a centrifugal separators performance, though, limited to determine the minimum size of a particle that can be treated. Therefore, in the results chapter of this study, the CFD-DEM analyses are honed to verify the consistency of these methods, in the absence of detailed particle size-frequency data.

3.7. Particle-laden Flow Modeling in CFD

3.7.1. Continuous Medium

The bowl of the centrifugal separator in which the mechanical separation process is occurred is comprised of three ‘revolute’ sub-assemblies: a conical bowl, a cylindrical bowl (dropping-bottom) and disk-stack. Hence equations defining the mainframe of this study should be expressed accordingly. In this section the conservation of mass and conservation of momentum equations in cylindrical coordinates will be briefly covered toward Reynolds Averaged Navier-Stokes equations utilized in CFD aspect of the study.

3.7.1.1. Conservation of Mass

Mass conservation for a flow through a channel exposed to centrifugal processing (without disk stack or conical part of centrifuge bowl) can be expressed as;

$$\frac{\partial \rho}{\partial t} + \frac{1}{r} \frac{\partial}{\partial r} (r \rho v_r) + \frac{1}{r} \frac{\partial}{\partial \theta} (\rho v_\theta) + \frac{\partial}{\partial z} (\rho v_z) = 0 \quad (3.9)$$

Eqn. 3.9 involves the three independent orthogonal velocity components, i.e., axial velocity, radial velocity and circumferential velocity are represented with u_z , u_r , u_θ , respectively. The circumferential velocity here is positive counterclockwise, that is, in the direction of increasing θ . When we consider the continuous substance –milk is incompressible throughout the process, Eqn. 3.9 simplifies into the form;

$$\frac{1}{r} \frac{\partial}{\partial r} (r u_r) + \frac{1}{r} \frac{\partial}{\partial \theta} (u_\theta) + \frac{\partial}{\partial z} (u_z) = 0 \quad (3.10)$$

As the density is a constant with regard to time and position whether the flow is steady or unsteady. The result is expressed in Eqn. 3.11;

$$\nabla \cdot V = 0 \quad (3.11)$$

will be valid for both scenarios and coordinate systems, Cartesian or cylindrical (White, 2000).

3.7.1.2. Conservation of Momentum

Conservation of Momentum equations or Navier-Stokes (N-S) equations are the backbone of defining viscous flow and many popular computer associated engineering (CAE) programs involving fluid dynamics simulations explicitly utilize localized numeric solutions of N-S equations (Reynolds Averaged Navier-Stokes, RANS). The N-S equations are derived from Newton's second law of motion, along with a viscous-stress parameter, related to velocity gradient and a pressure parameter.

Having derived from one of the most principal equations of physics, the applications of the N-S equations are virtually limitless. With proper adjustments to the equations, such as using Lagrangian schemes (as in this study) for discrete elements or leaving the mesh bonded geometries altogether (as in Harting et al., 2014), the applications vary from pipe and duct flow to stellar collision modeling. But the majority of fluid flow simulations on modern software packages deal with more day-to-day applications like pressure-drop calculation or power plant optimization.

According to problem definition investigated in this study, the N-S equation set is only described for cylindrical coordinates, as correlating both the solid-bowl and disk-stack to cylinders of different radii is more practical. For the incompressible, isothermal flow (density, $\rho=\text{const.}$, viscosity $\mu=\text{const.}$), with a velocity field of $\vec{V}=(u_z, u_r, u_\theta)$, the N-S equations take the form given below;

Cylindrical form of the Navier-Stokes equations for incompressible, isothermal Newtonian fluid (density, $\rho=\text{const.}$, viscosity $\mu=\text{const.}$) with a velocity field are given in Eqn.s 3.12-3.14;

r-component;

$$\begin{aligned} \rho \left(\frac{\partial u_r}{\partial t} + u_r \frac{\partial u_r}{\partial r} + \frac{u_\theta}{r} \frac{\partial u_r}{\partial \theta} - \frac{u_\theta^2}{r} + u_z \frac{\partial u_r}{\partial z} \right) \\ = - \frac{\partial P}{\partial r} + \rho g_r \\ + \mu \left[\frac{1}{r} \frac{\partial}{\partial r} \left(r \frac{\partial u_r}{\partial r} \right) - \frac{u_r}{r^2} + \frac{1}{r^2} \frac{\partial^2 u_r}{\partial \theta^2} - \frac{2}{r^2} \frac{\partial^2 u_r}{\partial \theta^2} + \frac{\partial^2 u_r}{\partial z^2} \right] \end{aligned} \quad (3.12)$$

z-component;

$$\begin{aligned} \rho \left(\frac{\partial u_z}{\partial t} + u_r \frac{\partial u_z}{\partial r} + \frac{u_\theta}{r} \frac{\partial u_z}{\partial \theta} + u_z \frac{\partial u_z}{\partial z} \right) \\ = -\frac{\partial P}{\partial z} + \rho g_z + \mu \left[\frac{1}{r} \frac{\partial}{\partial r} \left(r \frac{\partial u_z}{\partial r} \right) + \frac{1}{r^2} \frac{\partial^2 u_z}{\partial \theta^2} + \frac{\partial^2 u_z}{\partial z^2} \right] \end{aligned} \quad (3.13)$$

θ -component;

$$\begin{aligned} \rho \left(\frac{\partial u_\theta}{\partial t} + u_r \frac{\partial u_\theta}{\partial r} + \frac{u_\theta}{r} \frac{\partial u_\theta}{\partial \theta} + \frac{u_r u_\theta}{r} + u_z \frac{\partial u_\theta}{\partial z} \right) \\ = -\frac{1}{r} \frac{\partial P}{\partial \theta} + \rho g_\theta \\ + \mu \left[\frac{1}{r} \frac{\partial}{\partial r} \left(r \frac{\partial u_\theta}{\partial r} \right) - \frac{u_\theta}{r^2} + \frac{1}{r^2} \frac{\partial^2 u_\theta}{\partial \theta^2} - \frac{2}{r^2} \frac{\partial u_r}{\partial \theta} + \frac{\partial^2 u_\theta}{\partial z^2} \right] \end{aligned} \quad (3.14)$$

Although crucial to define and understand the behavior of fluid in a generalized flow domain, the N-S equations in the scope of this study will not be handled through an analytical solution, based on heavy assumptions. Instead, Reynolds Averaged Navier-Stokes (RANS) equations under ANSYS-Fluent mainframe will be utilized to solve the intricate nature of flow through centrifugal field. Therefore, some of the appropriate algorithms (aimed to adjust for low Re-number scenarios) are covered in the following title.

3.7.2. RANS Models for the Particle-laden Flow in Centrifugal Field

When it comes to picking the right modeling technique in CFD for a specific problem definition, the options are almost limitless. The possibility of turbulent flow in any portion of problem geometry opens up a myriad of RANS modeling methods. Literature focusing on solid-bowl centrifuges by handling the mathematical aspect by CFD is disappointingly scarce, as mentioned before. Specimen studies however, consider the $k - \varepsilon$ model, as expected. As the problem unfolds throughout the course of three years, it has revealed that finding the most reliable RANS algorithm is supposed to be one of the main outcomes of this study as the results of $k - \varepsilon$ algorithm is also needed to be validated. Therefore $k - \omega$ model is considered as an alternative, which later proved to be even more useful.

It is very important to underline that all the branches and additional functions of RANS models mentioned in this study are determined through time-consuming process of trial-and-error. A very good example of that is preferring the Renormalization Group-RNG $k - \varepsilon$ model over the Standard $k - \varepsilon$ model.

3.7.2.1. RNG $k - \varepsilon$ Model

Both $k - \varepsilon$ and $k - \omega$ being two-equation models, allow the calculation of a turbulent length scale and a time scale. Especially the *Standard $k - \varepsilon$* model became the de facto in fluid dynamics analyses in the field of mechanical engineering through its economic, robust and stable nature since its first introduction by Launder and Spalding (1974). So that the only studies involving CFD-DEM analyses of disk-stack centrifuges, try to solve the continuous medium equations (i.e. the Eulerian part of numerical solution) through Standard $k - \varepsilon$ algorithm.

The $k - \varepsilon$ model aims to model N-S equations for two parameters, as the name implies: a turbulence kinetic energy (k) and a dissipation rate (ε) where the latter is principally determined by the former. The calculation derives the turbulence kinetic energy from the equation directly when solution for dissipation rate is obtained through physical judgment.

Although tested properly, the Standard $k - \varepsilon$ model as seldom produced or populated the proper results, when compared to theoretical estimations of minimum particle diameter. This does not necessarily mean that the Standard $k - \varepsilon$ is outright false in terms of centrifuge modeling, but its ability to reflect the nature of sedimentation process under given conditions may be poor.

The search for a better compromise between the two (analytical and numerical) calculation methods directed the study towards using another $k - \varepsilon$ variant, which is RNG $k - \varepsilon$ model. The output of this tedious work is given in Appendix-A of this text.

As the name implies, RNG $k - \varepsilon$ model is a modified form of Standard model by a method called Renormalization Group. The properties specific to RNG $k - \varepsilon$ model are listed below;

- An additional term in dissipation rate (ε) calculation that practically increases the accuracy of the parameter in flows with a high strain rate.
- Swirl effect is optionally added (which is utilized) to improve accuracy of swirl calculation,
- An analytical equation is added for a variable Prandtl number whereas Prandtl number takes an arbitrary constant value in the *Standard $k - \varepsilon$* model,
- Most importantly, the RNG $k - \varepsilon$ adapts for low-Re number flows more successfully thanks to its effective viscosity calculation method, which is an analytically derived variant. The Standard $k - \varepsilon$ model is by nature a high-Reynolds number model which does not directly account for low-Re numbers (Ansys FLUENT 13.0, 2010).

To better employ the last feature, the mesh structure is adjusted and refined accordingly, providing a better boundary layer solution. The mathematical structure of RNG $k - \varepsilon$ model shows resemblance to the Standard $k - \varepsilon$ model:

$$\frac{\partial}{\partial t}(\rho k) + \frac{\partial}{\partial x_i}(\rho k u_i) = \frac{\partial}{\partial x_j} \left(\alpha_k \mu_{eff} \frac{\partial}{\partial x_j} \right) + G_k + G_b - \rho \varepsilon - Y_M + S_k \quad (3.15)$$

and

$$\begin{aligned} \frac{\partial}{\partial t}(\rho \varepsilon) + \frac{\partial}{\partial x_i}(\rho \varepsilon u_i) \\ = \frac{\partial}{\partial x_j} \left(\alpha_\varepsilon \mu_{eff} \frac{\partial \varepsilon}{\partial x_j} \right) + C_{1\varepsilon} \frac{\varepsilon}{k} (G_k + C_{3\varepsilon} G_b) - C_{2\varepsilon} \rho \frac{\varepsilon^2}{k} - R_\varepsilon + S_\varepsilon \end{aligned} \quad (3.16)$$

In Eqn.s 3-15 and 3.16, G_k represents the generation of turbulence kinetic energy due to the mean velocity gradients, G_b is the generation of turbulence kinetic energy due to buoyancy, and Y_M is the contribution of the fluctuating dilatation in compressible turbulence to the overall dissipation rate. Also α_k and α_ε are the inverse effective Prandtl numbers for k and ε , respectively. S_k and S_ε are user-defined source terms.

Turbulent viscosity is calculated through the Eqn. 3.17,

$$d\left(\frac{\rho^2 k}{\sqrt{\varepsilon\mu}}\right) = 1.72 \frac{\hat{v}}{\sqrt{\hat{v}^3 - 1 + C_v}} d\hat{v} \quad (3.17)$$

where;

$$\hat{v} = \frac{\mu_{eff}}{\mu} \text{ and } C_v \approx 100$$

Low-Re number handling ability of RNG $k - \varepsilon$ model stems from the correlation established between the effective turbulent transport character and the effective Reynolds number. For higher Reynolds numbers, Eqn. 3.18 is employed;

$$\mu_t = \rho C_\mu \frac{k^2}{\varepsilon} \quad (3.18)$$

with the coefficient $C_\mu = 0.0845$.

Finally, α_k and α_ε are computed using Eqn. 3.19,

$$\left| \frac{\alpha - 1.3929}{\alpha_0 - 1.3929} \right|^{0.6321} \left| \frac{\alpha + 2.3929}{\alpha_0 + 2.3929} \right|^{0.3679} = \frac{\mu_{mol}}{\mu_{eff}} \quad (3.19)$$

where $\alpha_0 = 1.0$. Also $\alpha_k = \alpha_\varepsilon \approx 1.393$, for high-Re number modeling.

Default values, wherever detected in the turbulence model, left at their default values as arbitrarily changing the model constants can severely affect the solution and converge characteristics of algorithm. Therefore, $C_{1\varepsilon}$ and $C_{2\varepsilon}$ values are directly assumed to be 1.42 and 1.68, respectively.

It is suggested that the RNG $k - \varepsilon$ model shows better adaptation to rapidly changing strain curvatures and more eligible for low-Re cases; a couple of advantages which makes the method apt for solving channel flow with extremely low Re numbers.

3.7.2.2. The Standard $k - \omega$ Model

The Standard $k - \omega$ model is an empirical model based on model transport equations for the turbulence kinetic energy (k) and the specific dissipation rate (ω), which can also be thought of as the ratio of ε to k .

As the $k - \omega$ model has been modified over the years, production terms have been added to both the k and ω equations, which have improved the accuracy of the model for predicting free shear flows.

The turbulence kinetic energy, k , and the specific dissipation rate, ω , are obtained from the transport equations in Eqn.s 3.20 and 3.21;

$$\frac{\partial}{\partial t}(\rho k) + \frac{\partial}{\partial x_i}(\rho k u_i) = \frac{\partial}{\partial x_j} \left(\Gamma_k \frac{\partial k}{\partial x_j} \right) + G_k - Y_k + S_k \quad (3.20)$$

and

$$\frac{\partial}{\partial t}(\rho \omega) + \frac{\partial}{\partial x_i}(\rho \omega u_i) = \frac{\partial}{\partial x_j} \left(\Gamma_\omega \frac{\partial \omega}{\partial x_j} \right) + G_\omega - Y_\omega + S_\omega \quad (3.21)$$

where G_k and G_ω represent the turbulence kinetic energy (k) generation and specific dissipation rate (ω) generation, respectively. Γ_k is the effective diffusivity of k and Γ_ω is the effective diffusivity of ω . Y_k and Y_ω represent the dissipation of k and ω due to turbulence. Finally S_k and S_ω are user-defined coefficients.

The effective diffusivities for the $k - \omega$ model are given by;

$$\Gamma_k = \mu + \frac{\mu_t}{\sigma_k} \quad (3.22)$$

$$\Gamma_\omega = \mu + \frac{\mu_t}{\sigma_\omega} \quad (3.23)$$

where σ_k and σ_ω are the turbulent Prandtl numbers for k and ω , respectively.

The turbulent viscosity, μ_t , is computed by following expression, using k and ω ;

$$\mu_t = \alpha^* \frac{\rho k}{\omega} \quad (3.24)$$

where α^* is employed to compensate for Low-Re numbers by buffering the turbulent viscosity and calculated with the formulation given in Eqn. 3.25:

$$\alpha^* = \alpha_\infty^* \left(\frac{\alpha_0^* + Re_t/R_k}{1 + Re_t/R_k} \right) \quad (3.25)$$

where the constituting parameters are summarized in Eqn.s 3.26-3.29,

$$Re_t = \frac{\rho k}{\mu \omega} \quad (3.26)$$

$$R_k = 6 \quad (3.27)$$

$$\alpha_0^* = \frac{\beta_i}{3} \quad (3.28)$$

$$\beta_i = 0.072 \quad (3.29)$$

Also for high Re-numbers, $\alpha^* = \alpha_\infty^* = 1$.

Production of turbulence kinetic energy (G_k) can be defined as in Eqn. 3.30;

$$G_k = -\overline{\rho u_i' u_j'} \frac{\partial u_j}{\partial u_i} \quad (3.30)$$

The production of specific dissipation rate (ω) is given by Eqn. 3.31;

$$G_\omega = \alpha \frac{\omega}{k} G_k \quad (3.31)$$

and the coefficient α is given by Eqn. 3.32;

$$\alpha = \frac{\alpha_\infty}{\alpha^*} \left(\frac{\alpha_0 + Re_t/R_\omega}{1 + Re_t/R_\omega} \right) \quad (3.32)$$

where $R_\omega = 2.95$. α^* and Re_t are given by Eqn. 3.25 and Eqn. 3.26, respectively. Again, for the high-Reynolds numbers, $\alpha = \alpha_\infty = 1$.

The dissipation of turbulence kinetic energy (Y_k) is given by Eqn. 3.33;

$$Y_k = \rho \beta^* f_{\beta^*} k \omega \quad (3.33)$$

where the piecewise function f_{β^*} is given in Eqn. 3.34

$$f_{\beta^*} = \begin{cases} 1 & \chi_k \leq 0 \\ \frac{1 + 680\chi_k^2}{1 + 400\chi_k^2} & \chi_k > 0 \end{cases} \quad (3.34)$$

where;

$$\chi_k \equiv \frac{1}{\omega^3} \frac{\partial k}{\partial x_j} \frac{\partial \omega}{\partial x_j} \quad (3.35)$$

with auxiliary functions and closure parameters expressed in Eqn.s 3.36-3.40;

$$\beta^* = \beta_i^* [1 + \xi^* F(M_t)] \quad (3.36)$$

$$\beta_i^* = \beta_\infty^* \left(\frac{4/15 + (Re_t/R_\beta)^4}{1 + (Re_t/R_\beta)^4} \right) \quad (3.37)$$

$$\xi^* = 1.5 \quad (3.38)$$

$$R_\beta = 8 \quad (3.39)$$

$$\beta_\infty^* = 0.09 \quad (3.40)$$

Where Re_t is given by Eqn. 3.26. The dissipation of ω is given by in Eqn. 3.41;

$$Y_\omega = \rho \beta f_\beta \omega^2 \quad (3.41)$$

where the contributing parameters are summarized in Eqn.s 3.42-3.44,

$$f_\beta = \frac{1 + 70\chi_\omega}{1 + 80\chi_\omega} \quad (3.42)$$

$$\chi_\omega = \left| \frac{\Omega_{ij}\Omega_{jk}\Omega_{ki}}{(\beta_\infty^*\omega)^3} \right| \quad (3.43)$$

$$\Omega_{ij} = \frac{1}{2} \left(\frac{\partial u_i}{\partial x_j} - \frac{\partial u_j}{\partial x_i} \right) \quad (3.44)$$

also,

$$\beta = \beta_i \left[1 - \frac{\beta_i^*}{\beta_i} \xi^* F(M_t) \right] \quad (3.45)$$

where the parameters β_i^* and $F(M_t)$ are defined by Eqn. 3.37 and Eqn. 3.46, respectively. The compressibility function, $F(M_t)$, is given by;

$$F(M_t) = \begin{cases} 0 & M_t \leq M_{t0} \\ M_t^2 - M_{t0}^2 & M_t > M_{t0} \end{cases} \quad (3.46)$$

with closure parameters summarized in Eqn.s 3.47-3.49;

$$M_t^2 \equiv \frac{2k}{a^2} \quad (3.47)$$

$$M_{t0} = 0.25 \quad (3.48)$$

$$a = \sqrt{\gamma RT} \quad (3.49)$$

For high-Reynolds numbers, $\beta_i^* = \beta_\infty^*$. In the incompressible scheme, $\beta^* = \beta_i^*$. The remaining constants are summarized below.

$$\alpha_\infty^* = 1, \alpha_\infty = 0.52, \alpha_0 = 1/9, \beta_\infty^* = 0.09, \beta_i = 0.072, R_\beta = 8 \\ R_\beta = 6, R_\omega = 2.95, \xi^* = 1.5, M_{t0} = 0.25, \sigma_k = 2.0, \sigma_\omega = 2.0$$

3.7.3. Particle-laden Flow in ANSYS Fluent Software: The CFD-DEM

The Computational Fluid Dynamics–Discrete Element Modeling (CFD-DEM) framework implemented in this study follows the method called the Euler-Lagrange approach. The liquid phase is treated as a continuum on which the mesh is fixed, whereas particles are solved by transferring their physical properties (momentum, mass and energy) from element to element on the Eulerian mesh frame, which is called the Lagrangian particle tracking. Discrete phase can be a number of solid, insoluble particles, as well as droplets or in some applications, spray. The discrete phase and continuous medium can be confined to a one-way interaction (continuous medium affecting the particles), a two-way interaction can be allowed (particles also can affect back the continuous medium) or an interaction between the two phases can be ignored altogether (Norouzi et al., 2016).

DEM calculations for every time step (in transient solver, flow time; in pseudo-transient solver, the particle time step) are advanced in this fashion: for any time and location in the flow region, the continuity and momentum equations are solved for continuous medium. After the solution for the iteration/time step is completed, particle equations of motion are solved for the properties adopted from the continuous phase calculation of current iteration/time step. Then equations of motion for continuous phase are solved again, for the following iteration/time step. If the continuous phase is solved in a steady-state solver, the time advancement is done only by particle time-stepping, which is called the pseudo-transient solution (ANSYS Fluent, 2010).

As applied in the context of this thesis, the Fluent CFD-DEM perspective of Euler-Lagrange approach becomes significantly simpler when particle-particle interactions can also be neglected. This scenario obviously requires a scarce amount of particles to be considered ($\dot{m}_{\text{particles}} \ll \dot{m}_{\text{fluid}}$) and this is an acceptable compromise in our study as discrete particles usually occupy an approximate volume fraction of %0.01 in raw bovine milk. This application is called ‘dilute phase’ modeling and represents the most applicable approach to solve CFD-DEM for spray dryers, coal, internal combustion, flue gasses and funnel modeling. Applications investigating the liquefaction character of materials or fluidized beds require dense-phase modeling which is not the inclination of this study. ANSYS Fluent calculates particle trajectories at every time step by implementing a force balance on every single particle which simply equates particle inertia with the forces acting on the particle, as in Eqn. 3.50:

$$\frac{d\vec{u}_p}{dt} = F_D(\vec{u} - \vec{u}_p) + \frac{\vec{g}(\rho_p - \rho)}{\rho_p} + \vec{F} \quad (3.50)$$

where \vec{F} is an additional acceleration (force/unit particle mass) term. Eqn. 3.51 gives the drag force per unit particle mass $F_D(\vec{u} - \vec{u}_p)$;

$$F_D = \frac{18\mu C_D Re}{\rho_p d_p^2} \frac{1}{24} \quad (3.51)$$

Here, \vec{u} is the fluid phase velocity, \vec{u}_p is the particle velocity, μ is the molecular viscosity of the fluid, ρ is the fluid density, ρ_p is the density of the particle, and d_p is the particle diameter. Re is the relative Reynolds number, defined in Eqn. 3.52.

$$Re \equiv \frac{\rho d_p |\vec{u}_p - \vec{u}|}{\mu} \quad (3.52)$$

The additional force term, \vec{F} , in Eqn. 3.50 also includes forces on particles that arise due to rotation of the reference frame. These forces arise when you are modeling flows in moving frames of reference. For rotation defined about the axis, for example, the forces on the particles in the Cartesian x- and y- directions can be written as in Eqn.s 3.53 and 3.54:

$$\left(1 - \frac{\rho}{\rho_p}\right) \Omega^2 x + 2\Omega \left(u_{p,y} - \frac{\rho}{\rho_p} u_y\right) \quad (3.53)$$

where $u_{p,y}$ and u_y are the particle and fluid velocities in the Cartesian y direction, Ω is the RPM, and;

$$\left(1 - \frac{\rho}{\rho_p}\right) \Omega^2 y + 2\Omega \left(u_{p,x} - \frac{\rho}{\rho_p} u_x\right) \quad (3.54)$$

where $u_{p,x}$ and u_x are the particle and fluid velocities in the Cartesian x direction.

The dispersion of particles due to turbulence in the fluid phase can be predicted using the stochastic tracking model or the particle cloud model. The stochastic tracking (random walk) model includes the effect of instantaneous turbulent velocity fluctuations on the particle trajectories through the use of stochastic methods. The particle cloud model tracks the statistical evolution of a cloud of particles about a mean trajectory. The concentration of particles within the cloud is represented by a Gaussian probability density function (PDF) about the mean trajectory. For stochastic tracking a model is available to account for the generation or dissipation of turbulence in the continuous phase. When the flow is turbulent, ANSYS Fluent will predict the trajectories of particles using the mean fluid phase velocity, \bar{u} , in the trajectory equations. Optionally, the instantaneous value of the fluctuating gas flow velocity can be involved with Eqn. 3.55 to predict the dispersion of the particles due to turbulence.

$$u = \bar{u} + u' \quad [N] \quad (3.55)$$

In the stochastic tracking approach, ANSYS Fluent predicts the turbulent dispersion of particles by integrating the trajectory equations for individual particles, using the instantaneous fluid velocity, $\bar{u} + u'(t)$, along the particle path during the integration.

By computing the trajectory in this manner for a sufficient number of representative particles (termed the “number of tries”), the random effects of turbulence on the particle dispersion can be included. Prediction of particle dispersion makes use of the concept of the integral time scale, T in the Eqn. 3.56:

$$T = \int_0^{\infty} \frac{u'_p(t)u'_p(t-\tau)}{u_p'^2} d\tau \quad (3.56)$$

The integral time is proportional to the particle dispersion rate, as larger values indicate more turbulent motion in the flow. It can be shown that the particle diffusivity is given by $\overline{u'_i u'_j} T$. For small “tracer” particles that move with the fluid (which is called the ‘zero drift velocity’), the integral time becomes the fluid Lagrangian integral time, T_L . Eqn. 3.57 describes the approximation to this time scale as;

$$T_L = C_L \frac{k}{\varepsilon} \quad (3.57)$$

Where C_L is to be determined as it is not well known. By matching the diffusivity of tracer particles, $\overline{u'_i u'_j} T$, to the scalar diffusion rate predicted by the turbulence model, v_t/σ , one can obtain ; T_L from Eqn.s 3.58 or 3.59.

$$T_L \approx 0.15 \frac{k}{\varepsilon} \quad (3.58)$$

for the $k - \varepsilon$ model and its variants, and;

$$T_L \approx 0.30 \frac{k}{\varepsilon} \quad (3.59)$$

when the Reynolds stress model (RSM) is used. For the $k - \omega$ models, substitute $\omega = \varepsilon/k$ into Eqn. 3.58. Similarly, the Large Eddy Simulation (LES) model uses the equivalent LES time scales. The trajectory equations, and any auxiliary equations describing heat or mass transfer to/from the particle, are solved by stepwise integration over discrete time steps. Integration of time in Eqn. 3.60 yields the velocity of the particle at each point along the trajectory, with the trajectory itself predicted by;

$$\frac{dx}{dt} = u_p \quad (3.60)$$

Note that Eqn. 3.50 and Eqn. 3.60 are a set of coupled ordinary differential equations, and Eqn. 3.50 can be expressed in the form of Eqn. 3.61;

$$\frac{du_p}{dt} = \frac{1}{\tau_p}(u - u_p) + a \quad (3.61)$$

where the term a includes accelerations due to all other forces except drag force. This set can be solved for constant u , a and τ_p by analytical integration. For the particle velocity at the new location u_p^{n+1} we get Eqn. 3.62;

$$u_p^{n+1} = u^n + e^{-\frac{\Delta t}{\tau_p}}(u_p^n - u^n) - a\tau_p \left(e^{-\frac{\Delta t}{\tau_p}} - 1 \right) \quad (3.62)$$

Eqn. 3.63 describes the new location x_p^{n+1} can be computed from a similar relationship;

$$x_p^{n+1} = x_p^n + \Delta t(u^n + a\tau_p) + \tau_p \left(1 - e^{-\frac{\Delta t}{\tau_p}} \right) (u_p^n - u^n - a\tau_p) \quad (3.63)$$

In these equations u_p^n and u^n represent particle velocities and fluid velocities at the old location.

3.8. The CFD-DEM Simulations in the Separation Field

Once the separator bowl rate reaches its optimum value and input rate (10 ton/h for our study) stabilizes, the process inside the centrifugal separator displays a steady-state behavior. Although disturbances may occur due to input rate, power supply, mechanical transmission (belt-transmission is preferred in many clarifying centrifuges) etc., errors originating from these parameters are seldom significant.

Under these assumptions, in this PhD study, the continuous fluid flow is assumed to be deterministic. The details of problem handled in this study as well as the respective steps in the aforementioned CFD solver are covered below.

3.8.1. Problem Definition

The original model of the actual machine involves 237 disks in a 15.1-liter bowl volume with a diameter of 390mm and height 400mm, handling an optimum 10 ton/h throughput. In the scope of this study, a 3-D, rotational region with one inlet and one outlet is considered in a steady-state scenario. As the simplified version of the actual centrifugal separator; this model involves 24 disks (Fig. 3.13), where *all* the geometric properties of disks were adopted right from the original model. The settling ratios of different particle diameters with various operating conditions are investigated, as summarized below.

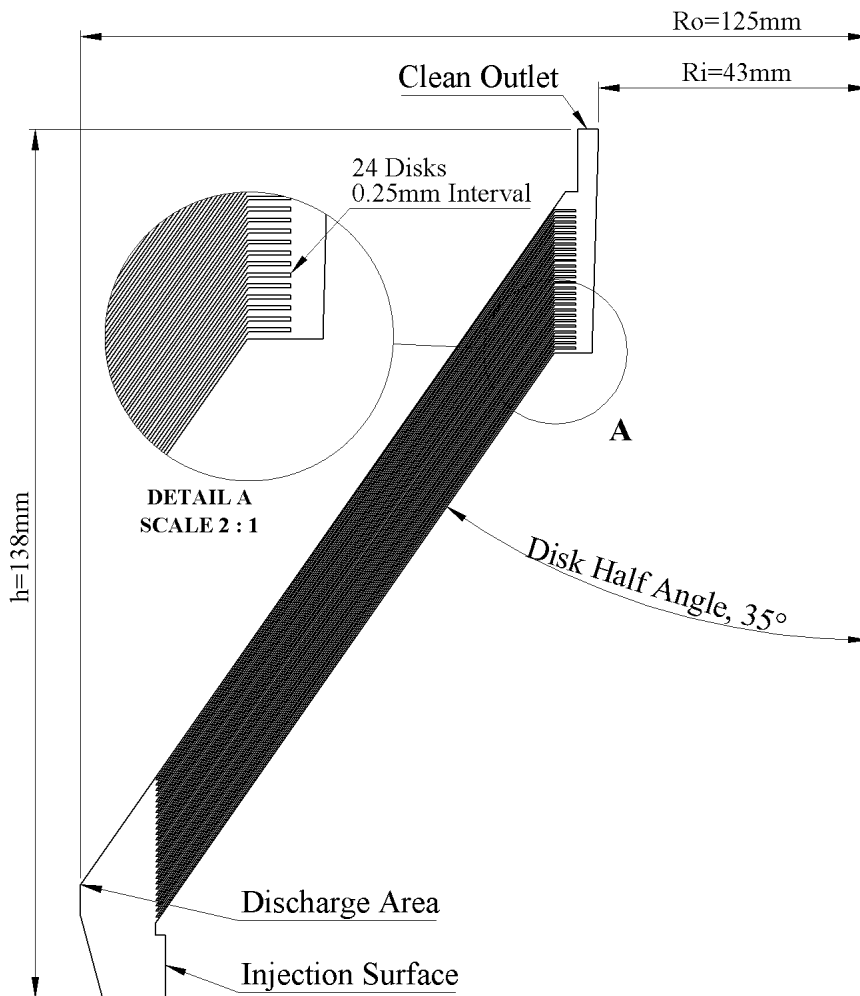


Figure 3.13. 24-disk bowl representation of two-phase clarifier.

A pressure-based solver is preferred, as there is no significant rise (or drop) in temperature during clarifying operation in actual application, hence a change in density. Processes involving heat input or dissipation may take place in a dairy processing plant e.g., pasteurization or homogenization (Mendlik, 1950, also Wilbey, 2004) and are optional. Since the main purpose of a ‘two-phase’ centrifugal separator is only to prepare milk to successive processes and not to heat-treat the fluid; no energy solver model is chosen for this study.

In the optimum operating rate of 7700 rpm, the centrifugal force reaches 6640g (in a counter-clockwise rotating reference frame) inside the separation field. Yet the ‘gravity’ is defined as 9.81 m/s^2 towards “-y” direction for consistency. Milk density is assumed to be 1035 kg/m^3 and viscosity $3.003 \times 10^{-3} \text{ Pa.s}$ which is constant against changing operating conditions (Reynolds number through disks being much lower than that of the rest of the bowl volume).

Steady state scheme is utilized for continuous phase solver, considering the centrifuge must reach to a steady behavior before the examples of ‘clarified’ milk can be collected. This behavior is observed after the raw milk is introduced; the exact duration of which is determined upon experience. However, The steady-state behavior is only applicable for continuous fluid: particles in the centrifugation field, although in a continuous medium, move randomly, i.e. stochastically (Stolarski, Nakasone, and Yoshimoto, 2006). In ANSYS Fluent, this requirement of particle-laden flow representation is compromised by a special algorithm called ‘unsteady particle tracking’ where the researcher is allowed to define a ‘time step’ in which the particle motion is calculated in a steady continuous fluid solver (Elghobashi, 1991, 1994).

A Moving Reference Frame (MRF) is implemented for centrifugal field representation. Considered as an Eulerian approach, the MRF model translates or rotates flow region without actually interacting with the mesh structure. Physical properties of both continuous phase and discrete phase are calculated in a control volume fashion. An alternative application where the domain itself is rotated, i.e. Mesh Movement (ANSYS FLUENT 13.0, 2010), requires transient conditions of continuous phase, which contradicts the mindset we preferred to utilize in terms of this study.

To sum up, the problem validation is realized at the optimum operating conditions of the machinery. Once the model is validated against the field test, the details of which will be covered in section 4.1.1, we advanced to perform simulations on the design points which previously were discussed and determined with the manufacturing company -also a contributor to our study, HAUS Centrifuge Technologies.

3.8.2. Pre-processing Setup and Particle Injections

Four variations of the same clarifier setup are utilized in pre-processing, based on the disk intervals hence, the rib height. In the original model, 0.25mm ribs set the gap between two consequent disks in disk-stack. This application ‘stacks’ the solid bowl with disks where the number of disks in the stack is limited to paring disk-distributor space. In our simplified model, adjusted rib heights generated the disk numbers given in Table 3.3. The solution domain is further simplified by slicing the model into 8 equal volumes (that is, the number of ribs, Fig. 3.14). Only the fluid domains are modeled in simulations, hence no fluid-solid interface (FSI) is considered (as in Genevaux et al., 2003 and Tu et al., 2015).

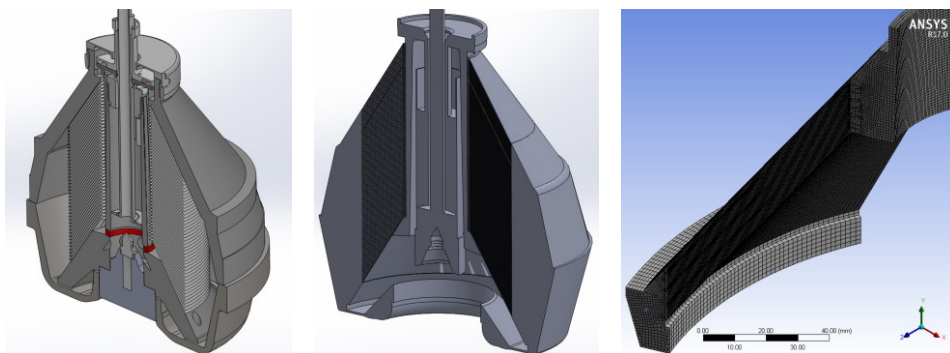


Figure 3.14. Actual simulation domain is obtained by a three-step evaluation.

A multizone (hexahedral-forced) mesh with 600,000 nodes and 345,000 elements is decided after numerous alternative structures implemented and failed to provide better results at lower element numbers. Hexa-dominant algorithm is preferred due to its ability to keep orthogonality and skewness parameters in check. Also, a three-layer element sizing is applied to disk intervals to better capture the wall boundary layers and a 5x38 element sizing is to fix number of elements -hence, 190 particles are injected on the ‘inlet’ surface. Fig. 3.15 gives a detailed view of 0.25mm disk interval geometry with hexahedral mesh.

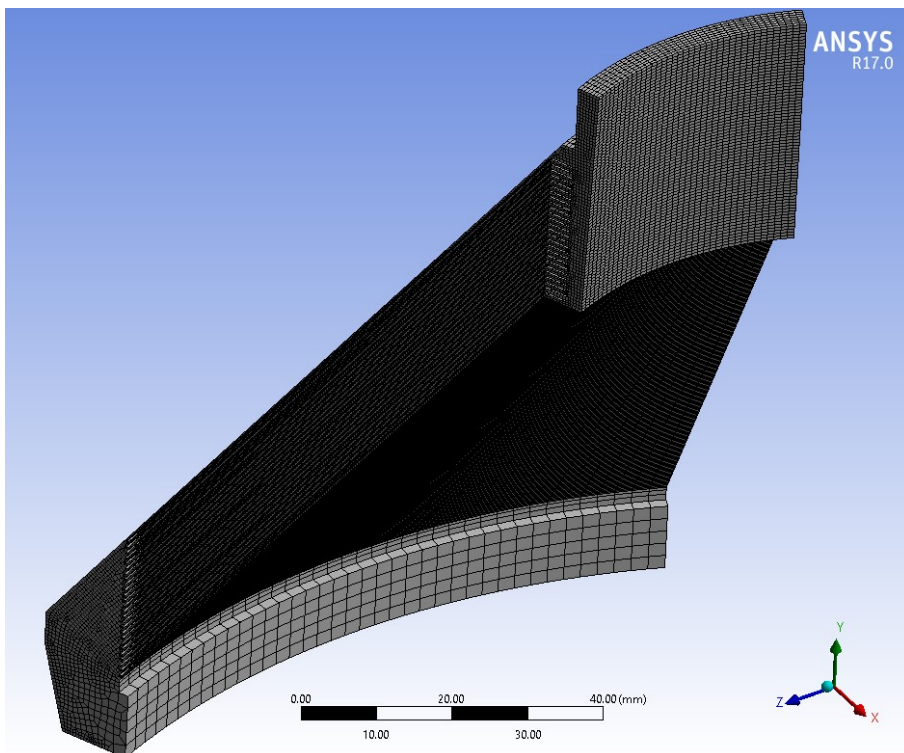


Figure 3.15. Detail of mesh view, 45° model with 0.25mm disk interval.

Table 3.3. The number of disks in the CFD modeling against the number of disks on the original model.

Rib Height [mm]	Disk Qty -Full-Scale Model-	Disk Qty -Simplified Model-
0.25	237	24
0.40	182	19
0.60	139	14
0.80	112	12

Particle properties required to perform simulations and model validation are partly assumed from published literature. BTSCC index was harvested from an actual machine operating in a dairy products compound in Tire/İzmir, the 3-D model of which was provided by the contributing company, HAUS Centrifuge Technologies. Somatic cell counts play an important role in data validation, since the study conducted has been revolved around the same machinery and same process. To keep the information concise, properties considering different simulation/test runs are given in Table 3.4.

Table 3.4. Some physical properties of Leukocytes with source publication.

Parameter	Source(s)	
Density [kg/m ³]	1561	Kempken, 1995
min. Diam. [μm]	6	Zlotnik, 1947
max. Diam. [μm]	20	Zlotnik, 1947
Avg. Diam. [μm]	16.5	Shekhawat, 2018
BTSCC Index (inlet)	690,000	See Section 4.1
SCC Index (clean)	84,000	See Section 4.1

3.8.2.1. Boundary Conditions

When handled as a black-box and in steady conditions, a clarifying separator acts like any single-in single-out (SISO) tool; an input through which the particle-laden flow is introduced and an output of clarified liquid. In this study, no solid discharge for the analysis duration is considered, that is 20 min., for milk clarifying application. As stated previously, a Moving Reference Frame (MRF) is utilized to represent rotation, hence the centrifugal field of the machinery.

Four typical boundary conditions are available through actual measurements from machinery; pressure readings (typically gage pressures) from input and output, bowl rate and input rate. Again, all these data bound to show slight variations from time to time, as stated before. A complete list of boundary conditions can be seen on Table 3.5. A ‘Wall’ indicates any surface either particle or fluid is in contact with.

Table 3.5. Boundary conditions set with applied modifications.

Boundary Type	Value	MRF Behavior	DEM Behavior
Wall (Discharge)	No-slip Wall	Rel. to Adj. Cell Zone	Trap
Wall (Other)	No-slip Wall	Rel. to Adj. Cell Zone	Reflect
Mass Flow Inlet	Varies (51.7 kg/h at validation point)	N/A	Reflect
Pressure Outlet	2.2 Bar	N/A	Escape

3.8.2.2. The DEM Setup

The particle size range considered in this thesis is based on earlier studies. Although DEM interface of ANSYS Fluent allow the researcher to input min., max. and average values as well as a spread parameter to calculate a distribution (i.e. Rosin-Rammler Distribution (Vesilind, 1980)), input and output data tracking becomes an ineffective work. This problem obliged the candidate to develop another control method for input and output figures: injecting the same number of particles for each simulation, only modifying the particle diameter and injection relative velocity, then compare results on a fractional basis.

This approach was also necessary as the actual BTSCC index from the field tests (see Section 4.1) required an average 500,000 particles to be modeled at each second of the solver time. Number of particles injected in DEM software is determined directly by the number of elements on the injection surface, unless the particle clouds are considered which, in our case, was out of possibility. Therefore, the injection surface is limited to 190 elements to provide a better aspect ratio on inlet surface of geometry. The element injection properties are detailed on Table 3.6.

Table 3.6. DEM Parameters

DEM Parameter	Status/Value
Interaction with Continuous Phase	Yes
Particle Length Scale	0.001 m
Particle Time Step Size	0.005 s
DEM Collision	No
Two-way Turbulence Coupling	No
Accuracy Control	Yes (Tolerance: 1×10^{-5})
Tracking Scheme	Trapezoidal (High-order), Implicit (Low-order)

4. RESULTS AND DISCUSSION

Particle-laden flow characteristics along with the sedimentation ability of a certain machinery have been investigated in this study. It is important to emphasize that, although there is a myriad of different applications available to centrifugal separators, this thesis aims to establish a base on which distinct operations on various separators can be scaled-up in a scientific point of view.

Validating the CFD-DEM results against field data, on the other hand, is a difficult task due to reasons summarized below. Empirical formulae detailed in the method section generally aim to define a singular particle's settling behavior in a 2-D space, that is a disk interval. The fact is that modeling the flow domain in two dimensions and reducing the number of disks to one (which otherwise will soar around a couple hundreds) dramatically simplifies many CFD pre- and post-processing steps. However, any data harvested from a 'running' centrifugal separator outlet reflects the effect of each disk along the disk-stack inside separator bowl. Therefore, the idea of collecting an outlet data and using this to validate a CFD-DEM model to validate any empirical method represents a far-fetched approach with minimum reliability. As a result, a 3-D model with the number of disks are reduced -decimated, to be more specific- is preferred to simulate the sedimentation process and to properly use the field data. Tests performed to investigate computational method approximation to particle sedimentation process involved a particular machine; a two-phase clarifying centrifuge, based on reasons mentioned above. This, of course, was a commercial machine, the features and operating conditions of which are well settled in time in the product range of the collaborating company. Although deciding on a single machine for investigating the scale-up abilities of a novel method may seem inadequate at first glance, the in-depth research framing multiple turbulence models and particle tracking schemes have confined the PhD candidate to pick the most common and invested type of machine and process. By the help of this very study, the candidate aims to investigate the particle settlement process in numerous machines with different continuous media and particle characteristics. These aspects will be summarized in the conclusion and title.

4.1. Problem Validation

Methods offered in scale-up studies provide minimum (or cut-off) diameters a specific centrifuge can separate from continuous phase. The physical principles on which those methods are established however, cannot deliver approximate fractions, as a performance parameter.

The core of this study, in fact, has been to determine how successfully a centrifuge can sediment these particles. In steady state operation, the clarifying centrifuge delivers an 87.83% separation performance after the system is reached the steady-state operation. That is, BTSCC index is dropped from 690,000 on the inlet example of raw milk to 84,000 on the outlet example. The basis for both example collecting procedure and validation runs of CFD-DEM model (see section 3.8.1 Fig. 3.13 for model definition), constraints in Table 4.1 are assumed.

Table 4.1. Process parameters for example collection.

Process Parameter	Value
Bowl Rate	7700 rpm
Throughput Rate	10 ton/h
Inlet Pressure	Atmospheric
Outlet Pressure	2.2 Bar

The measurements were performed by MAKÜ BİLTEKMER laboratory, Burdur/Türkiye in 27 Feb, 2019, by using fluoro-opto-electronic counting (*ISO 13366-2/AC:2008*); a variant of flow cytometry and a popular technology to analyze the characteristics of cells or particles (among the very similar examples of which are Gunasekera, Veal and Attfield, 2003; Koess and Hamann, 2008).

Flow cytometry provides a reliable well-established method to identify cells in solution and is most commonly used for evaluating peripheral blood, bone marrow, and other body fluids (Fig. 4.1).

Flow cytometry studies are used to identify and quantify the cells of the immune system and to characterize hematological malignancies. The two turbulence models under steady state conditions were tested against these figures. Results suggest that the Standard $k - \omega$ model gives better response to test data (Table 4.2).

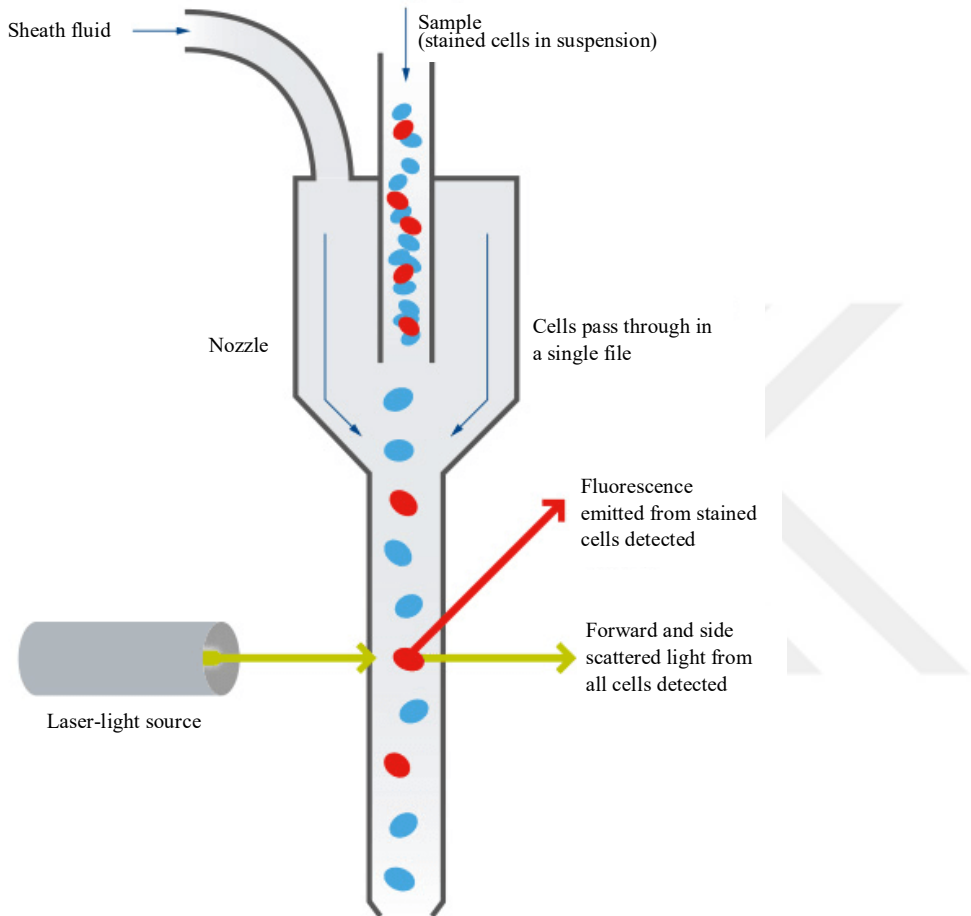


Figure 4.1. A schematic of a typical Flow Cytometry application (Abcam, 2019).

Table 4.2. Steady-state separation efficiency is validated through CFD-DEM modeling.

RANS	CFD-DEM	Field Test	Rel. Error
RNG k- ϵ	74.21%	87.83%	15.507%
Standard k- ω	91.05%	87.83%	3.666%

As seen on Table 4.2, the Standard k – ω model validates the field test at operation parameters pointed out in problem definition. To control the number of iterations, hence the particle time-steps, the residual criteria are arranged to demand a 10^{-3} limit for each parameter calculated (Fig. 4.3).

Residuals for RNG $k-\epsilon$ and Standard $k-\omega$ models can be seen on Fig. 4.2. Although parameters are inclined to group together, simulations do not converge during the run. A thorough observation of flow conditions can explain this behavior of CFD-DEM model utilized: the flow displays two different characters inside flow region that is laminar flow through disk-intervals and turbulent flow inside free flow region of bowl (see section 4.5).

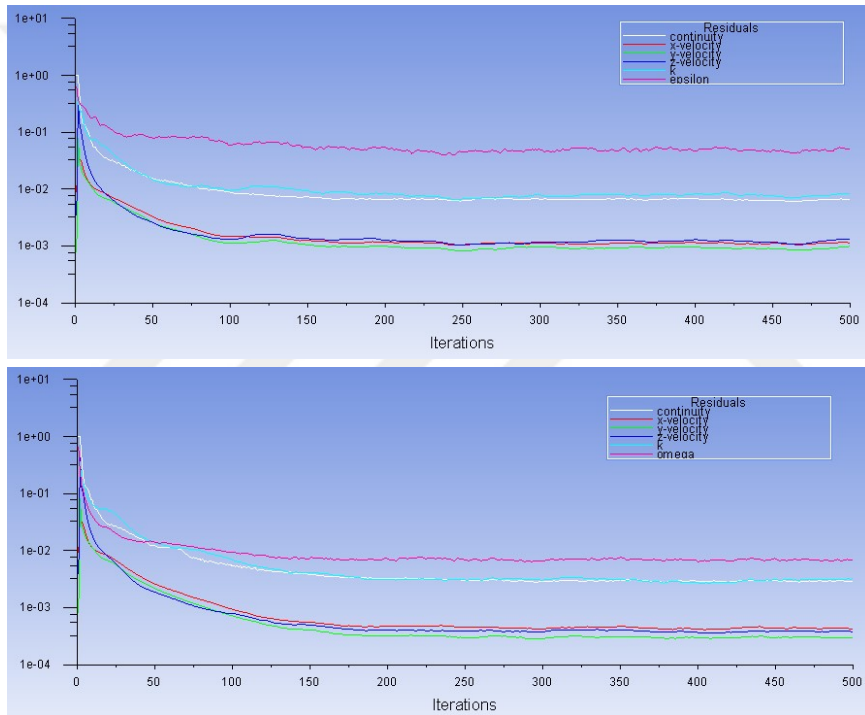


Figure 4.2. Residual graphics of RANS models applied to problem statement at steady state conditions: RNG $k-\epsilon$ (on top) and Standard $k-\omega$.

An alternative approach for that type of simulation would be to solve the domain in a ‘transient’ scheme, instead of steady-state work frame, this way removing the pseudo-transient character of discrete phase and binding the particle time-steps directly to solver time-steps. This is essentially a trade-off as real-time particle tracking causes several particles to become ‘incomplete’ at relatively larger time steps. Reducing the time-step beyond a certain limit (Figure 4.3), on the other hand, extends the duration for a single simulation run to days, in some cases, weeks.

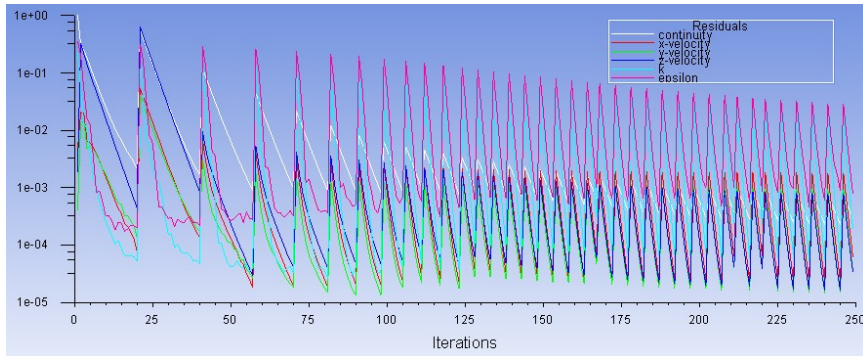


Figure 4.3. The CFD-DEM method for problem definition converges at every time step, at the expense of simulation time. Panel shows the solution for 10^{-5} s time steps.

The following titles will focus on different aspects of this CFD-DEM mainframe, comparing the results to theoretical calculations along with various scenarios considering critical parameters of centrifugal separation such as centrifugal forces and throughput ratios.

4.2. Sedimentation Performance for Various Cut-off Diameters

The four different disk intervals are tested for centrifugal separator formulae to obtain settling fractions, a point which these approaches fail to provide a basis on. The calculations regarding minimum particle diameters were conducted in a MATLAB GUI (MathWorks Inc., 2015), generated specifically to operate on Eqn.s 3.6-3.8 in this study, the details of which can be seen in Appendix-B. The results are summarized on Table 4.3 and Table 4.4. CFD-DEM Model response to various cut-off diameters of particles can be seen on Fig. 4.4.

Table 4.3. Minimum particle diameter calculation via theoretical approaches in different settler configurations.

Rib Height [mm]	Ambler (1959) [μm]	Leung (2007) [μm]	Kempken (1995) [μm]
0.25 (24 Disks, 1.436×10^{-2} kg/s)	0.707	0.738	1.428
0.40 (20 Disks, 1.709×10^{-2} kg/s)	0.845	1.494	1.707
0.60 (15 Disks, 1.714×10^{-2} kg/s)	0.977	1.727	1.974
0.80 (12 Disks 1.764×10^{-2} kg/s)	1.108	1.959	2.238

Table 4.4. Stokes' terminal velocities and total mass of injection for cut-off particles from Table 4.2 ($1\text{ng} = 10^{-6}\text{ mg}$).

Particle Diameter [μm]	Stokes' Velocity [m/s]	Particle Mass [ng]	Total Mass [ng]
0.707	8.41×10^{-6}	2.89×10^{-4}	0.0549
0.738	9.17×10^{-6}	3.29×10^{-4}	0.0624
0.845	1.20×10^{-5}	4.93×10^{-4}	0.0937
0.977	1.61×10^{-5}	7.62×10^{-4}	0.1448
1.108	2.07×10^{-5}	1.11×10^{-3}	0.2112
1.428	3.43×10^{-5}	2.38×10^{-3}	0.4522
1.494	3.76×10^{-5}	2.73×10^{-3}	0.5179
1.707	4.90×10^{-5}	4.07×10^{-3}	0.7724
1.727	5.02×10^{-5}	4.21×10^{-3}	0.7999
1.959	6.46×10^{-5}	6.14×10^{-3}	1.1675
1.974	6.56×10^{-5}	6.29×10^{-3}	1.1945
2.238	8.43×10^{-5}	9.16×10^{-3}	1.7407

Fig. 4.4 shows the erratic behavior of CFD-DEM model setup, as the particle size to be treated nears the critical (or cut-off) value assessed by the Stokes' law. Although Standard $k-\omega$ model barely reaches a mediocre R-squared value of 0.31, the RNG $k-\epsilon$ entirely fails to follow up as the particle diameter goes up, where the main inclination of the RANS model utilized should be better sedimentation ratios for larger diameter-particles.

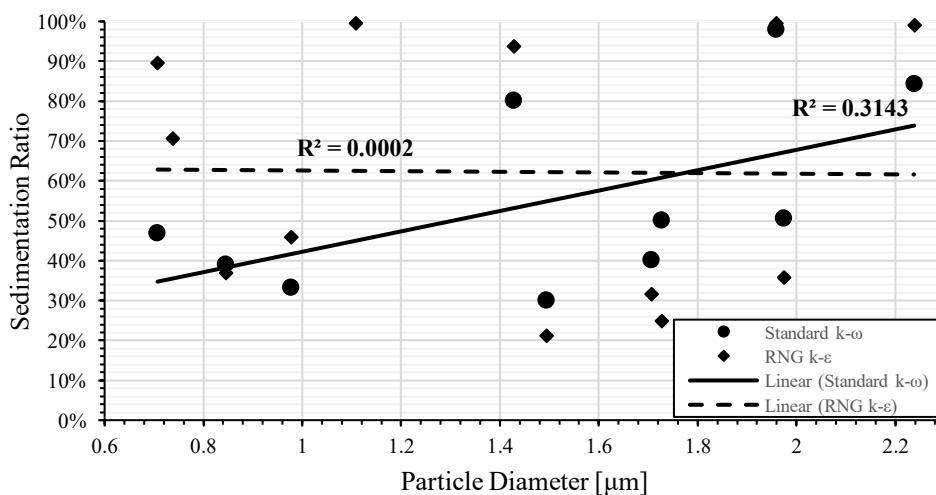


Figure 4.4. Settling efficiencies at cutoff diameters.

4.3. Scale-up Ability of the CFD-DEM Model

Reducing throughput rates allow substance to linger inside the solid-bowl for longer periods of time, exposed to centrifugal forces, therefore increasing the settling ability of an entire range of particles. Fig. 4.5 shows the relation between throughput rate and sedimentation percentage of the Zlotnik particle size range. Simulations are conducted using the standard $k - \omega$ RANS model for three alternative throughput rates, 5, 10 and 15 ton/h.

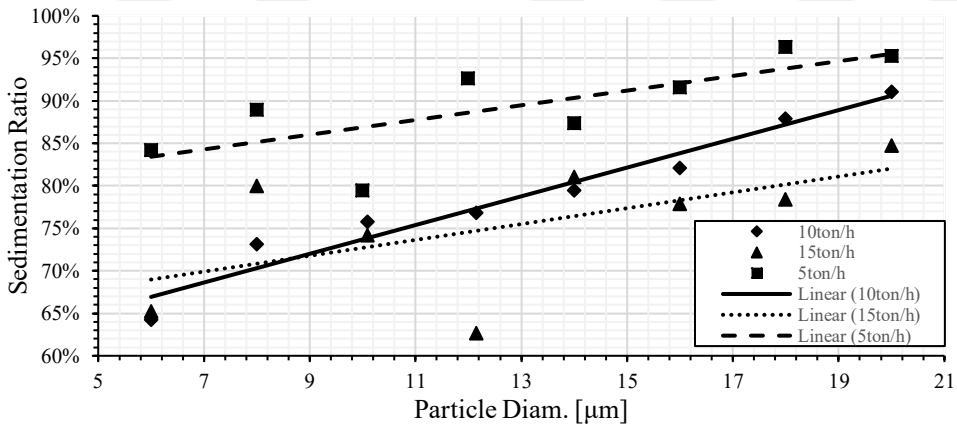


Figure 4.5. Sedimentation efficiencies at increasing throughput rates.

Contrary to throughput rates, bowl rate positively affects the separation performance only when increased: centrifugal forces increase with increasing bowl angular speeds. Three variations of bowl rates tested with RNG $k - \epsilon$ and the Standard $k - \omega$ turbulence models. Results can be seen on Fig. 4.6.

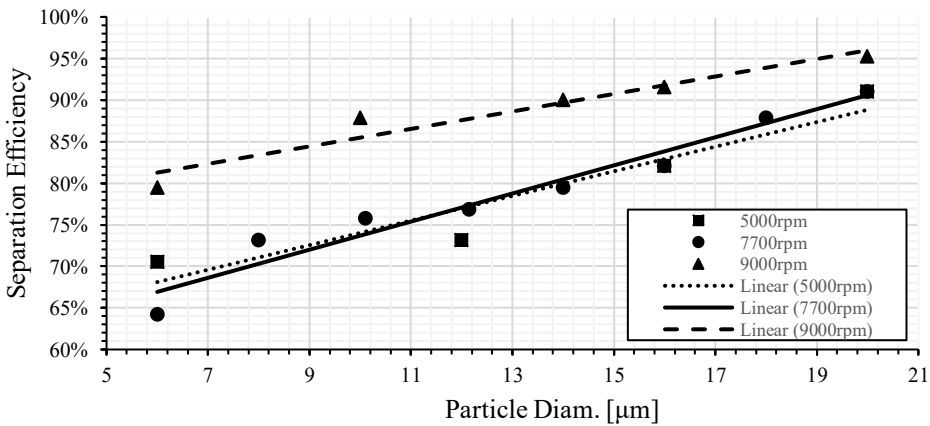


Figure 4.6. Separation efficiencies at increasing bowl rates.

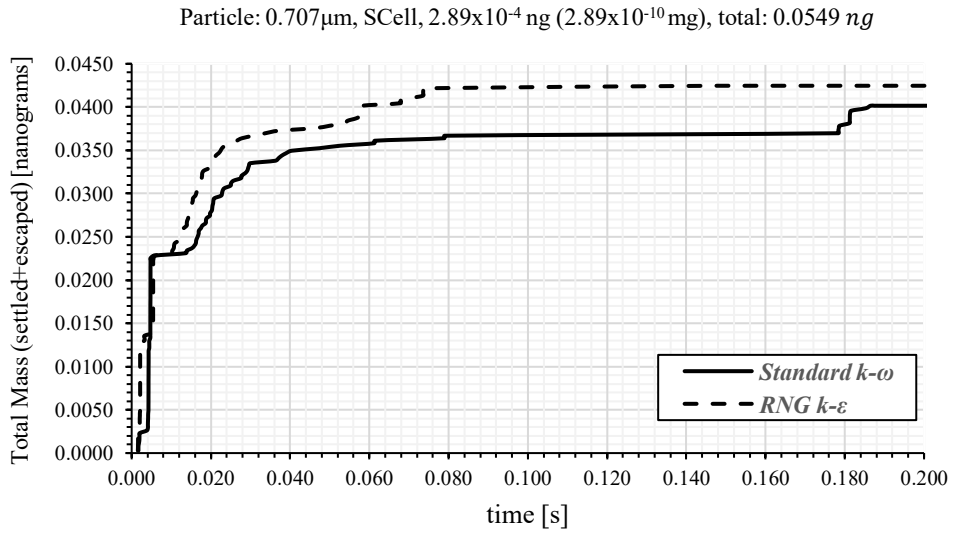
4.4. Particle Stagnation in Disk-stack

In the course of this study, numerous simulations were run in achieving the refined results by using a selection of RANS models, operating and boundary conditions etc. A peculiar result the PhD candidate observed time after time as the study developed, was that during every simulation, after a certain iteration/particle time step; some of the particles tracked were inclined to lose their relative kinetic energies and become ‘stagnant’, especially inside the disk-stack. This situation was first considered to be a ‘fluke’ originated from the absence or misinterpretation of an arbitrary parameter. After countless simulation runs spanning over three years however, the occurrence is now well-established. In retrospect, the particle stagnation became one of the important results of this study. When regarded a structural phenomenon instead of a calculation error which was the obvious option we considered first then immediately abandoned when every simulation uncovered a number of particles of this fate; particle stagnation may be the result of following issues;

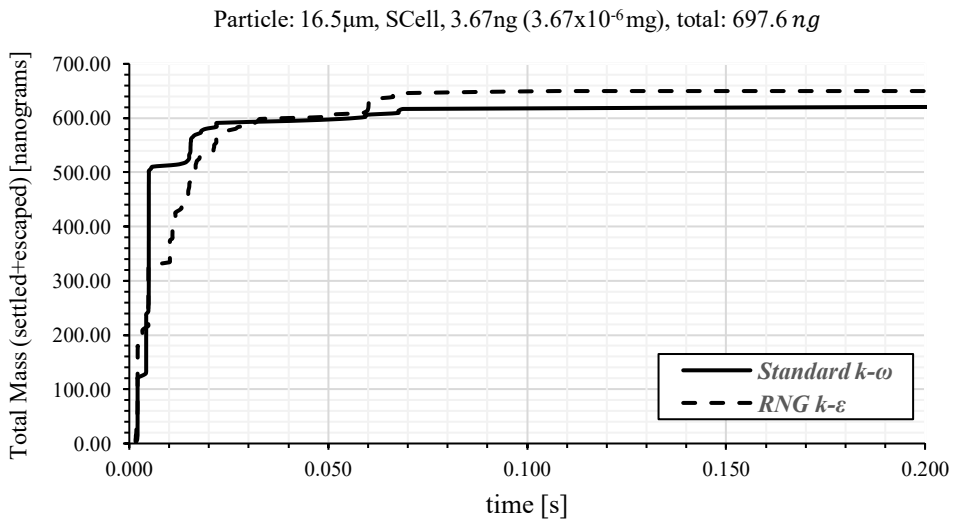
- Shear forces near the disk walls override the inertial forces acting on the particle,
- Uneven distribution of mass flow rate through the subsequent channels (see title 4.6),
- When outside of the disk-stack, particles may become stagnant due to cold spots where the continuous fluid itself lost relative velocity, become stagnant.

This situation however, is not an *entirely* unpleasant situation. In most cases, as there will be no trace of these particles (i.e. somatic cells) on the outlet samples, this phenomenon improves the sedimentation efficiency of a centrifuge. Data on Fig. 4.7 (next page) also in Fig 4.8 (for Shekhawat avg. (16.5 μ m) particle) are harvested to give an insight about particle stagnation, where total masses of injected particles are calculated as;

- **Ambler min. (0.707 μ m) particle;**
Total mass: 0.0549 ng, solved: 0.0425 ng (77.4% ; RNG $k - \epsilon$).
- **Shekhawat avg. (16.5 μ m) particle;**
Total mass: 697.6 ng, solved: 649.87 ng (93.2% ; RNG $k - \epsilon$).



(a)



(b)

Figure 4.7. Particle stagnation in disk-stack during the process occurs regardless the turbulence model employed. (a) cut-off particle and (b) average particle size. There are only slight differences between the two RANS models.

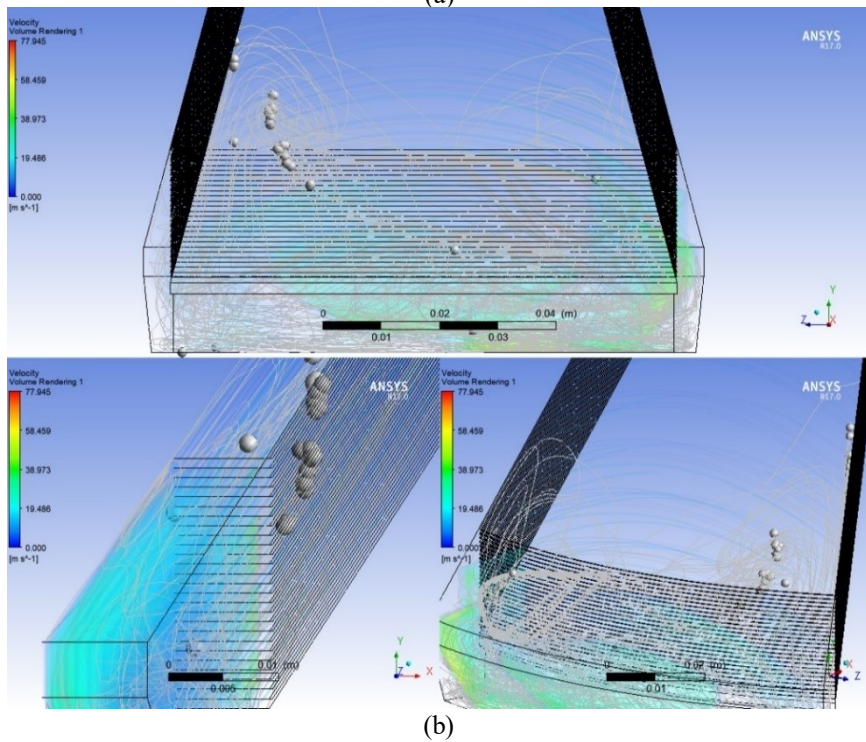
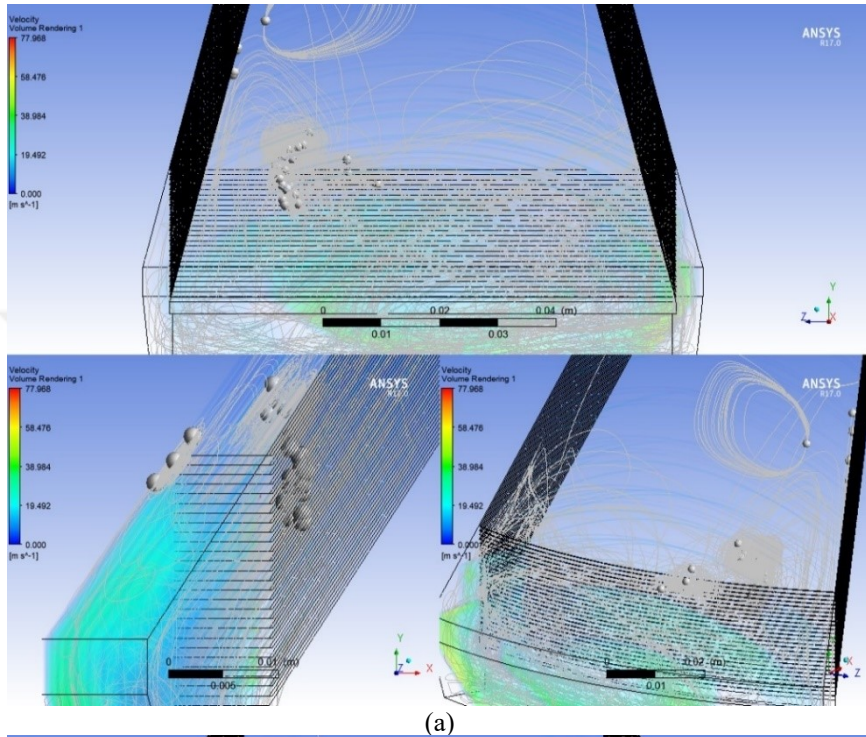


Figure 4.8. Particle tracks and occurrence of stagnation in disk-stack for Shekhawat avg. ($16.5\mu\text{m}$) particle with RNG $k - \epsilon$ (a) and the Standard $k - \omega$ (b) RANS models.

4.5. Turbulence Model Comparison for 3-D Flow Field

Discrete element behavior in any flow region is dominantly determined by viscous model applied. Inside a 3-D, simplified geometry (see Fig. 3.15) the flow characteristics of milk are investigated via two prominent turbulence models: RNG $k - \epsilon$ and the Standard $k - \omega$.

The simplified disk-stack representation to be utilized in the following simulations is prepared by maintaining the exact geometric details, alongside the process parameters like bowl outlet pressure and angular velocity. The only limited feature of the complete disk-stack assembly during CFD translation is indeed the number of disks, hence the throughput rate is reduced accordingly.

Locating as many disks as the centrifuge bowl can be stacked up with is the main mechanic of reducing the flow rate between individual disks. This ‘filtering’ effect of continuous medium generates extremely low flow rates, therefore allowing a laminar flow in the presence of drastic centrifugal forces. The interruption inside flow region by the presence of disk-stack also has a side-effect: the uniform pattern of the continuous medium on a stable centrifugal field is directly and negatively affected by disk-stack that splits the total throughput into uneven channel flows. We observed that the channels (disk intervals) are either overloaded during the process or there is no significant flow between certain disks. Either case supports the hypothesis of Leung, on computational fluid dynamics basis.

Both turbulence models are investigated in their abilities to represent this character: a laminar flow between the subsequent disks and an unsuppressed generation of eddies on the free volume of bowl; hence letting the particles sediment more quickly against the bowl walls. Pressure distributions calculated by both models, as well as relative velocity diagrams backed with vector tracking schemes and turbulence kinetic energy comparisons are displayed in comparison in the Fig. 4.9-4.13 in detail.

A preliminary analysis on how relative velocity varies through the separation field; both disk-stack and free flow regions (Fig. 4.9). The relative velocities, when the beach length just below the settler area is assumed to be critical length for Reynolds number, displays local Re numbers well above 10^5 level. flow character in the vicinity of settler. On the contrary, low-Reynolds numbers can be calculated in the same contour graph, indicating a laminar flow through disk-stack which is essential for sedimentation/particle filtering in a continuous process.

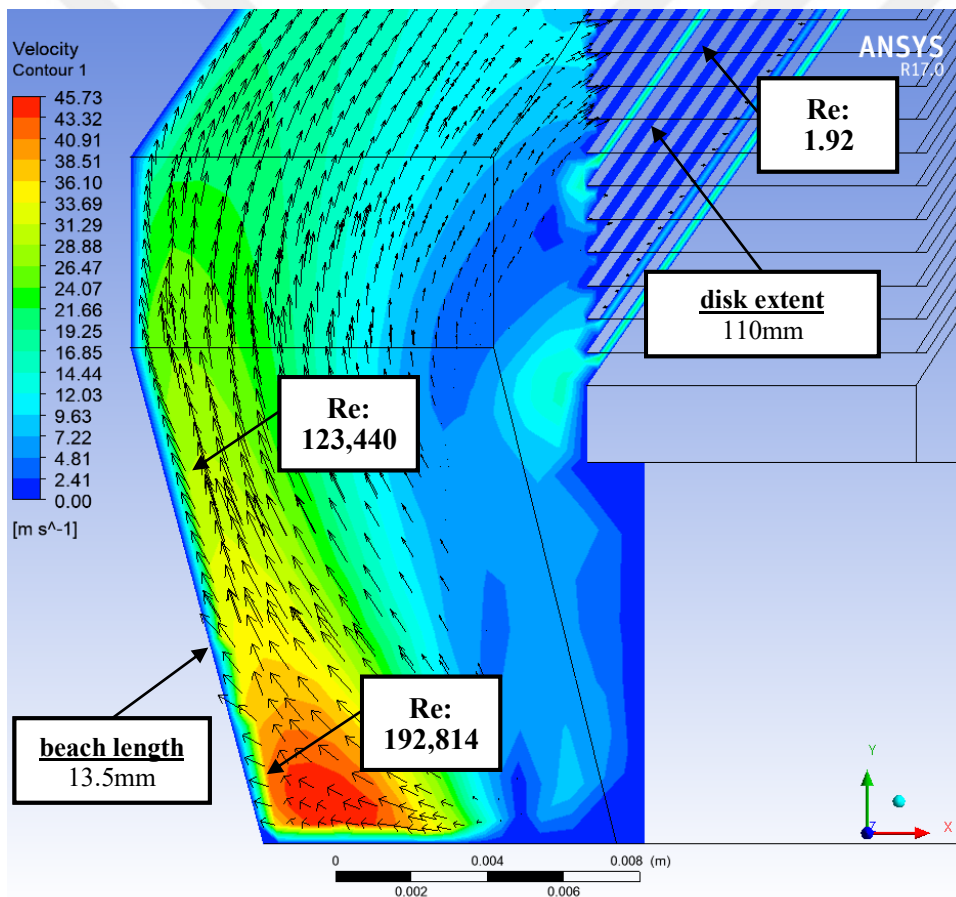


Figure 4.9. Reynolds number survey near settler beach and through disk interval.
Representation: Standard $k-\omega$; 7700 rpm, 1.436×10^{-2} kg/s throughput rate.

In terms of pressure distribution through the sedimentation zone (i.e. free-flow zone), the RANS methods show a similar solution on Fig. 4.10. Higher pressure fields between the disks are visible on the geometry (left column, for both methods), that is against the direction of rotation (toward $-y$).

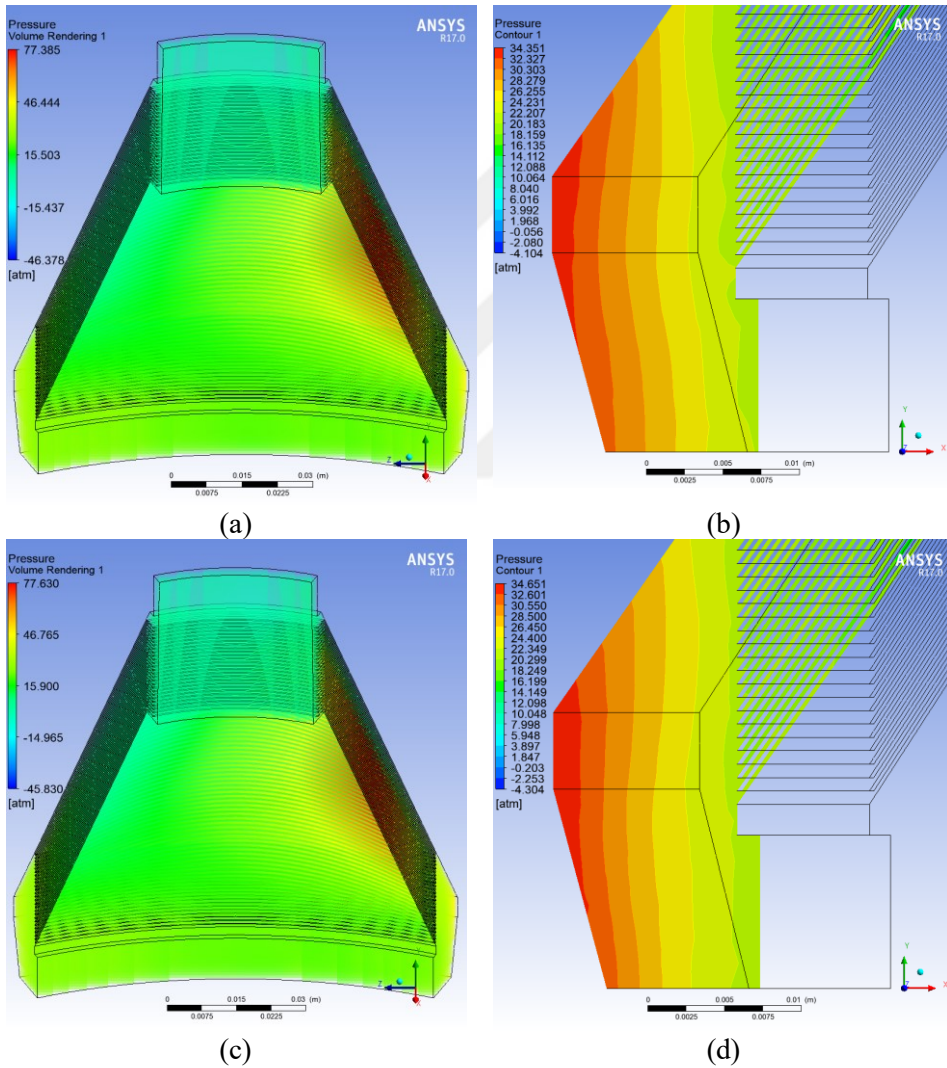


Figure 4.10. Pressure distribution in the flow region for RNG $k - \epsilon$ (a, b) and the Standard $k - \omega$ (c, d) RANS models where figures on the right represents the cross-section views.

The first significant distinction between the turbulence interpretation surfaces when the velocity contours are extracted (Figure 4.11). Having a very similar outlook on volume rendering (left column), a cross-plane section projection of velocity shows the adeptness of the Standard $k-\omega$ RANS modeling. The relative velocity distribution forms a well aligned, unidirectional flow field with the $k-\omega$ (right-bottom) while its counterpart resolves to a haphazard look both on velocity contours and vector field.

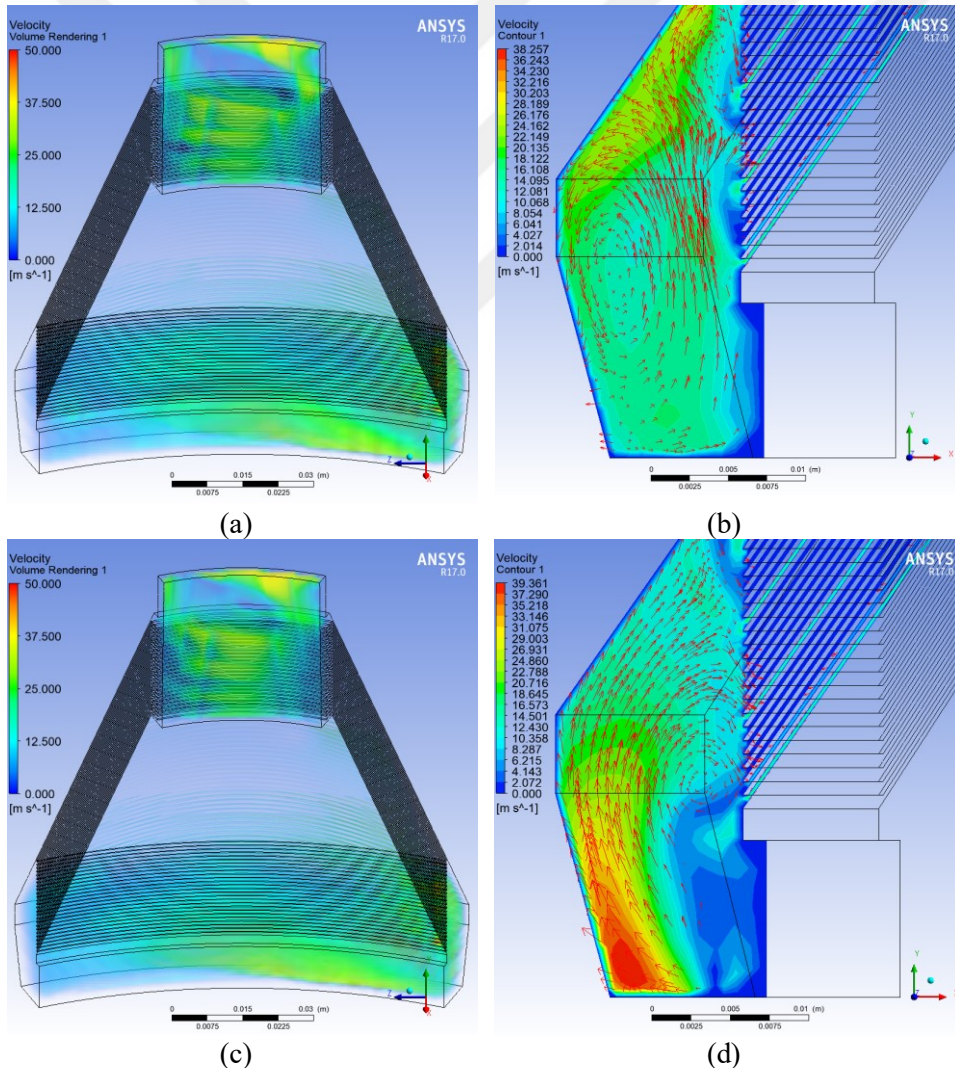


Figure 4.11. Velocity distribution in the flow region for RNG $k-\epsilon$ (a, b) and Standard $k-\omega$ (c, d) RANS models.

The Standard $k-\omega$ model grasps turbulence kinetic energy distribution more conveniently when compared to RNG $k-\varepsilon$, assessing from the cross-section view of $k-\omega$ model (Figure 4.12; bottom right). However, when the two volume renderings are compared, the RNG $k-\varepsilon$ shows a more restrained overview against the Standard $k-\omega$ which comes with several arbitrary hot point occurrences.

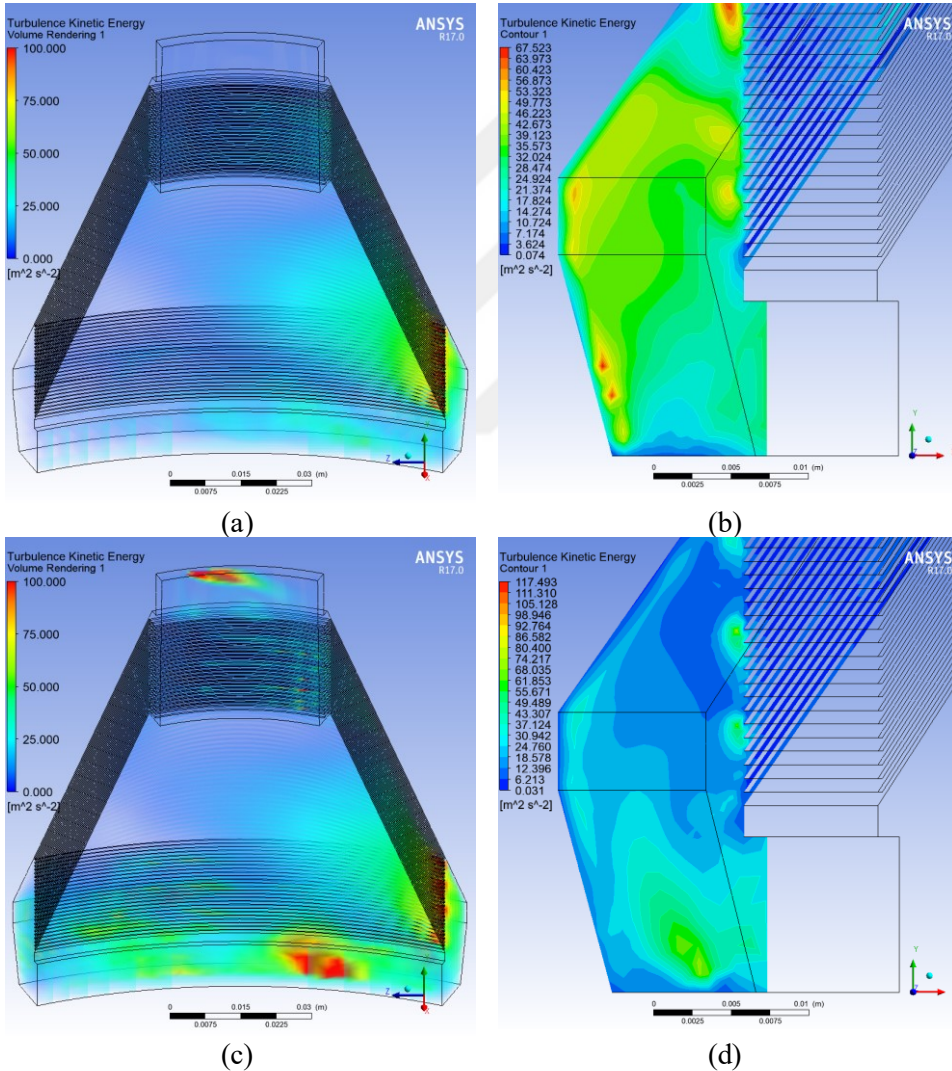


Figure 4.12. Turbulence Kinetic Energy distribution in the flow region for RNG $k-\varepsilon$ (a, b) and Standard $k-\omega$ (c, d) RANS models.

Instead of using residual monitor to assess the turbulence modeling, a surface monitor is set on the clarified liquid outlet: The throughput rate on the inlet (1.436×10^{-2} kg/s for this point), should be balanced out on the mass outflow. Fig. 4.13 shows both RANS methods quickly converge in about 35 iterations that is 0.035sec.

The only difference between the RNG $k-\epsilon$ and Standard $k-\omega$ models appears to be the transition to steady-state behavior on that surface. While the $k-\epsilon$ tends to stabilize more quickly, the method suffers a ‘dip’ in the first iterations. $k-\omega$ model on the other hand, shows a more ‘suppressed’ convergence character.

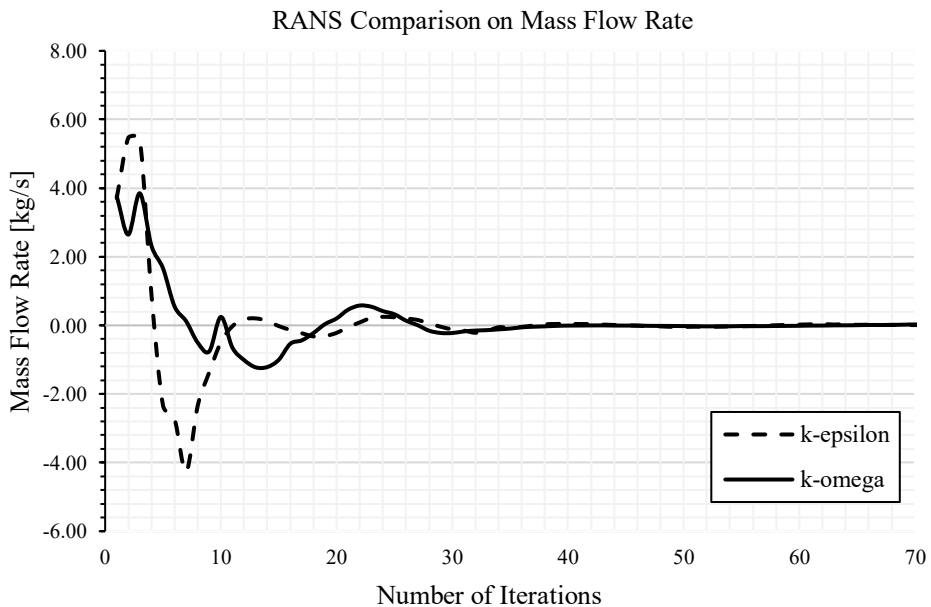


Figure 4.13. Mass flow rate quickly stabilizes for each calculation method.

5. CONCLUSION

In the context of this thesis study, the centrifugal sedimentation of a certain type of particles (somatic cells or leukocytes) inside a continuous medium (bovine milk) has been modeled in a computer aided engineering software, and its results compared to that of an actual field test.

In modeling the particle-laden flow phenomenon, a popular method called the Euler-Lagrange method has been employed, where the continuous medium was calculated via two different Locally Averaged Navier-Stokes (RANS) algorithms, namely RNG $k-\varepsilon$ and the Standard $k-\omega$, while the particulate flow is tracked with Lagrangian frame of reference.

For injected particle diameters, two different methods have been utilized:

The average somatic cell diameter, as well as the size range of cells are adopted from the relevant literature, the former having utilized in model validation on CFD-DEM software.

The minimum diameters that can be sedimented out have been calculated via methods, that benefits from an independent approach, again found in the literature. Since there are more than one convention in calculating the lower limit of treatable particles, multiple diameters have been tested.

Results, as mentioned above, delivered a significant compromise as to validity and scale-up abilities of CFD-DEM methodology in defining this intricate problem. Increasing diameter, hence the mass of an individual particle causes larger centrifugal-inertial forces to act on it, therefore the particles with higher diameters are more prone to sedimentation. Yet we can see this outcome by observing carefully the inclination, arranged in trendlines supported with RMS values.

As to practical results obtained in terms of designing better and more efficient centrifuges, the study showed us the results summarized below.

Despite the fact that density difference affects particles regardless of their size, it is also valid that larger diameter particles are sedimented out with less effort (i.e. settling time hence the energy consumed) with higher percentages,

Increasing disk interval (rib height) allows more particles to escape through the clarified fluid. Therefore, bowl space is stacked-up with as many disks as the machine design allows.

Reducing the disk interval does not necessarily improve the particle sedimentation, on the contrary, increases the number of particles that get stuck between the disks, therefore the particle stagnation. A good trade-off is then required to guarantee the separation efficiency only comes out of actually sedimented particles.

Assuming the mass flow load is distributed evenly throughout the disk-stack is simply incorrect; flow distribution is *altered* along the consecutive disks, therefore causing particles in some intervals where the flow rate nears zero kg/s, more particles reach to a stand-still (particle-stagnation).

Separation efficiency increases with decreasing throughput rate. 5 tons/h is selected in our study as the lower limit of throughput rate. By maintaining all other process and model parameters, the lower limit of throughput rate offsets the remaining two options, 10 tons/h (optimal rate) and 15 tons/h, in terms of better sedimentation of particles, as explained previously.

Finally, with increasing bowl speeds, the separation efficiency is dramatically increased: higher the centrifugal forces, better the chances of sedimentation for particles of every size.

For the last two hypotheses, a compromise must be made: reducing the throughput rate will also reduce the milk admittance, hence the entire compounds production capacity per unit time. Increasing the angular speeds of bowl, on the other hand, requires a heavier and larger machinery due to power requirements and dynamic loading effects.

In the course of the study, we also had the insight on topics below.

Multiple field examples from different times of year or a season, also different stages of process (initial introduction of milk, steady state operation etc.) would help us better improve the simulation structure.

The simulations in this study were implemented via BTSCC index only. We compared the input and clean output somatic cell counts to understand sedimentation capability of a specific centrifuge. A general sediment analysis including additional milk contaminants like pulverized hay and udder tissue would also yield field data to emphasize what ultimate range of particles can be treated in a milk clarifying centrifuge.

Simulation setup can be applied to alternate medium for scale-up purposes. Theoretically, with the same clarifying centrifuge configuration, different media can be treated. With adequate field tests and analyses supported with CFD-DEM, the machinery best suited for a specific application can be suggested to the third parties with accuracy, getting fewer complaints and rebate.

To summarize, this study focuses on successfully representing the discrete phase behavior in a centrifugal field by employing different turbulence models and a popular particle tracking scheme, that is, the Lagrangian frame of reference. The model and computational output show convenient results on and in the vicinity of validation point. Still the modeling approach can be further improved with detailed field data.

REFERENCES

- Abcam: Introduction to Flow Cytometry 2019. <https://www.abcam.com/protocols/introduction-to-flow-cytometry>. Last Accessed: 26/06/2019.
- Akbarzadeh, V., and Hrymak, A. N. 2016. Coupled CFD-DEM of particle-laden flows in a turning flow with a moving wall. **Computers and Chemical Engineering**, 86, 184–191. <https://doi.org/10.1016/j.compchemeng.2015.12.020>
- Ambler, C. M. 1959. The theory of scaling up laboratory data for the sedimentation type centrifuge. **Journal of Biochemical and Microbiological Technology and Engineering**, 1(2), 185–205. <https://doi.org/10.1002/jbmte.390010206>
- ANSYS Inc. 2010. Fluent Theory Guide. Ansys Inc. Southpointe, Canonsburg, PA.
- Arsalanloo, A., and Abbasalizadeh, M. 2017. Numerical study on deposition of particles in a 90° bend in the presence of swirling flow using Eulerian-Lagrangian method. **Powder Technology**, 320, 285–294. <https://doi.org/10.1016/j.powtec.2017.07.050>
- Aytekin, İ., and Boztepe, S. (2017). Süt Sığırlarında Somatik Hücre Sayısı, Önemi ve Etki Eden Faktörler. **Turkish Journal of Agriculture - Food Science and Technology**, 2(3), 112. <https://doi.org/10.24925/turjaf.v2i3.112-121.66>
- Baccioni, L., and Peri, C. 2014. Centrifugal separation. The Extra-Virgin Olive Oil Handbook. John Wiley & Sons, Ltd., ISBN 978-1-118-46045-0, West Sussex, United Kingdom.
- Bylund, G., and Svensson, C. 1995. Dairy processing handbook: The Chemistry of Milk. Tetra Pak Processing Systems AB, Lund, Sweden.
- Chang, Y. C., Chiu, T. Y., Hung, C. Y., and Chou, Y. J. 2019. Three-dimensional Eulerian-Lagrangian simulation of particle settling in inclined water columns. **Powder Technology**, 348, 80–92. <https://doi.org/10.1016/j.powtec.2019.02.052>
- Concha A., F. 2014. Solid-Liquid Separation in the Mining Industry. Springer International Publishing, ISBN 978-3-319-02483-7, Switzerland.
- Dosogne, H., Vangroenweghe, F., Mehrzad, J., Massart-Leën, A. M., and Burvenich, C. 2010. Differential Leukocyte Count Method for Bovine Low Somatic Cell Count Milk. **Journal of Dairy Science**, 86(3), 828–834. [https://doi.org/10.3168/jds.s0022-0302\(03\)73665-0](https://doi.org/10.3168/jds.s0022-0302(03)73665-0)
- Elghobashi, S. 1991. Particle-laden turbulent flows: direct simulation and closure models. **Applied Scientific Research**. <https://doi.org/10.1007/BF02008202>

- Elghobashi, S. 1994. On predicting particle-laden turbulent flows. **Applied Scientific Research**. <https://doi.org/10.1007/BF00936835>
- Flottweg Separation Technology, Separator Fetures: Disk-stack, 2018. <https://www.flottweg.com/engineering/separator-features/disk-stack> Last Accessed: 05/06/2019.
- GEA Westfalia, Nozzle Separators for Chemicals and Minerals, 2018. <https://www.gea.com/en/>. Last Accessed 05/06/2019.
- Genevaux, O., Habibi, A., and Dischler, J. M. 2003. Simulating Fluid-Solid Interaction. **Graphics Interface**. <https://doi.org/10.20380/gi2003.04>
- Gidaspow, D. 2012. Multiphase Flow and Fluidization: Continuum and Kinetic Theory Descriptions. Springer International Publishing, ISBN 978-3-319-45490-0, Switzerland.
- Gunasekera, T. S., Veal, D. A., and Attfield, P. V. 2003. Potential for broad applications of flow cytometry and fluorecence techniques in microbiological and somatic cell analyses of milk. **International Journal of Food Microbiology**. [https://doi.org/10.1016/S0168-1605\(02\)00546-9](https://doi.org/10.1016/S0168-1605(02)00546-9)
- Hagnestam-Nielsen, C., Emanuelson, U., Berglund, B., and Strandberg, E. 2009. Relationship between somatic cell count and milk yield in different stages of lactation. **Journal of Dairy Science**. <https://doi.org/10.3168/jds.2008-1719>
- Harting, J., Frijters, S., Ramaioli, M., Robinson, M., Wolf, D. E., and Luding, S. 2014. Recent advances in the simulation of particle-laden flows. **European Physical Journal: Special Topics**. <https://doi.org/10.1140/epjst/e2014-02262-3>
- HEINKEL Drying and Separation Group 2017. Horizontal Peeler Centrifuge Pharma, <https://www.heinkel.com>. Last Accessed 06/06/2019
- Hertz, H. 1882. Ueber die Berührung fester elastischer Körper. **Journal Fur Die Reine Und Angewandte Mathematik**. <https://doi.org/10.1515/crll.1882.92.156>
- Jayarao, B. M., Pillai, S. R., Sawant, A. A., Wolfgang, D. R., and Hegde, N. V. 2010. Guidelines for Monitoring Bulk Tank Milk Somatic Cell and Bacterial Counts. **Journal of Dairy Science**. [https://doi.org/10.3168/jds.s0022-0302\(04\)73493-1](https://doi.org/10.3168/jds.s0022-0302(04)73493-1)

- Jelen, P. 2000. Dairy Technology. **International Dairy Journal**.
[https://doi.org/10.1016/s0958-6946\(00\)00077-7](https://doi.org/10.1016/s0958-6946(00)00077-7)
- Kartushinsky, A., Tisler, S., Oliveira, J. L. G., and van der Geld, C. W. M. 2016. Eulerian-Eulerian modelling of particle-laden two-phase flow. **Powder Technology**, 301, 999–1007. <https://doi.org/10.1016/j.powtec.2016.07.053>
- Kempken, R., Preissmann, A., and Berthold, W. 1995. Assessment of a disc stack centrifuge for use in mammalian cell separation. **Biotechnology and Bioengineering**, 46(2), 132–138. <https://doi.org/10.1002/bit.260460206>
- Kilara, A. 2011. Dairy Ingredients for Food Processing. Wiley-Blackwell Publishing, ISBN 978-0-81-381746-0, Ames, IA, United States.
- Koess, C., and Hamann, J. 2008. Detection of mastitis in the bovine mammary gland by flow cytometry at early stages. **Journal of Dairy Research**.
<https://doi.org/10.1017/s0022029908003245>
- Lauder, B. E., and Spalding, D. B. 1974. The numerical computation of turbulent flows. **Computer Methods in Applied Mechanics and Engineering**.
[https://doi.org/10.1016/0045-7825\(74\)90029-2](https://doi.org/10.1016/0045-7825(74)90029-2)
- Leung, W. W. F. 2007. Centrifugal Separations in Biotechnology. Centrifugal Separations in Biotechnology, Elsevier Limited, ISBN 13: 978-1-85-617477-0, Oxford, United Kingdom.
- Li, N., Richoux, R., Boutinaud, M., Martin, P., and Gagnaire, V. 2014. Role of somatic cells on dairy processes and products: A review. **Dairy Science and Technology**. <https://doi.org/10.1007/s13594-014-0176-3>
- Lindner, J., Menzel, K., and Nirschl, H. 2013. Simulation of magnetic suspensions for HGMS using CFD, FEM and DEM modeling. **Computers and Chemical Engineering**. <https://doi.org/10.1016/j.compchemeng.2013.03.012>
- Liu, M. B., and Liu, G. R. 2010. Smoothed particle hydrodynamics (SPH): An overview and recent developments. **Archives of Computational Methods in Engineering**. <https://doi.org/10.1007/s11831-010-9040-7>
- Maskaniyan, M., Rashidi, S., and Esfahani, J. A. 2017. A two-way couple of Eulerian-Lagrangian model for particle transport with different sizes in an obstructed channel. **Powder Technology**, 312, 260–269.
<https://doi.org/10.1016/j.powtec.2017.02.031>
- MathWorks 2015. Creating Graphical User Interfaces, MATLAB User Guide. Mathworks, Inc., Natick, MA, United States.

- Melo, G. J. A. d., Gomes, V., Baccili, C. C., Almeida, L. A. L. d., and Lima, A. C. d. C. 2015. A robust segmentation method for counting bovine milk somatic cells in microscope slide images. **Computers and Electronics in Agriculture**, 115, 142–149. <https://doi.org/10.1016/j.compag.2015.05.018>
- Mendlik, F. 1950. Pasteurization. **Journal of the Institute of Brewing**. <https://doi.org/10.1002/j.2050-0416.1950.tb01526.x>
- Monaghan, J. J. 2005. Smoothed particle hydrodynamics. **Reports on Progress in Physics**. <https://doi.org/10.1088/0034-4885/68/8/R01>
- Náraigh, L., and Barros, R. 2016. Particle-laden viscous channel flows: Model regularization and parameter study. **European Journal of Mechanics, B/Fluids**, 59, 90–98. <https://doi.org/10.1016/j.euromechflu.2016.05.005>
- Ndimande, C. B., Cleary, P. W., Mainza, A. N., and Sinnott, M. D. 2019. Using two-way coupled DEM-SPH to model an industrial scale Stirred Media Detritor. **Minerals Engineering**. <https://doi.org/10.1016/j.mineng.-2019.03.001>
- Norouzi, H. R., Zarghami, R., Sotudeh-Gharebagh, R., and Mostoufi, N. 2016. Coupled CFD-DEM Modeling: Formulation, Implementation and Application to Multiphase Flows, Coupled CFD-DEM Modeling: Formulation, Implementation and Application to Multiphase Flows. John Wiley & Sons Ltd., ISBN 978-1-11-900513-1, Oxford, United Kingdom.
- Park, Y. W., and Haenlein, G. F. W. 2013. Milk and Dairy Products in Human Nutrition: Production, Composition and Health. Milk and Dairy Products in Human Nutrition: Production, Composition and Health. Wiley-Blackwell, ISBN 978-0-47-067418-5, West Sussex, United Kingdom.
- Records, A., and Sutherland, K. 2007. Decanter Theory: Decanter Centrifuge Handbook. Elsevier Science Ltd., ISBN 1-85617-369-0, Oxford, United Kingdom.
- Reinemann, D. J. 2013. Milking Machines and Milking Parlors. In Handbook of Farm, Dairy and Food Machinery Engineering. Elsevier Inc., ISBN 978-0-12-385881-8, NY, United States.
- Rola, J. G., Larska, M., Grzeszuk, M., Bocian, L., Kuta, A., Polak, M. P., and Rola, J. 2014. Bulk tank milk somatic cell counts in dairy herds with different bovine viral diarrhoea virus status in Poland. **Preventive Veterinary Medicine**, 116(1–2), 183–187. <https://doi.org/10.1016/j.prevetmed.-2014.06.007>

- Saidi, M. S., Rismanian, M., Monjezi, M., Zendeabad, M., and Fatehboroujeni, S. 2014. Comparison between Lagrangian and Eulerian approaches in predicting motion of micron-sized particles in laminar flows. **Atmospheric Environment**, 89, 199–206. <https://doi.org/10.1016/j.atmosenv.2014.01.069>
- Shekhawat, L. K., Sarkar, J., Gupta, R., Hadpe, S., and Rathore, A. S. 2018. Application of CFD in Bioprocessing: Separation of mammalian cells using disc stack centrifuge during production of biotherapeutics. **Journal of Biotechnology**. <https://doi.org/10.1016/j.jbiotec.2017.12.016>
- Spreer, E. 2017. Milk and Dairy Product Technology. Marcel Dekker, Inc., ISBN 978-0-82-470094-5, NY, United States.
- Stokes, G. G. 1851. On the Theories of the Internal Friction of Fluids in Motion, and of the Equilibrium and Motion of Elastic Solids. **Mathematical and Physical Papers Vol.1, 9**, 75–129. <https://doi.org/10.1017/CBO97805117022>
- Stolarski, T., Nakasone, Y., and Yoshimoto, S. 2006. Engineering Analysis with ANSYS Software. Elsevier Butterworth-Heinemann, ISBN 978-0-75-066875-X, Oxford, United Kingdom.
- Subramaniam, S. 2013. Lagrangian-Eulerian methods for multiphase flows. **Progress in Energy and Combustion Science**. <https://doi.org/10.1016/j.pecs.2012.10.003>
- The Panama Perspective 2018. Fight Against Agricultural Imports. <https://panamaadvisoryinternationalgroup.com/blog/news-from-panama/-fight-agricultural-imports/>. Last Accessed: 21/06/2019.
- Thunman, H., Leckner, B., Niklasson, F., and Johnsson, F. 2002. Combustion of wood particles - A particle model for Eulerian calculations. **Combustion and Flame**. [https://doi.org/10.1016/S0010-2180\(01\)00371-6](https://doi.org/10.1016/S0010-2180(01)00371-6)
- Triebel, H., Birnie G. D., and Rickwood, D. 2007. Centrifugal Separations in Molecular and Cell Biology. Butterworths & Co. Publishers Ltd., ISBN 978-0-40 870803-4, London, United Kingdom.
- Tsuji, Y., Tanaka, T., and Ishida, T. 1992. Lagrangian numerical simulation of plug flow of cohesionless particles in a horizontal pipe. **Powder Technology**. [https://doi.org/10.1016/0032-5910\(92\)88030-L](https://doi.org/10.1016/0032-5910(92)88030-L)
- Tu, J., Inthavong, K., and Wong, K. K. L. 2015. Computational Fluid Structure Interaction. Elsevier Science Ltd., ISBN 978-0-12-814770-2, Oxford, United Kingdom.

- Università Di Pavia 2018. http://fisica.unipv.it/Mihich/FM/7-PDF/7-PDF_1_sect05. Last Accessed: 02/06/2019.
- van der Linden, J. P. 1987. Liquid-Liquid Separation in Disc-stack Centrifuges. Delft University of Technology, Ph.D. Thesis, Netherlands.
- van Reis, R., Leonard, L. C., Hsu, C. C., and Builder, S. E. 1991. Industrial scale harvest of proteins from mammalian cell culture by tangential flow filtration. **Biotechnology and Bioengineering**, 38(4), 413–422. <https://doi.org/10.1002/bit.260380411>
- Vesilind, P. A. 1980. The Rosin-Rammler particle size distribution. **Resource Recovery and Conservation**, 5 (1980)275-277. [https://doi.org/10.1016/0304-3967\(80\)90007-4](https://doi.org/10.1016/0304-3967(80)90007-4)
- Walstra, P., Geurts, T. J., Noomen, A., Jellema, A., Van Boekel, M. A. J. S. 1999. Dairy Technology: Principles of Milk Properties and Processes. Marcel Dekker Inc., ISBN 978-0-82-470228-X, NY, United States.
- White, F. M. 2016. Fluid Mechanics 8th in SI units. McGraw-Hill Education, ISBN 978-9-38-596549-4, NY, United States.
- Wilbey, R. A. 2004. Homogenization of Milk, Encyclopedia of Dairy Sciences. Elsevier Science Ltd., ISBN 978-0-12-374407-4, London, United Kingdom.
- Zhang, Z., and Chen, Q. 2007. Comparison of the Eulerian and Lagrangian methods for predicting particle transport in enclosed spaces. **Atmospheric Environment**, 41(25), 5236–5248. <https://doi.org/10.1016/j.atmosenv.-2006.05.086>
- Zlotnik, I. 2012. Types of Cells Present in Cow's Milk. **Journal of Comparative Pathology and Therapeutics**, 57, 196-IN6. [https://doi.org/10.1016/s0368-1742\(47\)80025-6](https://doi.org/10.1016/s0368-1742(47)80025-6)

APPENDICES

APPENDIX A: RNG k – ϵ Model Survey

Continuous Medium: Bovine Milk
Particle: Somatic Cell (Leukocytes)
Software Ver.: ANSYS 17.0

Algorithm	RANS	Option 1	Option 2	Option 3	Option 4	Particle Diameter	Sedimentation %	Mass Outflow
Pressure Based	k- ϵ	Realizable	-	-	Non-equilibrium Wall Functions	0.1 μm	75.08%	PASS
Pressure Based	k- ϵ	Realizable	Enhanced Wall Treatment	-	-	0.1 μm	40.66%	PASS
Pressure Based	k- ϵ	Realizable	Standard Wall Functions	-	-	0.1 μm	45.90%	PASS
Pressure Based	k- ϵ	RNG	-	-	Standard Wall Functions	0.1 μm	37.05%	FAIL
Pressure Based	k- ϵ	RNG	Differential Viscosity Model	Standard Wall Functions	-	0.1 μm	3.61%	FAIL
Pressure Based	k- ϵ	RNG	Differential Viscosity Model	Swirl Dominated	Standard Wall Functions	0.1 μm	33.11%	FAIL
Pressure Based	k- ϵ	RNG	Differential Viscosity Model	Swirl Dominated	Non-equilibrium Wall Functions	0.1 μm	43.93%	FAIL

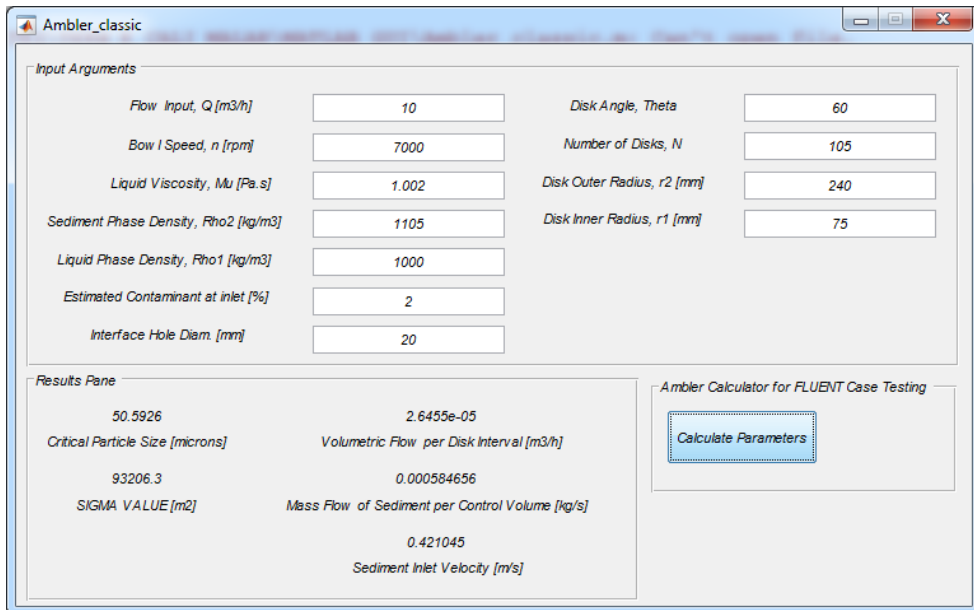
contd.

Algorithm	RANS	Option 1	Option 2	Option 3	Option 4	Particle Diameter	Sedimentation %	Mass Outflow
Pressure Based	k- ϵ	RNG	Differential Viscosity Model	-	Non-equilibrium Wall Functions	0.1 μm	0.00%	PASS
Pressure Based	k- ϵ	RNG	-	Swirl Dominated	Non-equilibrium Wall Functions	0.1 μm	0.00%	PASS
Pressure Based	k- ϵ	RNG	Differential Viscosity Model	Swirl Dominated	Enhanced Wall Treatment	0.1 μm	47.87%	FAIL
Pressure Based	k- ϵ	RNG	Differential Viscosity Model	Swirl Dominated	Scalable Wall Functions	0.1 μm	52.13%	FAIL
Pressure Based	k- ϵ	RNG	Enhanced Wall Treatment	-	-	0.1 μm	36.72%	FAIL
Pressure Based	k- ϵ	RNG	Swirl Dominated	Standart Wall Functions	-	0.1 μm	39.67%	FAIL
Pressure Based	k- ϵ	Standard	Enhanced Wall Treatment	-	-	0.1 μm	25.25%	FAIL
Pressure Based	k- ϵ	Standard	Non-equilibrium Wall Functions	-	-	0.1 μm	42.95%	FAIL
Pressure Based	k- ϵ	Standard	Standart Wall Functions	-	-	0.1 μm	8.20%	FAIL
Pressure Based	k- ϵ	Realizable	-	-	Non-equilibrium Wall Functions	10 μm	89.51%	FAIL

contd.

Algorithm	RANS	Option 1	Option 2	Option 3	Option 4	Particle Diameter	Sedimentation %	Mass Outflow
Pressure Based	k-ε	Realizable	Enhanced Wall Treatment	-	-	10 μm	14.10%	PASS
Pressure Based	k-ε	Realizable	Standart Wall Functions	-	-	10 μm	38.03%	PASS
Pressure Based	k-ε	RNG	-	-	Standart Wall Functions	10 μm	9.18%	FAIL
Pressure Based	k-ε	RNG	Differential Viscosity Model	Standart Wall Functions	-	10 μm	29.84%	FAIL
Pressure Based	k-ε	RNG	Differential Viscosity Model	Swirl Dominated	Scalable Wall Functions	10 μm	59.67%	FAIL
Pressure Based	k-ε	RNG	Enhanced Wall Treatment	-	-	10 μm	16.07%	FAIL
Pressure Based	k-ε	RNG	Swirl Dominated	Standart Wall Functions	-	10 μm	33.44%	FAIL
Pressure Based	k-ε	Standard	Enhanced Wall Treatment	-	-	10 μm	11.48%	FAIL
Pressure Based	k-ε	Standard	Standart Wall Functions	-	-	10 μm	0.66%	FAIL

APPENDIX-B: A MATLAB GUI for Centrifuge Separator Calculation



```
function varargout = Ambler_classic(varargin)
% AMBLER_CLASSIC MATLAB code for Ambler_classic.fig
%   AMBLER_CLASSIC, by itself, creates a new AMBLER_CLASSIC or
%   raises the existing
%   singleton*.
%   H = AMBLER_CLASSIC returns the handle to a new AMBLER_CLASSIC
%   or the handle to
%   the existing singleton*.
%   AMBLER_CLASSIC('CALLBACK',hObject,eventData,handles,...) calls the
%   local
%   function named CALLBACK in AMBLER_CLASSIC.M with the given
%   input arguments.
%   AMBLER_CLASSIC('Property','Value',...) creates a new
%   AMBLER_CLASSIC or raises the
%   existing singleton*. Starting from the left, property value pairs are
%   applied to the GUI before Ambler_classic_OpeningFcn gets called. An
%   unrecognized property name or invalid value makes property application
%   stop. All inputs are passed to Ambler_classic_OpeningFcn via varargin.
%   *See GUI Options on GUIDE's Tools menu. Choose "GUI allows only one
%   instance to run (singleton)".
gui_Singleton = 1;
gui_State = struct('gui_Name',    mfilename, ...
                  'gui_Singleton', gui_Singleton, ...
```



```

        'gui_OpeningFcn', @Ambler_classic_OpeningFcn, ...
        'gui_OutputFcn', @Ambler_classic_OutputFcn, ...
        'gui_LayoutFcn', [], ...
        'gui_Callback', []);
if nargin and and ischar(varargin{1})
    gui_State.gui_Callback = str2func(varargin{1});
end
if nargin
    [varargout{1:nargout}] = gui_mainfcn(gui_State, varargin{:});
else
    gui_mainfcn(gui_State, varargin{:});
end
function Ambler_classic_OpeningFcn(hObject, eventdata, handles, varargin)
handles.output = hObject;
guidata(hObject, handles);
function varargout = Ambler_classic_OutputFcn(hObject, eventdata, handles)
varargout{1} = handles.output;
function edit1_Callback(hObject, eventdata, handles)
function edit1_CreateFcn(hObject, eventdata, handles)
if ispc and and isequal(get(hObject,'BackgroundColor'),
get(0,'defaultUicontrolBackgroundColor'))
    set(hObject,'BackgroundColor','white');
end
function edit2_Callback(hObject, eventdata, handles)
function edit2_CreateFcn(hObject, eventdata, handles)
if ispc and and isequal(get(hObject,'BackgroundColor'),
get(0,'defaultUicontrolBackgroundColor'))
    set(hObject,'BackgroundColor','white');
end
function edit3_Callback(hObject, eventdata, handles)
function edit3_CreateFcn(hObject, eventdata, handles)
if ispc and and isequal(get(hObject,'BackgroundColor'),
get(0,'defaultUicontrolBackgroundColor'))
    set(hObject,'BackgroundColor','white');
end
function edit4_Callback(hObject, eventdata, handles)
function edit4_CreateFcn(hObject, eventdata, handles)
if ispc and and isequal(get(hObject,'BackgroundColor'),
get(0,'defaultUicontrolBackgroundColor'))
    set(hObject,'BackgroundColor','white');
end
function edit5_Callback(hObject, eventdata, handles)
function edit5_CreateFcn(hObject, eventdata, handles)
if ispc and and isequal(get(hObject,'BackgroundColor'),
get(0,'defaultUicontrolBackgroundColor'))
    set(hObject,'BackgroundColor','white');
end

```

```

end
function edit6_Callback(hObject, eventdata, handles)
if ispc andand isequal(get(hObject,'BackgroundColor'),
get(0,'defaultUicontrolBackgroundColor'))
    set(hObject,'BackgroundColor','white');
end
function edit7_Callback(hObject, eventdata, handles)
if ispc andand isequal(get(hObject,'BackgroundColor'),
get(0,'defaultUicontrolBackgroundColor'))
    set(hObject,'BackgroundColor','white');
end
function bowl_speed_Callback(hObject, eventdata, handles)
function bowl_speed_CreateFcn(hObject, eventdata, handles)
if ispc andand isequal(get(hObject,'BackgroundColor'),
get(0,'defaultUicontrolBackgroundColor'))
    set(hObject,'BackgroundColor','white');
end
function volumetric_flow_rate_Callback(hObject, eventdata, handles)
a double
function volumetric_flow_rate_CreateFcn(hObject, eventdata, handles)
if ispc andand isequal(get(hObject,'BackgroundColor'),
get(0,'defaultUicontrolBackgroundColor'))
    set(hObject,'BackgroundColor','white');
end
function disk_angle_Callback(hObject, eventdata, handles)
function disk_angle_CreateFcn(hObject, eventdata, handles)
if ispc andand isequal(get(hObject,'BackgroundColor'),
get(0,'defaultUicontrolBackgroundColor'))
    set(hObject,'BackgroundColor','white');
end
function inner_rad_Callback(hObject, eventdata, handles)
function inner_rad_CreateFcn(hObject, eventdata, handles)
if ispc andand isequal(get(hObject,'BackgroundColor'),
get(0,'defaultUicontrolBackgroundColor'))
    set(hObject,'BackgroundColor','white');
end
function outer_rad_Callback(hObject, eventdata, handles)
function outer_rad_CreateFcn(hObject, eventdata, handles)
if ispc andand isequal(get(hObject,'BackgroundColor'),
get(0,'defaultUicontrolBackgroundColor'))
    set(hObject,'BackgroundColor','white');
end
function disk_qty_Callback(hObject, eventdata, handles)
function disk_qty_CreateFcn(hObject, eventdata, handles)
if ispc andand isequal(get(hObject,'BackgroundColor'),
get(0,'defaultUicontrolBackgroundColor'))

```

```

    set(hObject,'BackgroundColor','white');
end
function liquid_viscosity_Callback(hObject, eventdata, handles)
function liquid_viscosity_CreateFcn(hObject, eventdata, handles)
if ispc andand isequal(get(hObject,'BackgroundColor'),
get(0,'defaultUicontrolBackgroundColor'))
    set(hObject,'BackgroundColor','white');
end
function liquid_density_Callback(hObject, eventdata, handles)
function liquid_density_CreateFcn(hObject, eventdata, handles)
if ispc andand isequal(get(hObject,'BackgroundColor'),
get(0,'defaultUicontrolBackgroundColor'))
    set(hObject,'BackgroundColor','white');
end
function sediment_density_Callback(hObject, eventdata, handles)
double
function sediment_density_CreateFcn(hObject, eventdata, handles)
if ispc andand isequal(get(hObject,'BackgroundColor'),
get(0,'defaultUicontrolBackgroundColor'))
    set(hObject,'BackgroundColor','white');
end
function Calc_Trigger_Callback(hObject, eventdata, handles)
Q=str2double(get(handles.volumetric_flow_rate,'string'));
mu=str2double(get(handles.liquid_viscosity,'string'));
N=str2double(get(handles.disk_qty,'string'));
rho_s=str2double(get(handles.sediment_density,'string'));
rho_l=str2double(get(handles.liquid_density,'string'));
inlet_cont_percent=str2double(get(handles.inlet_contaminant,'string'))/100;
interface_diameter=str2double(get(handles.interface_diam,'string'));
interface_h=str2double(get(handles.interface_height,'string'));
omega=2*pi*(str2double(get(handles.bowl_speed,'string')))/60;
outlet_r=str2double(get(handles.outer_rad,'string'))/1000;
inlet_r=str2double(get(handles.inner_rad,'string'))/1000;
theta=str2double(get(handles.disk_angle,'string'));
cutoff_diam=(((27*(Q/3600)*9.81*1*mu)/(2*pi*N*(rho_s-
rho_l)*omega^2*(outlet_r^3-inlet_r^3)*cotd(theta)))^0.5)*1e+6;
equivalent_area=2*pi*N*omega^2*(outlet_r^3-inlet_r^3)/(3*9.81*1*tand(theta));
volumetric_flow_DI=(Q/3600)/N;
mass_flow_contaminant_DI=volumetric_flow_DI*inlet_cont_percent*rho_s;
interface_area=(interface_diameter/1000)*pi*(interface_h/1000);
inlet_velocity=volumetric_flow_DI/interface_area;

set(handles.sigma,'string',equivalent_area);
set(handles.cut_off_pd,'string',cutoff_diam);
set(handles.CV_flowrate,'string',volumetric_flow_DI);
set(handles.contaminant_massflow,'string',mass_flow_contaminant_DI);

```

```
set(handles.contaminant_inletvel,'string',inlet_velocity);
```

```
ReynoldsNr=rho_l*inlet_velocity*interface_h/mu;
```

```
Darcyf=24/ReynoldsNr;
```

```
DarcyDeltaP=Darcyf*(rho_l/2)*inlet_velocity^2/interface_h;
```

```
set(handles.hydraulic_diam1,'string',interface_h);
```

```
set(handles.rho_liquid1,'string',rho_l);
```

```
set(handles.mu_liquid1,'string',mu);
```

```
set(handles.average_velocity1,'string',inlet_velocity);
```

```
set(handles.Re1,'string',ReynoldsNr);
```

```
set(handles.darcy_fl,'string',Darcyf);
```

```
set(handles.pressure_drop1,'string',DarcyDeltaP);
```

```
function inlet_contaminant_Callback(hObject, eventdata, handles)
```

```
function inlet_contaminant_CreateFcn(hObject, eventdata, handles)
```

```
if ispc andand isequal(get(hObject,'BackgroundColor'),  
get(0,'defaultUicontrolBackgroundColor'))
```

```
    set(hObject,'BackgroundColor','white');
```

```
end
```

```
function interface_diam_Callback(hObject, eventdata, handles)
```

```
function interface_diam_CreateFcn(hObject, eventdata, handles)
```

```
if ispc andand isequal(get(hObject,'BackgroundColor'),  
get(0,'defaultUicontrolBackgroundColor'))
```

```
    set(hObject,'BackgroundColor','white');
```

```
end
```

```
% -----
```

```
function Untitled_1_Callback(hObject, eventdata, handles)
```

```
function interface_height_Callback(hObject, eventdata, handles)
```

```
function interface_height_CreateFcn(hObject, eventdata, handles)
```

```
if ispc andand isequal(get(hObject,'BackgroundColor'),
```

```
get(0,'defaultUicontrolBackgroundColor'))
```

```
    set(hObject,'BackgroundColor','white');
```

```
end
```

RESUME

Personal Information

Name and Surname : Orçun EKİN

Place and Date of Birth : Aydın, 15/10/1984

Education

Undergraduate (BSc):

Bursa Uludağ University (2002-2007)

Faculty of Engineering and Architecture

Mechanical Engineering Department

Postgraduate (MSc):

Bursa Uludağ University (2007-2011)

Institute of Natural and Applied Sciences

Mechanical Engineering Program

Postgraduate (PhD):

Aydın Adnan Menderes University (2014-2019)

Graduate School of Natural and Applied Sciences

Mechanical Engineering Program

Foreign Languages : English, German

Scientific Activities

Proceeding, Full Text

Ekin O., Çerçi Y., Asker M., “Aydin İli için Parabolik Çanak Tipi Güneş Takip Sisteminin Tasarimi ve Analizi”, ULIBTK’15: 20. Ulusal Isı Bilimi ve Tekniği Kongresi, Sep 2015.

Çerçi Y., **Ekin O.**, Yurddaş A., “A Thermal Resistance Investigation of Red Colored Perforated Clay Bricks by Numerical Modeling”, 3rd International Congress on Construction and Building Research, Dec 2015.

Çerçi Y., **Ekin O.**, Coşkun D., Güçlüer S., Ünlü K. A., Ersöz Ö. R., “An Investigation of Water Heating Process in A Paraboloid Solar Collector”, 3rd International Conference on Advances in Mechanical Engineering Istanbul, Dec 2017.

Deniz C., Çerçi Y., **Ekin O.**, Güçlüer S., Ünlü K. A., “A Study of Specular Error of Parabolic Solar Collector By Deflectometry”, 34th International Physics Congress of The Turkish Physical Society, Aug 2018.

Ekin O., Çerçi Y., “A Comparison of Turbulence Models Characterizing the Flow Through an Inclined Channel Exposed to Centrifugal Forces”, 3rd International Symposium on Industrial Design Engineering, Nov 2018.

Çerçi Y., Ünlü K. A., **Ekin O.**, Güçlüer S., Coşkun D., “Investigation of Pressure Losses in a Water Heating System of a Paraboloid Solar Dish Collector”, 3rd International Symposium on Industrial Design Engineering, Nov 2018.

Contact

e-mail: orcun.ekin@adu.edu.tr

Address: Adnan Menderes Üniversitesi, Mühendislik Fakültesi, Makina Mühendisliği Bölümü, PK:09100 Efeler/AYDIN.

Phone: +90 (256) 213 7503

25/06/2019

AYDIN